AD-A254 756

AGE

Form Approved
OMB No. 0704-0188

1. AGENCY USE ONLY (Leave blank)

3. REPORT TYPE AND DATES COVERED
Quarterly 6 Apr - 8 Apr 92

4. TITLE AND SUBTITLE
Soft X-Ray Projection Lithography

5. FUNDING NUMBERS
F49620-92-J-0264

6. AUTHOR(S)
Dr Quinn

7. PERFORMING ORGANIZATION NAME(S) AND ADDRESS(ES)
Optical Society of America
2010 Massachusetts Avenue N.W.
Washington, DC 20036

8. PERFORMING ORGANIZATION REPORT NUMBER
AFOSR-TR- 92 0738

9. SPONSORING/MONITORING AGENCY NAME(S) AND ADDRESS(ES)
AFOSR/NE
Bldg 410
Bolling AFB DC 20332-6448

10. SPONSORING/MONITORING AGENCY REPORT NUMBER
2301/As

11. SUPPLEMENTARY NOTES

12a. DISTRIBUTION/AVAILABILITY STATEMENT
UNLIMITED

This document has been approved for public release and sale; its distribution is unlimited.

12b. DISTRIBUTION CODE

13. ABSTRACT (Maximum 200 words)

CONFERENCE WAS HELD

14. SUBJECT TERMS

15. NUMBER OF PAGES

16. PRICE CODE

17. SECURITY CLASSIFICATION OF REPORT	18. SECURITY CLASSIFICATION OF THIS PAGE	19. SECURITY CLASSIFICATION OF ABSTRACT	20. LIMITATION OF ABSTRACT
UNCLASS	UNCLASS	UNCLASS	UL

POSTCONFERENCE EDITION

Sponsored by
Air Force Office of Scientific Research
Defense Advanced Research Projects Agency
National Science Foundation

for the
Optical Society of America

1992 OSA Technical Digests

Vol. 1 **Noninvasive Assessment of the Visual System** Santa Fe, NM (Jan. 26-28)
Postconference edition: ISBN 1-55752-216-2 [*U.S. List Price:* $75 (paperback) / *OSA Member Price:* $48 (paperback)]

Vol. 2 **Laser Applications to Chemical Analysis** Salt Lake City, UT (Jan. 27-30)
Postconference edition: ISBN 1-55752-214-6 [*U.S. List Price:* $75 (paperback) / *OSA Member Price:* $48 (paperback)]

Vol. 3 **Ophthalmic and Visual Optics** Santa Fe, NM (Jan. 29-30)
Postconference edition: ISBN 1-55752-218-9 [*U.S. List Price:* $66 (paperback) / *OSA Member Price:* $43 (paperback)]

Vol. 4 **Advances in Color Vision** Irvine, California (Jan. 31-Feb. 1)
Postconference edition: ISBN 1-55752-220-0 [*U.S. List Price:* $66 (paperback) / *OSA Member Price:* $43 (paperback)]

Vol. 5 **Optical Fiber Communication** San Jose, California (Feb. 3-7)
Postconference edition: ISBN 1-55752-222-7 [*U.S. List Price:* $92 (paperback) / *OSA Member Price:* $60 (paperback)]

Vol. 6 **Compact Blue-Green Lasers** Santa Fe, NM (Feb. 19-21)
Postconference edition: ISBN 1-55752-226-X [*U.S. List Price:* $75 (paperback) / *OSA Member Price:* $48 (paperback)]

Vol. 7 **Physics of X-Ray Multilayer Structures** Jackson Hole, WY (Mar. 2-5)
Postconference edition: ISBN 1-55752-228-6 [*U.S. List Price:* $66 (paperback) / *OSA Member Price:* $43 (paperback)]

Vol. 8 **Soft-X-Ray Projection Lithography** Monterey, CA (April 6-8)
Postconference edition: ISBN 1-55752-230-8 [*U.S. List Price:* $66 (paperback) / *OSA Member Price:* $43 (paperback)]

Vol. 9 **Diffractive Optics: Design, Fabrication and Applications** New Orleans, LA (April 13-15)
Postconference edition: ISBN 1-55752-234-0 [*U.S. List Price:* $75 (paperback) / *OSA Member Price:* $48 (paperback)]

Vol. 10 **Integrated Photonics Research** New Orleans, LA (April 13-15)
Postconference edition: ISBN 1-55752-232-4 [*U.S. List Price:* $92 (paperback) / *OSA Member Price:* $60 (paperback)]

Vol. 11 **Signal Recovery and Synthesis IV** New Orleans, LA (April 14-16)
Postconference edition: ISBN 1-55752-236-7 [*U.S. List Price:* $66 (paperback) / *OSA Member Price:* $43 (paperback)]

Vol. 12 **Conference on Lasers and Electro-Optics** Anaheim, CA (May 10-15)
Postconference edition: ISBN 1-55752-238-3 [*U.S. List Price:* $92 (paperback) / *OSA Member Price:* $60 (paperback)]

Vol. 13 **Quantum Electronics and Laser Science** Anaheim, CA (May 10-15)
Postconference edition: ISBN 1-55752-240-5 [*U.S. List Price:* $92 (paperback) / *OSA Member Price:* $60 (paperback)]

Vol. 14 **Surface Roughness and Scattering** Tucson, AZ (June 1-3)
Postconference edition: ISBN 1-55752-242-1 [*U.S. List Price:* $75 (paperback) / *OSA Member Price:* $48 (paperback)]

Vol. 15 **Optical Interference Coatings** Tucson, AZ (June 1-5)
Postconference edition: ISBN 1-55752-244-8 [*U.S. List Price:* $75 (paperback) / *OSA Member Price:* $48 (paperback)]

Vol. 16 **Nonlinear Dynamics in Optical Systems** Austria (June 8-12)
Postconference edition: ISBN 1-55752-259-6 [*U.S. List Price:* $75 (paperback) / *OSA Member Price:* $48 (paperback)]

Vol. 17 **Optical Amplifiers and Their Applications** Santa Fe, NM (June 24-26)
Postconference edition: ISBN 1-55752-246-4 [*U.S. List Price:* $75 (paperback) / *OSA Member Price:* $48 (paperback)]

Vol. 18 **Nonlinear Optics: Materials, Fundamentals, & Applications** Maui, HI (August 17-21)
Postconference edition: ISBN 1-55752-248-0 [*U.S. List Price:* $75 (paperback) / *OSA Member Price:* $48 (paperback)]

Vol. 19 **Adaptive Optics for Large Telescopes** Maui, HI (August 17-21)
Postconference edition: ISBN 1-55752-250-2 [*U.S. List Price:* $75 (paperback) / *OSA Member Price:* $48 (paperback)]

Vol. 20 **Photon Correlation and Scattering** Boulder, CO (August 24-26)
Postconference edition: ISBN 1-55752-252-9 [*U.S. List Price:* $66 (paperback) / *OSA Member Price:* $43 (paperback)]

Vol. 21 **High-Resolution Fourier Transform Spectrometry** Boulder, CO (August 27-29)
Postconference edition: ISBN 1-55752-254-5 [*U.S. List Price:* $66 (paperback) / *OSA Member Price:* $43 (paperback)]

Vol. 22 **Persistent Spectral Hole-Burning: Science and Applications** Switzerland (September 12-18)
Postconference edition: ISBN 1-55752-263-4 [*U.S. List Price:* $75 (paperback) / *OSA Member Price:* $48 (paperback)]

Vol. 23 **OSA Annual Meeting** Albuquerque, NM (September 20-25)
Postconference edition: ISBN 1-55752-256-1 [*U.S. List Price:* $75 (paperback) / *OSA Member Price:* $48 (paperback)]

.... still more to come.

Order by phone, fax, or mail. To charge by phone, call (202) 416-1907. (We accept VISA MasterCard, Diner's Club, and AMEX.) Fax your order and charge information to (202) 416-6120. Mail your order to: OSA Publications Dept., **ATTN: Susan Bornt,** 2010 Massachusetts Ave., NW, Washington, DC 20036.

Orders are accepted up to six months in advance of the meeting.

Soft-X-Ray Projection Lithography

Summaries of papers presented at the
Soft-X-Ray Projection Lithography Topical Meeting

April 6–8, 1992
Monterey, California

1992 Technical Digest Series
Volume 8

POSTCONFERENCE EDITION

Sponsored by
Air Force Office of Scientific Research
Defense Advanced Research Projects Agency
National Science Foundation

for the
Optical Society of America

Optical Society of America
2010 Massachusetts Avenue, NW
Washington, DC 20036

Articles in this publication may be cited in other publications. In order to facilitate access to the original publication source, the following form for the citation is suggested:

> Name of Author(s), "Title of Paper," in Soft-X-Ray Projection Lithography Technical Digest, 1992 (Optical Society of America, Washington, D.C., 1992), Vol. 8, pp. xx–xx.

ISBN Numoer

Conference Edition	1-55752-229-4
Postconference Edition	1-55752-230-8
(Note: Postconference Edition includes postdeadline papers.)	
1992 Technical Digest Series	1-55752-261-8

Library of Congress Catalog Card Number

Conference Edition	92-80613
Postconference Edition	92-80614

This material is based upon work supported by the National Science Foundation. Any opinions, findings, and conclusions or recommendations expressed in this publication are those of the author(s) and do not necessarily reflect the views of the National Science Foundation.

CONTENTS

SUNDAY, APRIL 5, 1992

STEINBECK LOBBY

5:00 pm–7:00 pm REGISTRATION

MONDAY, APRIL 6, 1992

STEINBECK LOBBY

7:30 am–12:00 m REGISTRATION/SPEAKER CHECK-IN

STEINBECK FORUM

8:30 am–8:45 am
OPENING REMARKS
N. M. Ceglio, *Lawrence Livermore National Laboratory*
W. T. Silfvast, *University of Central Florida*

STEINBECK FORUM

8:45 am–10:05 am
MA KEYNOTE SESSION
N. M. Ceglio, *Lawrence Livermore National Laboratory, Presider*

8:45 am
MA1 LSI lithography: present status and future trends, Shoichiro Yoshida, *Nikon Corp., Japan.* Current photolithographic methods employ shorter wavelength light for finer resolving power. For the next generation LSIs in which resolution of 0.2 μm or less is called for, x-ray lithography and electron beam exposure system will be used. Also as an extension of the conventional projection photolithographic methods, soft x-ray lithography is expected to become more prominent. **(p. 2)**

9:25 am
MA2 Lithography—the technology to be used is ????, Robert W. Hill, *Hill Associates, Inc.* There is great indecision int he semiconductor industry as to what the lithography technology will be for the back half of the 1990's (1995–2000). When applied against an idealized process requirement model, all technologies have problems which make the choice extremely expensive and difficult. Technologies considered are: optical extensions, e-beam technologies, ion beam technologies, and x-ray technologies. This paper discusses the main technologies with a description of the advantages and disadvantages. **(p. 3)**

STEINBECK LOBBY

10:05 am–10:35 am COFFEE BREAK

MONDAY, APRIL 6, 1992—*Continued*

STEINBECK FORUM

10:35 am–11:55 am
MA KEYNOTE SESSION—*continued*
W. T. Silfvast, *University of Central Florida, Presider*

10:35 am
MA3 Where are we in the development of soft x-ray projection lithography? Richard R. Freeman, *AT&T Bell Laboratories.* The current state of development of soft x-ray projection lithography is reviewed and compared to the advances required in both science and engineering in order to make it a commercial success. **(p. 4)**

11:15 am
MA4 State of soft-x-ray projection lithography in Japan, Shigetaro Ogura, *Kobe Design Univ., Japan.* Introducing the activities and typical results obtained, particularly in Japan, the state of x-ray projection lithography in Japan is briefly reviewed and discussed. **(p. 5)**

11:55 am–1:30 pm LUNCH on your own

STEINBECK LOBBY

1:00 pm–5:30 pm REGISTRATION/SPEAKER CHECK-IN

STEINBECK FORUM

1:30 pm–3:30 pm
MB SYSTEMS ISSUES
Jeff Bokor, *AT&T Bell Laboratories, Presider*

1:30 pm (Invited)
MB1 Design considerations for a "front end" illumination system for soft x-ray projection lithography, N. M. Ceglio, *Lawrence Livermore National Laboratory.* We define the "front-end" or illumination system to include all those components necessary to produce the x-rays, and to transport them to and appropriately illuminate the mask. We will provide a systematic discussion of the constraints that limit the design of an illumination system for soft x-ray projection lithography. **(p. 8)**

2:00 pm
MB2 XUV projection lithography system design based on single-surface reflecting optics, Brian E. Newnam, V. K. Viswanathan, *Los Alamos National Laboratory.* The rationale, design, and potential capabilities of an XUV projection lithography system using 60–70-nm illumination and single-surface reflectors are described. **(p. 9)**

2:20 pm
MB3 Wavelength issues in soft-x-ray projection lithography, A. M. Hawryluk, N. M. Ceglio, *Lawrence Livermore National Laboratory.* The operating wavelength for a soft-x-ray projection lithography stepper is of considerable interest. However, the choice of wavelength is not a free variable because it will influence other systems parameters. The ideal system would operate at a wavelength where the optics and multilayer mirrors are easy to fabricate, conventional sources exist, resists are sensitive, and resist processing is viable. Having analyzed the choice of wavelength from a systems point of view, we are reporting our results. **(p. 12)**

2:40 pm–3:00 pm COFFEE BREAK

3:00 pm (Invited)
MB4 0.35 micron step and scan manufacturing lithography tool, B. Kuyel, *AT&T Bell Laboratories.* Micrascan-92 is a 248 nm, 0.5 NA, 4X step and scan lithography tool designed for 0.35 μm manufacturing. The lithographic requirements for 0.35 μm device technology, and basic principles of operation of MS-92 are described. **(p. 13)**

STEINBECK FORUM

3:30 pm–5:00 pm
MC SOURCES: 1
Martin Richardson, *University of Central Florida, Presider*

3:30 pm
MC1 X-ray plasma source design, Charles Cerjan, *Lawrence Livermore National Laboratory.* Simulations of x-ray conversion efficiency are presented which are compared to experimental results. The important optimization issues of pulse formatting and material choice are discussed. **(p. 16)**

3:50 pm (Invited)
MC2 X-ray production ~130 Å from laser-produced plasmas for projection x-ray lithography applications, R. L. Kauffman, D. W. Phillion, R. Spitzer, *Lawrence Livermore National Laboratory.* Absolute x-ray production in the region around 130 Å is measured using two different techniques for wavelength discrimination: a broad band channel defined by a grazing incidence carbon x-ray mirror and a Be transmission filter coupled with a Si XUV solid state diode that measures x-rays in the 177 Å to 111 Å region. We also measure x-ray production in a narrow band around 130 Å defined by a near normal incidence synthetic multilayer mirror. In addition, we measure spectra using a transmission grating spectrometer. The spectra show that a relatively narrow feature in Sn near 130 Å enchances x-ray production making this element an optimum choice for this wavelength region. **(p. 17)**

MONDAY, APRIL 6, 1992—*Continued*

4:20 pm
MC3 Laser-plasma source development for projection x-ray lithography, Paul D. Rockett, John A. Hunter, Richard E. Olson, *Sandia National Laboratories, Albuquerque;* Glenn D. Kubiak, Kurt W. Berger, *Sandia National Laboratories,;* Harry Shields, Michael Powers, *Jamar Technology Co., Inc.* An extensive series of experiments and calculations have been performed to improve our understanding of the conversion processes from laser light to XUV radiation. **(p. 18)**

4:40 pm
MC4 Continuous emission source covering the 50- to 300-angstrom band, Stuart Bowyer, *Center for EUV Astrophysics.* We have developed a continuous emission source for use in the soft x-ray and extreme ultraviolet spectral regions. The source and its characteristics are described. **(p. 20)**

TUESDAY, APRIL 7, 1992

STEINBECK FORUM

8:00 am–11:30 am REGISTRATION/SPEAKER CHECK-IN

8:30 am–11:30 am
TuA OPTICS
John H. Bruning, *GCA/TROPEL, Presider*

8:30 am (Invited)
TuA1 Issues associated with the design and construction of an imaging system for soft-x-ray lithography, F. Zernike, *SVG Lithography Systems, Inc.* The necessary optical fabrication technologies and techniques that may be used in the construction of a soft-x-ray projection system are discussed. **(p. 26)**

9:00 am (Invited)
TuA2 Condenser optics, partial coherence, and imaging for soft-x-ray projection lithography, Gary E. Sommargren, Lynn G. Seppala, *Lawrence Livermore National Laboratory.* This paper discusses a condenser design for coupling a laser-produced plasma x-ray source to a 5:1 projection system and its effect on partially coherent imaging. **(p. 29)**

9:30 am
TuA3 Physical optics modeling in soft-x-ray projection lithography, William C. Sweatt, *Sandia National Laboratories;* George N. Lawrence, *Applied Optics Research.* We are developing a diffraction-based model to analyze soft-x-ray projection lithography systems including the effects of partial coherence, imperfect optics and alignment, and source variations. **(p. 32)**

9:50 am–10:10 am COFFEE BREAK

10:10 am
TuA4 Practical tolerancing and performance implications for XUV projection lithography reduction systems, V. K. Viswanathan, *Los Alamos National Laboratory.* The effects of beam-induced thermal distortion of the mirror surfaces and misalignments on the imaging performance of two types of reflective projection optical designs are compared. **(p. 36)**

10:30 am
TuA5 Tolerances of a reflective imaging system, Masaaki Itou, Tsuneo Terasawa, *Hitachi, Ltd., Japan.* Optical surface figure tolerances of a four-mirror imaging system are discussed. Ray-tracing calculations show the tolerance of each mirror to be $< \sim 1$ nm. **(p. 37)**

10:50 am
TuA6 1x reflective x-ray optics, R. F. W. Pease, N. I. Maluf, *Stanford Univ.;* D. A. Markle, *Ultratech Stepper;* G. Owen, *Hewlett Packard Co.* An objection that is often raised to 1x lithography in general is the perceived difficulty of making masks. It is shown that the assumptions customarily made to extrapolate 5x level are fallacious. In particular, evidence is presented that error distributions do not, as is commonly assumed, lie on a Gaussian. Even more importantly, the errors are not distributed evenly over the mask: it is shown how this fact, in particular, grately eases the supposed difficulty of making 1x masks. **(p. 39)**

TUESDAY, APRIL 7, 1992—*Continued*

11:10 am
TuA7 Precision bending of substrate for high performance x-ray optics, D. D. Allred, Y. Shi, M. Berrondo, R. T. Perkins, F. Yuan, L. V. Knight, A. Reyes-Mena, *Brigham Young Univ.* We have investigated producing aspheric mirrors for x-rays with order-of-magnitude improvements in surface finish, figure, and lightness for x-ray mirror blanks. **(p. 40)**

11:30 am–1:00 pm LUNCH on your own

STEINBECK LOBBY

12:30 pm–5:30 pm REGISTRATION/SPEAKER CHECK-IN

STEINBECK FORUM

1:00 pm–4:10 pm
TuB MULTILAYERS
Richard H. Stulen, *Sandia National Laboratories, Presider*

1:00 pm (Invited)
TuB1 Multilayer mirror technology, D. G. Stearns, R. S. Rosen, *Lawrence Livermore National Laboratory;* S. P. Vernon, *Vernon Applied Physics.* We describe recent advances in the fabrication and characterization of multilayer coatings for soft-x-ray projection lithography. **(p. 44)**

1:30 pm
TuB2 Controlling short wavelength x-ray multilayer period variation of focusing optics, J. B. Kortright, K. Nguyen, P. Denham, *Lawrence Berkeley Laboratory;* D. L. Windt, *AT&T Bell Laboratories.* Experimental techniques and results are described for tailoring the variation of multilayer period across the surfaces of focusing optics that have an axis of symmetry. **(p. 46)**

1:50 pm
TuB3 Structural modification of Mo-Si x-ray multilayer mirrors: ion-assisted sputter deposition, S. P. Vernon, *Vernon Applied Physics;* D. G. Stearns, R. S. Rosen, *Lawrence Livermore National Laboratory.* The structural properties and soft x-ray normal incidence reflectivity of Mo-Si multilayers fabricated using ion-assisted dc magnetron sputter deposition are reported. **(p. 49)**

2:10 pm
TuB4 Multilayer performance for soft-x-ray Schwarzschild optics, Georgy Gutman, Kevin Parker, James L. Wood, *Ovonic Synthetic Materials Co., Inc.;* Richard Watts, *National Institute of Standards and Technology.* Some of the problems involved in fabrication multilayer coatings for soft-x-ray objectives are discussed. Cost-efficient techniques for control and characterization of coating uniformity and reflectivity on figured optics are described. Recent results are presented. **(p. 50)**

2:30 pm
TuB5 Multilayer damage and repair issues in soft-x-ray projection lithography, D. P. Gaines, R. C. Spitzer, *Brigham Young Univ.;* N. M. Ceglio, *Lawrence Livermore National Laboratory.* Current soft x-ray projection lithography (SXPL) system designs require multilayer coated optics to operate at levels approaching predicted maximums for near normal incidence reflectivity. Effects that (potentially) degrade multilayer performance in the SXPL environment are discussed. Appropriate repair strategies are suggested, and preliminary results are presented. **(p. 54)**

2:50 pm–3:30 pm COFFEE BREAK

3:30 pm
TuB6 Silicide layer growth rates in Mo/Si multilayers, R. S. Rosen, D. G. Stearns, *Lawrence Livermore National Laboratory;* M. A. Viliardos, M. E. Kassner, *Oregon State Univ.;* S. P. Vernon, *Vernon Applied Physics.* Growth rates of the silicide layers in Mo/Si multilayers were determined at temperatures of 260–342 °C and times of 0.5–2000 hours. **(p. 55)**

3:50 pm
TuB7 Investigation of distortion and damage of Mo-Si multilayer reflective coatings with high-intensity UV radiation, Howard A. Bender, William T. Silfvast, *Univ. Central Florida/CREOL;* Kenneth M. Beck, *Univ. Central Florida.* Measurements of optical distortion and damage thresholds for Mo-Si multilayer reflective coatings under pulsed irradiation have yielded values of 260 mJ/cm² and 500 mJ/cm², respectively, using 308 nm excimer radiation to simulate soft-x-ray flux. Calculated values indicate higher thresholds. **(p. 59)**

STEINBECK FORUM

4:10 pm–5:20 pm
TuC METROLOGY
Chris Evans, *NIST, Presider*

4:10 pm (Invited)
TuC1 An undulator facility for precision optical testing, David Attwood, *Lawrence Berkeley Laboratory.* An undulator facility for spatially coherent radiation, tunable from 130 Å to 70 Å and beyond is described. Its use for interferometry of coated optics for projection lithography is discussed. **(p. 62)**

4:40 pm
TuC2 Propagation error in precision Fizeau interferometry, Chunsheng Huang, *GCA Tropel.* A general analytical form of the propagation error from an interferometer optical system is derived. Influence of the third order aberrations is investigated as numerical examples. **(p. 63)**

5:00 pm
TuC3 Status of the soft-x-ray/XUV optical metrology program at the National Institute of Standards and Technology, Richard Watts, David Ederer, Thomas Lucatorto, Charles Tarrio, *National Institute of Standards and Technology.* We describe the final design parameters and expected performance of a new monochromator/reflectometer optical characterization facility being built at NIST. **(p. 67)**

STEINBECK LOBBY

8:00 am–11:30 am REGISTRATION/SPEAKER CHECK-IN

STEINBECK FORUM

8:30 am–10:10 am
WA IMAGING EXPERIMENTS
R. F. W. Pease, *Stanford University, Presider*

8:30 am (Invited)
WA1 Soft-x-ray projection lithography experiments using Schwarzschild imaging optics, D. A. Tichenor, G. D. Kubiak, M. E. Malinowski, R. H. Stulen, S. J. Haney, K. W. Berger, L. A. Brown, W. C. Sweatt, *Sandia National Laboratories;* J. E. Bjorkholm, R. R. Freeman, M. D. Himel, A. A. MacDowell, D. M. Tennant, O. R. Wood, II, J. Bokor, T. E. Jewell, W. M. Mansfield, W. K. Waskiewicz, D. L. White, D. L. Windt, *AT&T Bell Laboratories.* Projection imaging experiments are described. A Schwarzschild objective is illuminated with 14-nm radiation using an ellipsoidal condenser and a laser plasma source. **(p. 70)**

9:00 am
WA2 Large-area, high-resolution pattern replication using a two-aspherical-mirror system, Hiroo Kinoshita, Kenji Jurihara, Tutomu Mizota, Tuneyuki Haga, Yasuhiro Torii, *NTT LSI Laboratories, Japan;* Hisataka Takenaka, *NTT Interdisciplinary Research Laboratories, Japan.* We have fabricated and assembled a prototype—reduction optics consisting of two aspherical mirrors—to clarify the characteristics of large exposure area. **(p. 72)**

9:20 am (Invited)
WA3 Soft x-ray projection imaging using a 1:1 ring-field optic, A. A. MacDowell, *AT&T Bell Laboratories;* J. E. Bjorkholm, K. Early, R. R. Freeman, M. Himel, P. P. Mulgrew, L. H. Szeto, D. W. Taylor, D. M. Tennant, O. R. Wood, II, J. Bokor, L. Eichner, T. E. Jewell, W. K. Waskiewicz, D. L. White, D. L. Windt, *AT&T Bell Laboratories;* F. Zernike, *SVG Lithography Systems, Inc.* A Mo/Si multilayer coated 1:1 ring-field optical system has been used to carry out projection imaging using soft-x-ray radiation at 12.7 nm. **(p. 75)**

9:50 am
WA4 Schwarzschild microscope for carbon Kα radiation, Katsuhiko Murakami, Hiroshi Nakamura, Tetsuya Oshino, Masayuki Ohtani, Hiroshi Nagata, *Nikon Corp., Japan.* A Schwarzschild objective coated with NiCr/C multilayers was designed and fabricated for C Kα radiation. Imaging results using this objective as a microscope are presented. **(p. 79)**

10:10 am–10:30 am COFFEE BREAK

STEINBECK FORUM

10:30 am–11:50 am
WB SOURCES: 2
David Attwood, *Lawrence Berkeley Laboratory, Presider*

10:30 am (Invited)
WB1 Characterization and control of laser plasma flux parameters for soft-x-ray projection lithography, Martin Richardson, William T. Silfvast, *Univ. Central Florida/CREOL.* We discuss particle and plasma emission measurements of, and particle interdiction techniques for, laser plasma sources designed to meet the needs of soft-x-ray projection lithography. **(p. 84)**

11:00 am
WB2 Laser driver for projection x-ray lithography, Lloyd A. Hackel, Raymond J. Beach, *Lawrence Livermore National Laboratories.* A projection x-ray lithography system requires a laser system with output of approximately 1 J/pulse, 2 to 3 ns pulselength, and a repetition rate of 400 Hz. We have designed a laser-diode-pumped Nd:YLF rod laser system meeting these requirements. We discuss the detailed design criteria for the laser and the experiments which support the design. **(p. 85)**

11:20 am
WB3 Small-scale tokamak for x-ray lithography, S. Suckewer, *Princeton Univ.;* L. Bromberg, D. Cohn, *Massachusetts Institute of Technology.* We have compared the total radiated power of a small tokamak and a small synchrotron, taking into account the spectral intensity distribution of line radiation from the tokamak plasma and of continuum radiation from the synchrotron. Based on related calculations, we discuss the usefulness of a small tokamak for x-ray projection and proximity lithography and simple methods to change the dominant lines in the plasma radiation spectrum. **(p. 86)**

11:40 am–1:30 pm LUNCH on your own

STEINBECK LOBBY

1:00 pm–4:30 pm REGISTRATION/SPEAKER CHECK-IN

STEINBECK FORUM

1:30 pm–2:40 pm
WC RESISTS
Gary N. Taylor, *AT&T Bell Laboratories, Presider*

1:30 pm (Invited)
WC1 Resist alternatives for sub-0.35-μm lithography using highly attenuated radiation, R. R. Kunz, M. A. Hartney, M. Rothschild, *MIT Lincoln Laboratory.* Resist films that fully attenuate the exposing radiation cannot be processed as conventional resists. Alternative resist chemistries that can accommodate highly absorbed radiation will be the topic of this presentation. **(p. 88)**

WEDNESDAY, APRIL 8, 1992—*Continued*

2:00 pm
WC2 Chemically amplified soft-x-ray resists: sensitivity, resolution, and molecular photodesorption, Glenn D. Kubiak, Robert Q. Hwang, Michelle T. Schulberg, *Sandia National Laboratories;* Kathy R. Early, *AT&T Bell Laboratories.* We present sensitivity, resolution, and photodesorption yield results for chemically amplified resists, studied using lithographic exposures at 140 Å, atomic force microscopy, and time-of-flight mass spectrometry, respectively. **(p. 89)**

2:20 pm
WC3 Ray-PN resist for soft-x-ray projection lithography, K. Early, D. M. Tennant, D. Jeon, P. P. Mulgrew, A. A. MacDowell, O. R. Wood, II, *AT&T Bell Laboratories;* G. D. Kubiak, D. A. Tichenor, *Sandia National Laboratories.* We have imaged 0.1 μm lines/spaces in 50- and 70-nm thick films of Ray-PN resist at 14-nm wavelength using ~10 mJ/cm². Processing conditions are presented. **(p. 92)**

2:40 pm–3:00 pm COFFEE BREAK

STEINBECK FORUM

3:00 pm–4:20 pm
WD MASKS
William Oldham, *University of California-Berkeley, Presider*

3:00 pm (Invited)
WD1 Mask technologies for soft-x-ray projection lithography at 13 nm, D. M. Tennant, A. A. MacDowell, P. P. Mulgrew, J. Z. Pastalan, W. K. Waskiewicz, D. L. Windt, O. R. Wood, II, *AT&T Bell Laboratories.* We investigate the materials and processing methods that show promise for patterning transmissive and reflective masks for use with λ = 13 nm soft-x-ray imaging systems. **(p. 98)**

3:30 pm (Invited)
WD2 X-ray mask inspection and qualification, James Wiley, *KLA Instruments Corp. Abstract not available at press time.* **(p. 100)**

4:00 pm
WD3 Reflection mask repair for soft-x-ray projection lithography, Andrew M. Hawryluk, David P. Gaines, *Lawrence Livermore National Laboratory,* Diane Stewart, *Micrion Corp.* Soft-x-ray projection lithography (SXPL) will use a reflective mask consisting of an x-ray multilayer mirror, patterned with a thin (~50–100 nm) layer of gold. Pattern repair techniques that do not degrade the multilayer mirror reflectivity must be developed if SXPL is to become an acceptable choice for lithography. Mask repair results from both clear and opaque mask repair experiments are discussed and analyzed. **(p. 101)**

Keynote Session

MA 8:45am–11:55am
Steinbeck Forum

Natale M. Ceglio, *Presider*
Lawrence Livermore National Laboratory

William T. Silfvast, *Presider*
University of Central Florida

LSI Lithography: Present Status and Future Trends

Shoichiro Yoshida
Nikon Corporation
Fuji Building, 2-3, Marunouchi 3-chome
Chiyoda-ku, Tokyo 100, Japan

The current photolithographic methods employ shorter wavelength light for finer resolving power as exemplified in the rapid transition from g-line to i-line steppers now taking place. The application of new technological attempts like phase-shift or partial illumination methods will further pursuit this trend. Then comes the deep-UV lithography with Eximer laser used as the light source, with which it seems possible to attain 0.25μm resolution for production LSIs.

For the next generation LSIs in which resolution of 0.2μm or less are called for. X-ray lithography and Electron Beam Exposure System come into picture, though from production point of view the X-ray seems to have the upper hand. Also as extension of the conventional projection photolithographic methods, expectation of the soft X-ray lithography will come upfront.

Technically many breakthroughs on such technologies as new photoresist matching the X-ray exposures, improved alignment accuracy, better reliability on drives and system integration as a whole are to be realized for production application. For higher throughput, development of better X-ray optics and elements are of course indispensable.

So far D-RAM generations have changed in a cycle of about three years, technological bottlenecks, difficulties in matching user's needs and economic factors including better return on investments, and delivery requirements will force gradually longer cycle of generation changes.

(The speaker would like to touch on the subject of future photolithographic technology which are expected to develop into soft-X-ray lithography and their problems.)

Lithography - "The technology to be used is ????".

Robert W. Hill, Hill Associates, Inc.

There is great indecision in the semiconductor industry as to what the lithography technology will be for the back half of the 1990's (1995-2000). When applied against an idealized process requirements model, all technologies have problems which make the choice extremely ex pensive and difficult. Technologies considered are: optical extensions, e beam technologies, ion beam technologies, and x-ray technologies. This paper discusses the main technologies with a description of the advantages and disadvantages.

WHERE ARE WE IN THE DEVELOPMENT OF SOFT X-RAY PROJECTION LITHOGRAPHY?

Richard R. Freeman, AT&T Bell Laboratories
Crawfords Corner Road, Holmdel, NJ 07733

Since the first suggestion of doing projection lithography with soft x-rays was made by Hawryluk and Seppala, and Silvfast and Wood nearly 4 years ago, there has been a flood of activity on many of the basic principles and technologies. Foremost among these has been the development of high reflectivity coatings for mirrors that operate near 130 angstroms, the demonstration of diffraction-limited reduction imaging over a small field, and the design of high efficiency laser plasmas for compact illumination sources. Current work includes construction and repair of reflection masks, designs for large field cameras, and illuminators to couple them to the source, and development of advanced methods to measure and ultimately fabricate precision spherical and aspherical mirrors for large field cameras.

Yet a great deal of work has to be done before soft x-ray projection lithography can become even a prototype lithography system, much less a commercial competitor. Examples of new science and engineering that must be developed include: the fabrication of precision aspherical mirrors, the fabrication of mechanically rigid, precision mirror mounts and the accurate alignment of the mirrors on the structure; the development of a compact, high efficiency, high average power laser source for the laser plasma and the control of the debris from the plasma; the production of a high quality imaging resist, probably multilayer, that will allow good linewidth control on the processed wafer; an alignment and registration system capable of supporting sub 1/4 micron printed features; a technique to guarantee defect-free reflecting mask substrates and the implementation of a mask and wafer differential scanner for the step and scan production of large chips.

The State of Soft X-ray Projection Lithography in Japan

Shigetaro Ogura

Kobe Design University,8-1-1 Gakuennishi Nishi-ku,Kobe, Japan

Soft X-ray projection type Lithography has been expected to be most atractive technology in future electronics device production,paticularly since the realization of normal incidence soft x-ray mirror [1] . For instance,Kinoshita et al [2] and other groups [3,4] have already shown the feasibility of this technology,adopting a Schwartzschild optical system composed of normal mirrors. If neglecting process speed or throughput,it is widely accepted the projection type lithography is the one of most fascinateing candidate for future excess 1 G electronics device fabrication. For realizing this technology as a successor of Excimer and/or proximity x-ray lithography, a long range research and development have already started in Japan, at first individual necessitate component such as conpact SR source,typically SiC substrate mirror and multilayer mirror fabrications ,including optical design works [5] for this purpose.

Introducing the activities and typical results obtained paticularly in Japan,the state of x-ray projection lithography in Japan will be briefly revived and discussed.

[1] T.Barbee,Jr.,SPIE 563,2-28(1985)

[2] H.Kinoshita et al,1991 Technical Digest of Soft-X-ray Projection Lithography,57-59(1991)

[3] O.R.Wood et al,ibid,40-42(1991)

[4] M.Itoh et al.ibid,116-118(1991)

[5] Y.Watanabe et al,J.J.A.P.B30,3053-3057(1991)

Systems Issues

MB 1:30pm–3:30pm
Steinbeck Forum

Jeffrey Bokor, *Presider*
AT&T Bell Laboratories

Design Considerations for a "Front End" Illumination System for Soft X-ray Projection Lithography

N. M. Ceglio
Lawrence Livermore National Laboratory
Livermore, CA 94550

We define the "front-end" or illumination system to include all those components necessary to produce the x-rays, and to transport them to and appropriately illuminate the mask. We will provide a systematic discussion of the constraints that limit the design of an illumination system for soft x-ray projection lithography.

XUV Projection Lithography System Design Based on Single-Surface Reflecting Optics*

Brian E. Newnam and V. K. Viswanathan
Chemical and Laser Sciences Division, MS J564
Los Alamos National Laboratory
Los Alamos, NM 87545
505/667-7979

Optical projection lithography using exposure wavelengths less than 100 nm is being developed to produce integrated circuits with feature sizes less than 0.2 μm while providing a total depth of focus (DOF) of ~1 μm. With such short wavelengths, all-reflective projection systems with reflective masks will be required. Since six to seven reflections at normal incidence will be necessary to attain large, diffraction-limited images ≥1 cm^2, high mirror reflectance is very important for future high- volume production. As a result, present attempts to develop soft-x-ray projection lithography are focused mainly around 13 nm [1-3] where relatively high reflectance ~60% has been attained with Mo/Si multilayer mirrors.

There are, however, a number of difficult challenges associated with use of multilayer reflectors. These include: 1) repair of coating defects at interior layers of the reflection masks, 2) narrow spectral bandwidth (~2-3% FWHM, net after 6-7 reflections) that restricts the useful exposure source power, 3) intensity variations in the image plane due to reflector sensitivity to angle-of-incidence variations, 4) potential reflectance degradation due to x-radiation-induced chemical and structural changes, 5) periodic removal of degraded coatings and recoating on expensive mirror substrates, 6) metrology at the operating soft-x-ray wavelength and, of course, 7) the initial coating costs. Furthermore, at soft-x-ray wavelengths such as 13 nm, diffraction-limited performance of the projection system requires that the rms surface figure error for each of the projection mirrors (~4-5) must be ≤0.5 nm. This tolerance includes both source-induced thermal distortion as well as initial polishing imprecision.

For the ≤0.15-μm lithographic production desired near the end of this century, we propose to bypass the problems posed by soft-x-ray multilayer reflectors

*Work supported by Los Alamos Laboratory Directed R&D under the auspices of U.S. Dept. of Energy.

and, instead, to develop a lithographic exposure tool to operate at the shortest wavelength at which mirrors with single reflecting surfaces have sufficient reflectance. This approach should facilitate mask repair, allow for broadband sources, eliminate coating-dependent parameters, use surface metrology at visible wavelengths, and reduce fabrication and maintenance costs. We have evaluated the merits and problems of a system design based on an exposure wavelength of **~60 nm** in the extreme ultraviolet (XUV). Polished CVD-SiC with 35-40% reflectance at normal incidence at for wavelengths longer than 60 nm [4] is the primary mirror candidate. (Diamond would have even higher reflectance if it can be produced with sufficiently smooth surfaces.) Obviously, the useful bandwidth of such a reflector for lithography will be limited only by imaging considerations. For each mirror at this wavelength, the surface figure error budget is 4.5 times larger than at 13 nm, or ~2 nm rms, which is about the SOA polishing capability of some optical fabrication shops (~λ/200 at 600 nm).

The predicted lithographic resolution with 60-nm illumination is 0.15 μm with 0.8-μm DOF, assuming process parameters K_1=0.7 and K_2=0.5. A 60-nm system should also be extendable to ≤0.1-μm lithography by implementing either reflective phase-shift masks and/or annular illumination. On first consideration, it would seem that the low (~0.1%) light throughput of the SiC-reflector projection optics would necessitate a very powerful photon source. However, the very high absorption coefficient of carbon-based photoresists in the XUV, e.g. ~45 μm^{-1} at 60 nm, corresponds to a very high sensitivity <1 $mJ/cm,^2$ that is an offsetting factor. High absorption also implies that processing by surface-imaging/reactive-ion etch probably will be required. With some caveats, this appears feasible since Hartney [5] and coworkers at MIT Lincoln Laboratories have attained sharp features with shallow absorption depths <0.075-μm. Potential 60-nm radiation sources include lasers, e.g. an XUV free-electron laser [6], as well as weaker, broadband sources of synchrotron radiation, e.g. bending magnets [1, 6, 7] and laser-induced plasmas [8-10]. Taking into account the various offsetting factors (mirror reflectance, bandwidth, and resist absorption), the average source power requirement at 60 nm would be a factor of two to five times lower than at 13 nm.

We describe the components (optics, resist, and sources) considered in the design of a 60-nm projection lithographic system. Included is our design of a concentric, two-mirror projection camera [11] that, with 60 nm illumination, attains the desired of 0.15-μm resolution with less than 0.01-μm distortion over a

diffraction-limited 25-mm x 25-mm image field, without scanning. A smaller version of this camera design can produce even larger fields in the scanning mode.

1. D. L. White, et al., "Soft-X-Ray Projection Lithography with 20X Reduction and 0.1-μm Resolution," in *X-Ray/EUV Optics for Astronomy, Microscopy, Polarimetry, and Projection Lithography*, R. B. Hoover and A. B. C. Walker, Jr. eds., Proc. SPIE Vol. 1343, 204 (1991).

2. D. A. Tichenor, et al., "Diffraction-Limited Soft-X-Ray Projection Imaging Using a Laser Plasma Source," Opt. Lett. 16, 1557 (1991).

3. N. M. Ceglio and A. M. Hawryluk, "Soft-X-Ray Projection Lithography System Design," in OSA Proc. on *Soft-X-Ray Projection Lithography*, J. Bokor, ed. (Opt. Soc. Am., Washington, DC 1991), Vol. 12, pp. 5-10.

4. S. Mrowka et al., "Reflectivity of Silicon Carbide in the Extreme Ultraviolet," in *X-Ray Instrumentation in Astronomy*, J. L. Culhane, ed., Proc. SPIE Vol. 597, 160 (1985).

5. M. A. Hartney, "Surface-Imaging Lithography," in OSA Proc. on *Soft-X-Ray Projection Lithography*, op. cit., pp. 120-123.

6. B. E. Newnam, "Extreme-Ultraviolet Free-Electron Laser-Based Projection Lithography Systems," Opt. Eng. 30, 1100 (1991).

7. K. Nguyen, D. Attwood, and T. K. Gustafson, "Source Issues Relevant to X-Ray Lithography," in OSA Proc. on *Soft-X-Ray Projection Lithography*, op. cit., pp. 62-67.

8. R. L. Kauffman and D. W. Phillion, "X-Ray Production Efficiency at 130 Å from Laser-Produced Plasmas," in OSA Proc. on *Soft-X-Ray Projection Lithography*, op. cit., pp. 68-71.

9. C. Cerjan and M. D. Rosen, "Laser-Produced Plasma Soft-X-Ray Generation," in OSA Proc. on *Soft-X-Ray Projection Lithography*, op. cit., pp. 72-75.

10. P. D. Rockett, et al., "XUV Conversion Efficiency in a Low-Intensity KrF Laser Plasma for Projection Lithography," in OSA Proc. on *Soft-X-Ray Projection Lithography*, op. cit., pp. 76-79.

11. V. K. Viswanathan and B. E. Newnam, "Development of Reflective Optical Systems for XUV Projection Lithography," in OSA Proc. on *Soft-X-Ray Projection Lithography*, op. cit., pp. 30-33.

Wavelength Issues in Soft-X-Ray Projection Lithography

A. M. Hawryluk, N. M. Ceglio
Lawrence Livermore National Laboratory
Livermore, CA 94550

The operating wavelength for a soft-x-ray projection lithography stepper is of considerable interest. However, the choice of wavelength is not a free variable because it will influence other systems parameters. The ideal system would operate at a wavelength where the optics and multilayer mirrors are easy to fabricate, conventional sources exist, resists are sensitive, and resist processing is viable. Having analyzed the choice of wavelength from a systems point of view, we are reporting our results.

0.35 micron Step and Scan Manufacturing Lithography Tool

B. Kuyel, Sematech
2607 Montopolis Drive, Austin, TX 78741

Micrascan-92 is a 248 nm, 0.5 NA, 4X Step and Scan lithography tool designed for 0.35 micron manufacturing. It is capable of printing 22x32.5 mm field on 8" wafers with 50 W/hr throughput with the required overlay on the critical process levels. The optical projection lithography technology used in MS-92 is compatible with I-Line, DUV, and VDUV exposures. The step and scan technology, on the other hand, is extendible to meet the requirements of projection X-Ray applications.

The lithographic requirements for 0.35 micron device technology, and basic principles of operation of MS-92 will be described. The system "Base Specifications" will be reviewed from the point of view of what is required from a 0.35 micron lithography tool for a high volume DRAM and ASIC production applications. Overall system architecture and the subsystem functions will be described. Some of the issues unique to a development of a new and a complex technology, in a time frame compatible with the needs of semiconductor manufacturing industry, will be addressed. A few lessons learned in reducing the risk and improving the confidence levels in the realization of a new lithographic concept as a manufacturing worthy tool will be shared.

Monday, April 6, 1992

Sources 1

MC 3:30pm–5:00pm
Steinbeck Forum

Martin C. Richardson, *Presider*
University of Central Florida

X-ray Plasma Source Design Issues

Charles Cerjan
Lawrence Livermore National Laboratory
POB 808, L-296
Livermore, CA 94550
Ph: 510/422-4490 FAX: 510/294-4320

The optimization of soft x-ray production from a laser-produced plasma source is an important issue for several current lithography schemes. Recent experiments at Lawrence Livermore National Laboratory by R. Kauffman, D. Phillion, and R. Spitzer, indicate that the required conversion efficiency can be achieved using moderate laser intensities for a few select materials. Computer simulations of these experiments delineate the critical phenomena underlying these high conversion efficiencies, especially the role of the coupled hydrodynamic expansion and radiation flow in the plasma. By driving the plasma emission out of local thermodynamic equilibrium, photon output in the desired spectral region can be much greater than the black-body emissivity. These conditions can only be achieved under certain conditions which are determined by the incident laser intensity, essentially the electron temperature, and the excited electronic state populations within each ionization stage. Reliable simulations of the experiments require fairly detailed atomic physics databases since the prediction of photon output occurs in such a narrow spectral range. The computer program LASNEX is capable of coupling the hydrodynamic motion and a radiation field described by detailed atomic physics rates for laser produced plasmas. Two-dimensional simulations using this code are compared to the experimental results and are shown to be reliable in their interpretation of these results.

X-Ray Production ~ 130 Å from Laser-Produced Plasmas for Projection X-ray Lithography Applications*

R. L. Kauffman, D. W. Phillion, and R. Spitzer
Lawrence Livermore National Laboratory
P. O. Box 5508
Livermore, Ca. 94550

X ray production in the region around 130 Å from laser-produced plasmas has been investigated for using them as a possible source for projection x-ray lithography. The dependence of production efficiency on target material, intensity, and pulse length has been extensively studied using a 0.53 μm wavelength laser with a maximum output of 0.3 J. Production efficiency of 1% into a 3 Å bandwidth has been demonstrated from a Sn target for intensities around 10^{11} W/cm^2 using an 8 ns pulse. Absolute x-ray production in the region around 130 Å is measured using two different techniques for wavelength discrimination. A broad band channel defined by a grazing incidence carbon x-ray mirror and a Be transmission filter coupled with a Si XUV solid state diode measures x-rays in the 177 Å to 111 Å region. We also measure x-ray production in a narrow band around 130 Å defined by a near normal incidence synthetic multilayer mirror. Filters, mirrors, and detectors have been absolutely calibrated at synchrotrons to obtain absolute yields. In addition, we measure spectra using a transmission grating spectrometer. The spectra show that a relatively narrow feature in Sn near 130 Å enhances x-ray production making this element an optimum choice for this wavelength region. The intensity scaling data suggest that laser spot size and two-dimensional expansion of the plasma play an important role in optimizing x-ray production for these sub-joule irradiation conditions. In future experiments we plan to extend these measurements to larger spot sizes using a higher power laser to better understand the effects of two-dimensional plasma expansion on x-ray production. We also plan to extend these studies using a 1 μm laser to investigate the wavelength dependence on conversion efficiency.

*Work performed under the auspices of the U. S. Department of Energy by the Lawrence Livermore National Laboratory under contract No. W-7405-Eng-48.

Laser-Plasma Source Development for Projection X-ray Lithography

Paul D. Rockett, John A. Hunter, and Richard E. Olson
Sandia National Laboratories, Albuquerque, New Mexico 87185 (505/845-7466)

Glenn D. Kubiak and Kurt W. Berger
Sandia National Laboratories, Livermore, California 94551

Harry Shields and Michael Powers
Jamar Technology Co. Inc., 3956 Sorrento Valley Blvd., San Diego, CA 92121

A Sandia/AT&T team is utilizing optics coated for reflection at 14 nm for projection x-ray lithography. An excimer laser-plasma source of XUV radiation has provided illumination for this work, demonstrating the viability of a laser-plasma x-ray source for ultra-large scale integration. The issues of designing such a source for projection lithography are distinct from synchrotron sources and require understanding the UV to XUV conversion process, mitigating debris from the laser-target, and establishing long-term reliability. We are approaching these problems in parallel by studying the conversion process in solid and thin-film targets, by designing an advanced tape drive as a long-lasting low-mass laser-target, and by choosing to work with excimer lasers as off-the-shelf industrial components.

This paper reports our work on improving our understanding of XUV conversion in laser-plasma x-ray sources in the 0.4-2.8 x 10^{11} W/cm^2 range. By elucidating the processes of plasma heating and radiation transport, we hope to manipulate the plasma to optimize yield into a 4.5% band about 14 nm. Present work with a KrF laser at 248 nm and with a XeCl laser at 308 nm have demonstrated efficiencies of .5% to .8% laser light into 14 nm light.

Experiments were conducted with the Sandia KrF LPS (Laser Plasma Source) using both solid and low-mass targets at 0.7 x 10^{11} W/cm^2, 1.2 x 10^{11} W/cm^2, and 2.8 x 10^{11} W/cm^2. The laser pulselength was approximately 36 ns, and data were recorded with absolutely calibrated x-ray diodes (XRD's), which were filtered with either material filters, a multilayer mirror, or were viewed through a grating monochromator. Longer pulse experiments were performed at Jamar Technology Inc. with ACEL (Advanced Compact Excimer Laser), a XeCl laser with a 47 ns pulselength to evaluate the opportunity of driving a longer XUV pulse.

Data regarding absolute conversion efficiency and the x-ray time history have been used with radiation-hydrodynamic calculations to gain a better understanding of the conversion process.

Mass-limited target conversion efficiency was studied using gold coated on a 1.3μm plastic backing. This extended the work reported last year at 0.7 x 10^{11} W/cm^2 up to an intensity of 2.8 x 10^{11} W/cm^2. The results showed burnthrough occurring at a gold depth greater than 300 nm for .28 TW/cm^2 and at 220 nm for .12 TW/cm^2, as opposed to 50 nm for .07 TW/cm^2.[1] This established the coating thickness that would be required to produce the same XUV emission as seen from a solid target.

Long-pulse XUV generation was attempted with the Jamar XeCl laser, utilizing a 47 ns 308 nm pulse and an incident intensity of 4 x 10^{10} W/cm^2. We quickly determined, however, that the XUV pulse about 14 nm (as indicated by the multilayer filtered XRD - a 12% BW about 14 nm) lasted for only 20 ns of the 47 ns laser duration. A review of prior KrF data corroborated this result.

A detailed study of pulselength and timing relative to the incident laser pulse was then conducted with an NBS XRD sitting behind our grating monochromator with wide slits. The large slits permitted a 6% BW about 14 nm and a 4% BW about 32 nm. The LPS provided a 32 ns 248 nm pulse. As expected one sees a growing pulselength with increasing XUV photon energy, however, the 14 nm was confirmed to last for only approximately 20 ns, regardless of intensity up to 2.8 x 10^{11} W/cm^2. The 32 nm signal lasted for the full 32 ns, however, all XUV signals began some 7 ns after the toe of the incident laser pulse. The conversion physics revealed in these results will be discussed in terms of LASNEX models of this interaction.

REFERENCES

1. P. Rockett, J. Hunter, R. Kensek, R. Olson, G. Kubiak, and K. Berger, "XUV Conversion Efficiency in a Low-Intensity KrF Laser Plasma for Projection Lithography," OSA Proc. on Soft X-ray Projection Lithography, **Vol. 12**, Monterey, CA, April 10-12 1991.

*This work was supported in part by the U. S. Department of Energy under contract DE-AC04-76DP00789.

A Continuous Emission Source Covering the 50 to 300 Angstrom Band

Stuart Bowyer

Center for EUV Astrophysics
2150 Kittredge Street
Berkeley, CA 94720
(510) 642-1648

Introduction

Because of the growing importance of extreme ultraviolet radiation, there is considerable interest in high intensity laboratory sources for this spectral range. A variety of sources have been proposed for these wavelengths, and many of these are described in the classic book of Samson (1967). Most of these sources have substantial limitations, especially those that are intended for use below 1200 Å. We (Paresce *et al.* 1971) and others have developed continuous discharge sources which are stable and maintenance-free and which provide a large number of intense lines at wavelengths down to ~300 Å. Soft X-ray sources of the type developed and refined by Henke (1975) are capable of producing substantial amounts of soft X-ray radiation. However, these sources have severe limitations for use at wavelengths longer than ~50 Å. For example, much of the radiation produced is continuum radiation with rather low flux at any specific line. In addition, the flux is peaked at shorter wavelengths. When dispersed by a grazing incidence monochromator, wavelengths at first order and many higher orders emerge from the exit slit, rather than a true monochromatic flux which is usually desired. Essentially the only sources available that can provide reasonable flux levels at wavelengths between 50 and 300 Å are capacitive discharge sources with attendant problems of severe electromagnetic interference, and plasma discharge sources.

We have developed a plasma discharge source which produces a substantial number of lines with high intensity in the wavelength band from 50 to 300 Å. This device is based on a design described by Finley *et al.* (1979). That source has undergone some six revisions since its inception, and the current configuration is described herein. It is stable, easy to use, and easy to maintain.

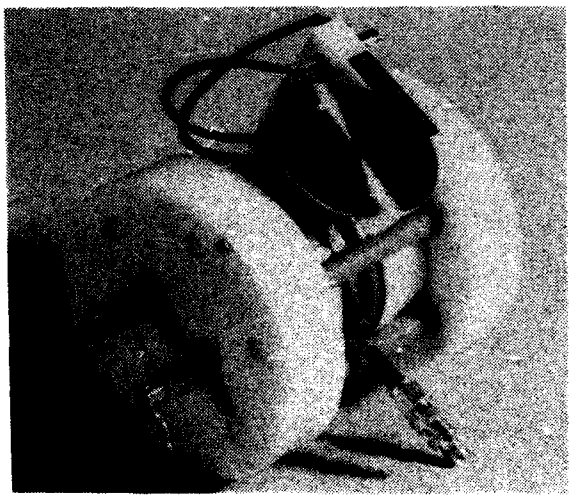

Fig. 1. Photograph of the source.

The Source

A picture of the source is shown in Figure 1; a cutaway schematic is shown in Figure 2. Electrons emitted from a cathode are constrained to follow magnetic field lines in very tight helices until they are scattered to an anode. An anomalously high energy electron distribution is thereby developed in the discharge region

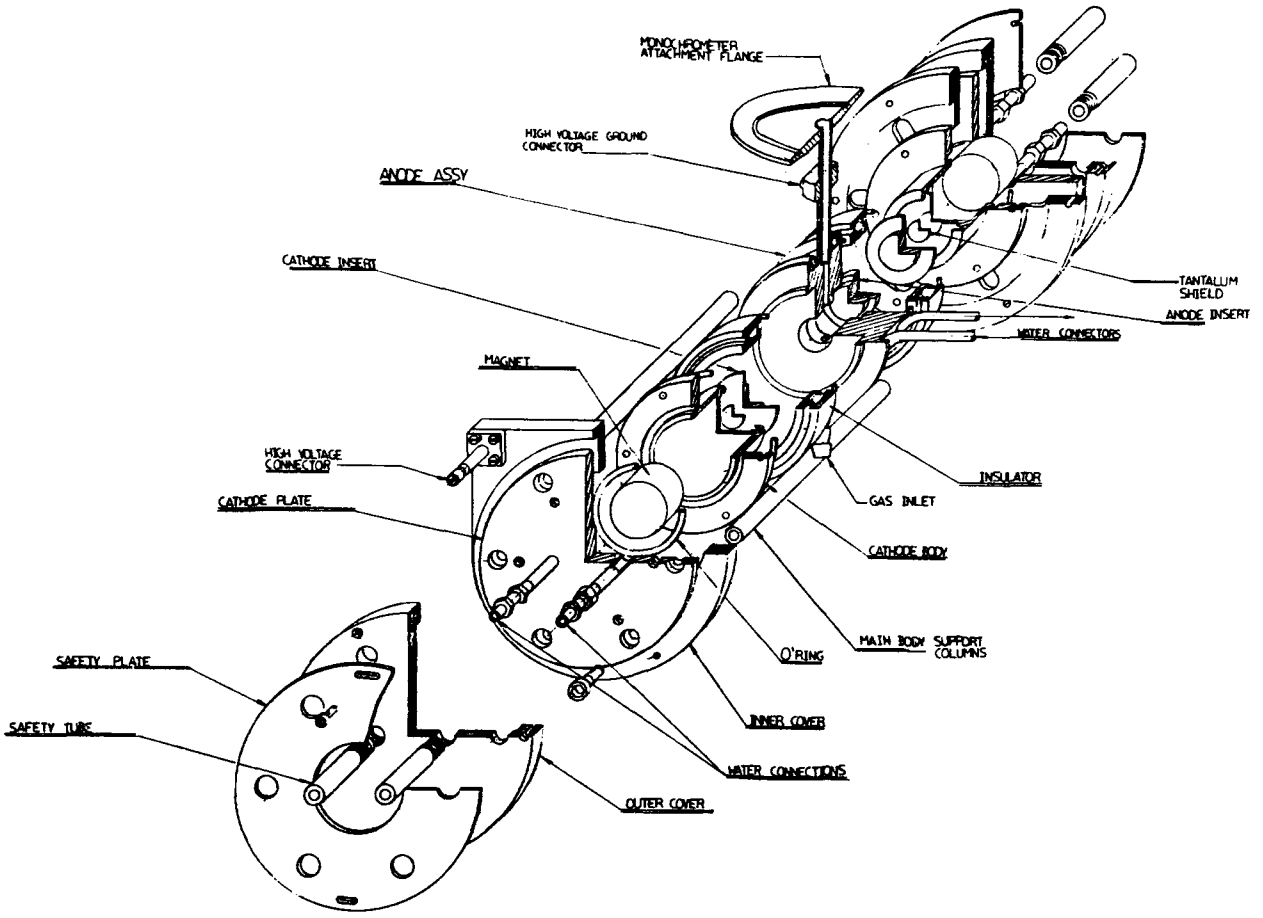

Fig. 2. Cutaway schematic of the source.

between the two anodes. These electrons excite a variety of lines, including both lines intrinsic to the discharge gas and, equally important, lines produced by the excitation of highly ionized material sputtered from the cathode faces. The axial magnetic field is produced by a pair of rare earth magnets placed inside the cathode bodies, and the magnetic circuit is completed by six bolts which clamp the unit together. Considerable heat is generated in the cathode bodies, and cooling water is circulated through them. The anode is also water-cooled. The source is powered by a ~2 ampere high-voltage power supply.

In operation, the pressure in the gas discharge region is controlled by pumping on the source while adjusting the input gas flow rate. The pressure inside the discharge region is difficult to measure. Relative readings, however, are sufficient for optimizing the discharge. The discharge characteristics of this source are pressure dependent. Under normal conditions, the discharge is confined to the central anode region. At the high pressure limit, a glow discharge takes place throughout the lamp. As the pressure is lowered, a critical pressure is reached below which a discharge cannot be sustained.

As the source is being operated, material is continually sputtered off the cathode faces. However, the geometry of the source is such that after more than a hundred hours of operation, we have observed no metal deposited downstream of the source. Most of the sputtered metal is deposited on ridges at the edges of the anode. When the cathode pieces are replaced, the anode insert can be removed and a clean one can be installed, if necessary.

The longevity of the cathode pieces depends on the material used and the operating characteristics of the discharge. The source is designed to minimize the possibility of sputtering through to the water jacket by the addition of an insert behind the center of the cathode piece. When the cathode piece itself is sputtered through, the emission characteristics of the source change dramatically, indicating that maintenance is required.

Output Characteristics

The spectrum shown in Figure 3 is that of a neon discharge with magnesium cathodes. A magnesium cathode gives very thorough coverage of the region from 120 to 190 Å, with extremely bright Mg III lines at 232 Å. The spectrum shown in Figure 4 is that of a neon discharge with aluminum cathodes.

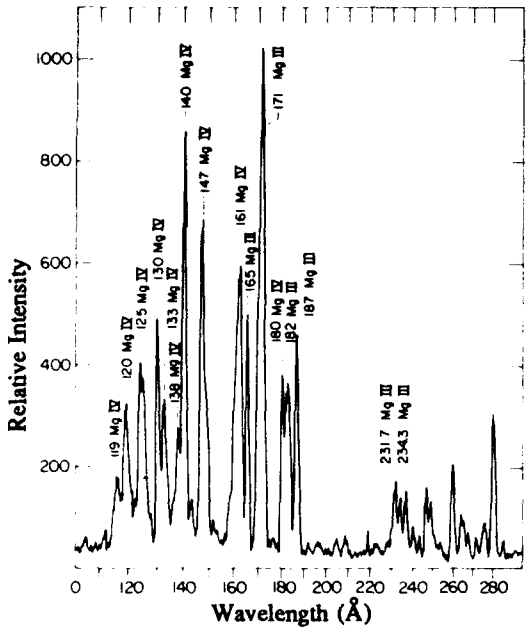

Fig. 3. Spectrum of magnesium and neon.

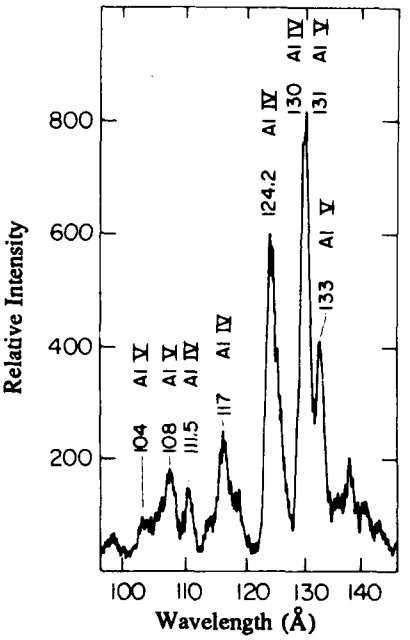

Fig. 4. Spectrum of aluminum and neon.

In general, metal line intensities increase more rapidly with the discharge current than do gas lines since the sputtering rate is roughly proportional to the square of the current. This is because increasing the voltage (and thus the current) increases the energy of the impacting ions, thus raising the sputtering yield. The gas line intensities (especially the lines from higher ionized species) are less strongly dependent on the current.

Finley *et al.* (1979) characterized some of the operating characteristics of the source. They showed that the pressure dependency of individual lines varies greatly for different species. The short wavelength aluminum line intensities are strongly pressure dependent, dropping to half of their peak value when the pressure is increased by only 25%. The Ne IV lines drop to half of their original value, while the Ne III lines drop by a third, when the pressure is increased by a factor of 3. The aluminum 234 Å line drops off much less sharply with pressure than the aluminum 161 Å line. Given that the gas column between the discharge region and the entrance slit to the monochromator represents $<10^{-6}$ of an optical depth and that the collision frequency of the ions is $<10^{6}$ s^{-1}, self-absorption and collisional deexcitation are of minimal importance. Thus the change in line intensities is probably accounted for by the lowered kinetic energies of the ions and electrons due to the increased frequency of collisions. The intensities of the metal lines decrease much more rapidly with increasing pressure than the gas lines because the sputtering rate decreases, lowering the metal vapor density.

The best combination for the 50–170 Å region has been found to be an argon discharge with aluminum cathodes. Lines between 170 and 200 Å are provided only by magnesium. Above 200 Å, a neon discharge with aluminum cathodes is most satisfactory. Lines of argon and neon beyond 300 Å are quite intense with a discharge current of 300 mA or lower. At these discharge currents, the aluminum sputtering rate is negligible, and the lamp can be used for days without significant erosion of the cathode. Argon was found to be effective in exciting metallic lines, while increasing the sputtering rate only slightly.

Typical Operating Parameters

The operational parameters of the source depend upon the source gas used, the pressure of the gas in the discharge area, the applied voltage, the character of the high voltage power supply, the value of the ballast resistor, and the condition of the cathodes. Consequently, no "standard" operating parameters can be specified; each user must characterize his own particular experimental setup. In particular, the character of the radiation is

sensitive to the pressure in the discharge region in the source, and this pressure is intrinsically unknown. As a practical matter, one measures the pressure at some point near the source and obtains a pressure reading which is related to the source discharge pressure by the intervening conductance.

Within the context of these limitations, we show typical operating parameters of the source in Figures 5, 6, and 7. These measurements were made with a fresh magnesium cathode and with neon as a source gas. The pressure was measured in a monochromator at a point immediately adjacent to the source attachment flange. The voltages indicated reflect the total voltage drop across the high voltage power supply and the ballast resistors.

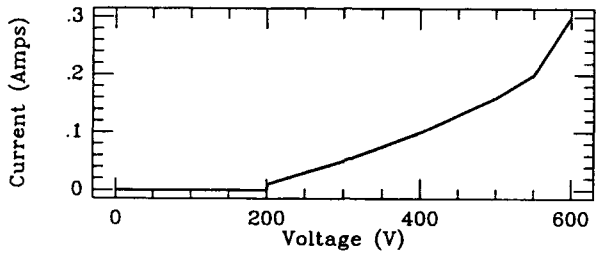

Fig. 5. Source current as a function of voltage. Pressure ~10^{-3} torr.

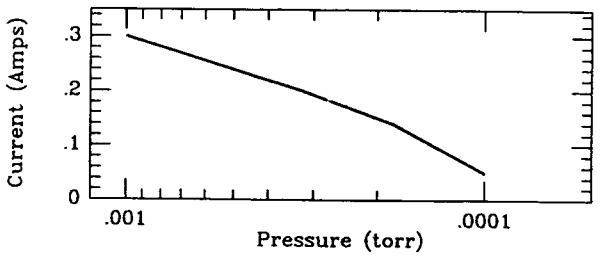

Fig. 6. Source current as a function of pressure. The voltage was initially set to provide 600 V at 0.3 amps and was not adjusted thereafter.

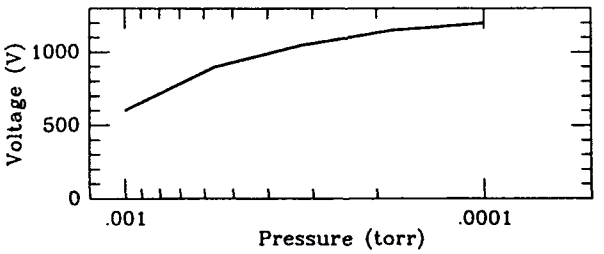

Fig. 7. Voltage as a function of pressure. The voltage was initially set to provide 600 V at 0.3 amps and was not adjusted thereafter.

Conclusions

With a limited number of cathode materials and exciting gases, this source provides nearly 40 usable lines between 50 and 300 Å, many of which are available from a single cathode-gas combination. The source is quiet, continuous, and stable over most of the cathode lifetime. It is well suited to calibrating photon-counting instruments. Although the cathodes eventually fail because of the erosion by sputtering, their longevity is sufficient for even long calibration runs. When the cathodes do becomes exhausted, the refurbishment procedure is sufficiently simple that the source can be back on-line in less than 30 minutes.

References

Finley, D.S., S. Bowyer, F. Paresce, and R.F. Malina, Applied Optics, **18**, 649 (1979).

Henke, B.L., and M.L. Tester, Adv. X-Ray Anal., **18**, 76 (1975).

Paresce, F., S. Kumar, and S. Bowyer, Applied Optics, **10**, 1904 (1971).

Samson, J.A.R., *Techniques of Vacuum Ultraviolet Spectroscopy* (New York: Wiley), 1967.

Optics

TuA 8:30am–11:30am
Steinbeck Forum

John H. Bruning, *Presider*
GCA Tropel Division

ISSUES ASSOCIATED WITH THE DESIGN AND CONSTRUCTION OF AN IMAGING SYSTEM FOR SOFT X-RAY LITHOGRAPHY

F. Zernike
SVG Lithography Systems, Inc.
Wilton, CT 06897

Soft x ray projection lithography allows the printing of feature sizes of .1μm and smaller with reasonable depth of focus because the very short wavelength allows a small numerical aperture. Because attainable mirror reflectivities are low in this wavelength region, the number of mirrors has to be kept to a minimum. Here again the low numerical aperture helps. Compared to present deep UV (248nm.) systems, there are a number of clearcut differences that impact the design and the construction of such a system.

First, as mentioned, the system has only a few elements. This is an advantage where the figure tolerance of the surfaces, that is the random deviation of the actual surface from the desired figure, is concerned. On the other hand, the fact that there are only a few elements to adjust puts a comparatively tighter tolerance on the dimension of each component; the "radius" tolerance of the elements and the tolerance on the spacings between them. To be successful the optical design should pay proper attention to what is mechanically possible.

Second, most, if not all of the surfaces will be aspheric. It is well known that aspheric surfaces are more difficult to make than spherical ones, and the tight "radius" tolerance makes this even more so. In addition, aspheric mirrors have an axis (like a lens) and are therefore more difficult to align than spherical ones.

Third, to obtain low scatter at this wavelength, the surface roughness required is at the high end of what can at present be done for modest spatial frequencies. In addition, to obtain good multi-layer coatings, it may be necessary to maintain this low surface roughness at much higher spatial frequencies than are measurable with optical means.

Fourth, the coatings on the mirrors are angle sensitive, and this has an

influence on the wavefront performance of the system. It may also cause the field dependence of the transmission of the objective to become non uniform. This would then have to be compensated in the illumination system.

Because there are only a few elements in the system, the surface tolerance on each element can be a larger fraction of the total allowable wavefront error than in a multi-element system. Again, the advantage is not as large as might be expected because the smaller number of elements does not allow the balancing of the low order aberrations of one element against those of another. Of course the most important point is that the wavefront error is expressed in units of the operating wavelength, and this unit is forty times smaller than the visible wavelength at which most elements are normally measured. Assuming twenty transmissive elements in a deep UV system, and four mirrors in the soft x ray system, it can easily be shown that the soft x ray mirrors need to have surface figures that are an order of magnitude better than those of the lens elements in the deep UV system. This is better than the best presently attainable surfaces.

To make better surfaces, the first requirement is for a method to measure them; the resolution of present visible (633nm) interferometers is not good enough. However, by going to a deep UV wavelength this situation can be improved. Once a measurement method exists work to improve the figure quality can start.

During testing, and in the final application, the elements need to be mounted in such a way that they are not distorted by the mount itself. Clearly the element should be tested in the "as used" condition. This is not different from present technology, except that the allowable amount of figure distortion is again much smaller.

After coating, the elements will have to be tested at the wavelength at which they are used, and at angles closely equal to those in the final application.

Finally there is the matter of system construction and alignment. As mentioned, careful design of the mounts will be necessary to make

sure that the elements wil not be distorted. However in general the techniques to be used would be extensions of presently used ones.

As mentioned above, the alignment of aspheres is more difficult than that of spheres, since they have an axis. This makes optical alignment of the aspheres in the system impractical. A more promising method is to align each asphere to its mount, using a high resolution interferometer, and to then align the mounts to each other mechanically. If the mounts are made to tight tolerances, this can result in coarse alignments that are good to about two micrometers. In general one would look for a coarse alignment technique that allows the elements to be placed close enough to their nominal positions so that the aberrations of the resulting transmitted wavefront are small enough to be analyzed and to be corrected in fine alignment by small adjustments to the positions of the elements.

Since the system is totally reflective, it should be possible to do fine alignment interferometrically at a longer wavelength. How well this can be done will depend on the particular design and the dependence of its aberrations on misalignments of each of the elements, and on the resolution of the interferometer used.

In conclusion, the task of making and verifying very high surface quality, tightly dimensioned, smooth aspheres is perhaps one of the larger challenges in the making of a soft x ray projection system. If the optical and mechanical designs are done in concert, the assembly and the fine alignment of the system should be extensions of presently used techniques.

Condenser Optics, Partial Coherence and Imaging for Soft X-Ray Projection Lithographapy

Gary E. Sommargren and Lynn G. Seppala

Lawrence Livermore National Laboratory
P.O. Box 808
Livermore, CA 94550

INTRODUCTION:

In this paper we have concentrated on the design and implications of condenser systems for an all reflective soft x-ray projection system. The optical system for a soft x-ray projection lithography system has five main components: the source, condenser (illumination system), mask, imaging system and wafer. Each component is characterized by several parameters, some of which are:

Laser produced plasma source: Energy per pulse and repetition rate of laser, target material, spot size on target, conversion efficiency.

Condenser: Collection solid angle, number and reflectivity of mirrors, position of pupils and source image relative to the imaging system, partial coherence factor.

Mask: Reflectivity, flatness.

Imaging System: Number and reflectivity of mirrors, f/# at the wafer, de-magnification, field size and shape.

Wafer: Sensitivity of resist, flatness.

The throughput (wafers per hour) of a soft x-ray projection lithography system must be comparable to that of optical lithography while providing increased resolution without a significant reduction in the depth of field. System design involves choosing a consistent set of parameters for all five components which meet these goals.

Recent design studies indicate that the imaging system will nominally be a distortion corrected, axially symmetric, four mirror 5:1 ring field (1mm by 25mm at the wafer) reduction imaging system, f/6 and telecentric at the wafer, producing 0.1um features at a wavelength of 13nm. This was used as a baseline for design of the condenser.

CONDENSER DESIGN:

The primary function of the condenser system is to provide uniform illumination at the mask with the proper degree of partial coherence. To maximize wafer throughput, the condenser must collect and transfer the x-rays as efficiently as possible. Thus, the first condenser mirror should have a large collection solid angle while at the same time be sufficiently far from the source to accomodate debris shielding and not too large or curved such that fabrication and coating are impossible. An f/2 system has been chosen as a reasonable compromise. This first collection mirror acts as the pupil of the condenser system. Then, depending on the type of illumination, this pupil is imaged either onto the mask or the pupil of the imaging system. In either case, to minimize x-rays losses the illumination should not overfill the minimum dimension of the ring field. Therefore, to take full advantage of the imaging system, the illumination must be scanned circumferentially over the full ring field at the mask. These numerous requirements preclude the use of a simple single element condenser.

Critical illumination:

In critical illumination, the source is imaged onto the mask. For x-ray efficiency, the image of the source just fills the width of the ring field, while the pupil (first mirror of the condenser) is imaged onto the pupil of the imaging system. The ratio of the numerical apertures of the condenser and imaging systems at the mask, which defines the degree of partial coherence, must also be set at a predetermined value. The first order condenser design to achieve this requires at least two mirrors. A 25x three element condenser design will be described in which the entire ring field can most easily be filled circumferentially by scanning the laser beam on the target. Because exposure of the resist requires multiple x-ray pulses per field, scanning will also tend to average source non-uniformities.

Köhler illumination:

Köhler illumination generally provides better uniformity than critical illumination. Here the pupil of the condenser is imaged onto the mask. Again for x-ray efficiency, the pupil just fills the width of the ring field while the source is imaged onto the pupil of the imaging system. The size of the image relative to the pupil now defines the degree of partial coherence which must set at a given value. The first order design requires two mirrors. To fill the ring field circumferentially, an additional mirror must be angularly scanned at an intermediate image of the source. Several designs have been explored, including 300x three and four mirror configurations.

EFFECTS OF PARTIAL COHERENCE:

Image quality depends not only on the properties of the imaging system, but on the illumination system as well. Hopkins[1] was the first to express this mathematically. The intensity of the image is given as a four dimensional convolution integral whose kernel contains the object (mask), the amplitude point spread function, and the mutual coherence function at the object. The amplitude point spread function is the Fourier transform of the pupil of the imaging system, where the pupil is a complex quantity that defines the finite extent of the pupil and the aberrations of the imaging system. The mutual coherence function is the Fourier transform of the incoherent "effective source" produced by the illumination system, including vignetting and aberrations. When the width of the mutual coherence function is small compared to the width of the amplitude point spread function the imaging is incoherent. When it is much larger, the imaging is coherent. When they are comparable, the imaging is said to be partially coherent. Codes have been written using Hopkins' formulation to plot images of mask patterns. They are being used to evaluate subtle effects of the condenser as well as the imaging system on the performance of the total optical system.

1. H. H. Hopkins, "On the diffraction theory of optical images," Proc. Roy Soc. London, Ser. A, **217**, 408-432 (1953).

PHYSICAL OPTICS MODELING IN SOFT-X-RAY PROJECTION LITHOGRAPHY

William C. Sweatt
Photometrics and Optical Development Division
Sandia National Laboratories
Albuquerque, NM 87185-5800
(505) 845-8566

George N. Lawrence
Applied Optics Research
4455 N. Osage Rd.
Tucson, AZ 85718
(602) 299-1933

INTRODUCTION

Sandia National Laboratories is designing the illuminator for a soft-x-ray projection lithography system,[1,2,3] (see figure) using incoherent, 14-nm wavelength radiation generated by a laser-plasma source. The condenser optic is an off-axis elliptical mirror arranged to give Köhler illumination. The system that images the mask onto the wafer is an off-axis section of a Schwarzchild reflective microscope. As we design the illuminator, we need to be able to calculate its effects on the image quality of the whole system; this includes partial coherence effects, mirror surface quality, alignment and focusing, and source variations. In this paper, we discuss the detailed diffraction analysis that we are performing for this purpose and a few of our results.

KÖHLER ILLUMINATION IN IDEAL SYSTEMS

Our illuminator uses Köhler geometry, in which the x-ray source is imaged into the entrance pupil of the Schwarzchild microscope. In an ideal Köhler system, the illumination is uniform across the mask, regardless of the source uniformity. Furthermore, from any point on the mask, the illuminating pencil of light is aimed at the center of the entrance pupil. Köhler geometry also gives control over the coherence properties of the illumination; one simply changes the size of the source image in the entrance pupil. At one extreme, a very small source image gives coherent illumination. This is characterized by sharp edges on features in the image plane and, unfortunately, hot spots (due to ringing) in the intensity pattern. A large image of the source produces incoherent illumination. There are no hot spots in the image, but the edges of the features are rounded and not sharp. For projection lithography, the optimum balance between these two extremes seems to be a source image size of 50% to 70% of the entrance pupil diameter.

KÖHLER ILLUMINATION IN A SOFT-X-RAY SYSTEM

Our system, which is shown in the figure, is composed entirely of mirrors, since there are no refractive materials available for 14-nm radiation. The condenser optic is an off-axis section of an elliptical mirror. It images the soft-x-ray source into an off-axis entrance pupil of a Schwarzchild microscope. This is the simplest and most efficient system available offering good image quality at this wavelength. Note that the condenser optic is not located immediately upstream from the object mask as is typical.

If our condenser is perfectly made and aligned, we will have all of the advantages of Köhler illumination, save one; there is a small variation in intensity because the ellipse is off-axis. Unfortunately, aberrations in such a system are almost unavoidable; this may significantly degrade the imagery in our system. These aberrations result for two reasons: First, off-axis elliptical mirrors are very hard to make without leaving a small amount of aberration. Second, off-axis mirrors are hard to align, and very small alignment errors can induce significant third-order coma and astigmatism.

Another significant difference between this illuminator and a more usual one is that the condenser mirror is mounted far upstream of the object mask. If this mirror introduces any aberration, the beam will change shape as it propagates toward the mask. At the mask, the intensity profile will be altered, and the aberrations themselves will be distorted in that higher order terms will be introduced. Finally, aberrations and focusing defects in the condenser could upset the aberration balance in the Schwarzchild microscope.

PREVIOUS ANALYSIS OF ILLUMINATION SYSTEMS

H. H. Hopkins wrote the seminal papers[4,5] on the effects of partial coherence in illumination systems. His early development assumed uniform irradiance from a circular source and diffraction-limited condenser optics. Later, he and M. J. Yzuel studied misalignment and defocus between the "perfect" condenser optics and the imaging system. They also proposed a ray-trace-based analysis technique for modeling aberrated condensers.[6] D. S. Goodman[7] analytically studied the effects of third-order aberrations in condenser optics.

These analytical developments give insight about the effects of image quality defects in condenser optics. As such, they are very valuable for generating starting points for design studies. Unfortunately, our system is not well represented by these models, particularly the effects of the propagation of the aberrated beam, and the coupling with the illuminator aberrations and alignment with the off-axis Schwarzchild microscope. We need a modeling capability sophisticated enough to handle the complexity of this system.

OPTICAL MODELING

There are purported to be numerous pieces of proprietary software that can analyze condenser/imaging systems. We decided, however, that our needs would best be served if we modified an existing physical optics analysis code, GLAD,[8] so that it could model partially coherent systems. This code is extremely versatile. It can model the propagation of a wavefront through almost any conceivable optical system. This includes systems that contain aspheric surfaces, surfaces with arbitrary aberration functions, tilted and decentered elements, and arbitrarily shaped apertures and masks. All that needs to be added to the code is the source geometry and a loop to sum the intensity contributions at the wafer from an array of randomly phased source points.

In modeling a system, we assume that the source is a collection of randomly phased point sources. We propagate the wavefront from each of these point sources, one at a time, through the condenser optics to the object mask. We multiply the wavefront by the mask function, and then propagate it through the imaging optics to the wafer. At the wafer, we sum the intensities from all of the wavefronts. This method is not new, but implementing it with such a versatile computer code with full diffraction analysis capability may well be.

We will report on the image degradation resulting from errors in the condenser. This will include mirror fabrication errors, tilt and defocus of the condenser mirror, and decenter and defocus of the entrance pupil.

REFERENCES

[1] D. A. Tichenor, et al., *Opt. Let.* 16:1557 (1991).
[2] G. D. Kubiak, et al., *J. Vac. Sci. Tech.* B9 in press (1991).
[3] D. A. Tichenor, et al., "Soft X-ray Projection Lithography Experiments Using Schwarzchild Imaging Optics," to be presented at OSA's SXPL Topical Meeting, Monterey (1992).
[4] H. H. Hopkins, *Proc. Roy. Soc. (London)* A208:263 (1953).
[5] H. H. Hopkins, *Proc. Roy. Soc. (London)* A217:408 (1953).
[6] H. H. Hopkins and M. J. Yzuel, *Optica Acta* 17(3):157 (1970).
[7] D. S. Goodman, *SPIE* 922:108 (1988).
[8] GLAD is a proprietary product of Applied Optics Research, 4455 N. Osage Rd. Tucson AZ, 87518.

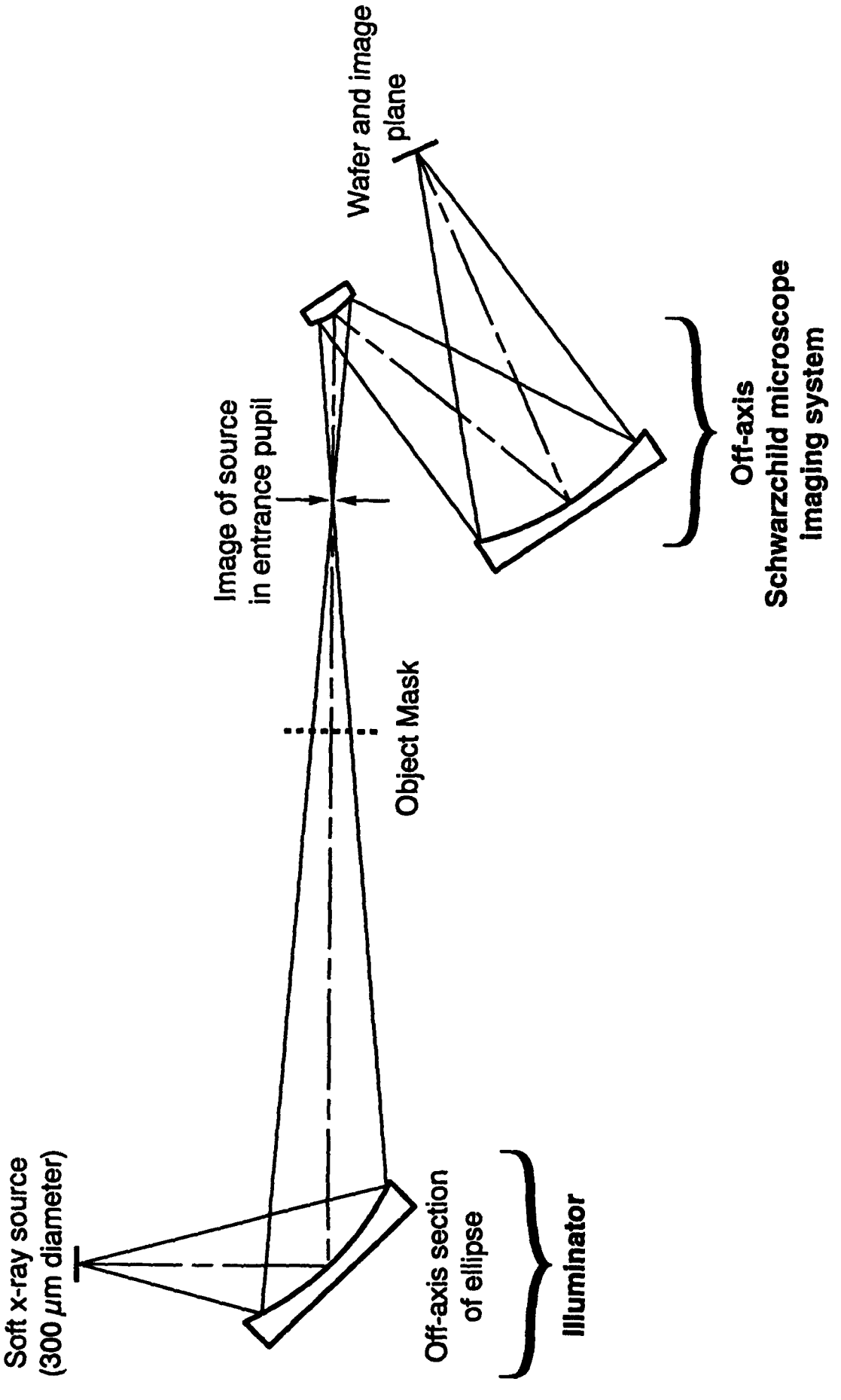
Soft x-ray source
(300 μm diameter)
Off-axis section
of ellipse
Illuminator
Object Mask
Image of source
in entrance pupil
Wafer and image
plane
Off-axis
Schwarzchild microscope
imaging system
TA0325.04

*Practical Tolerancing and Performance Implications for XUV Projection Lithography Reduction Systems**

V. K. Viswanathan
Chemical and Laser Sciences Division, MS J564
Los Alamos National Laboratory
Los Alamos, New Mexico 87545
505/667-1688

The design aspects of candidate reflective optical systems for projection lithography using extreme-ultraviolet (XUV) exposure wavelengths from approximately 10 to 20 nm have been discussed by various authors.[1-3] The very demanding requirements for XUV-projection systems include the ability to resolve 0.1-μm features over at least a 25 mm x 25 mm image field with less than 0.01-μm distortion while providing a minimum of 1-μm total depth of focus. Other practical considerations affecting system imaging capability include thermal distortion of the mirror surfaces due to absorption of a fraction of the incident radiation beam and alignment tolerances. We present our analyses of the magnitude of these latter two effects on two types of reflective projection optical designs. We use the usual criteria for manufacturing and alignment errors[4] and Zernike polynomials[5] to represent the thermal and other distortions induced by the incident flux. We find that concentric, symmetric two-mirror systems[2] are significantly less sensitive to thermal and alignment errors than off-axis, four-mirror systems.

1. T. E. Jewell, J. M. Rodgers, and K. P. Thompson, "Reflective systems design study for soft x-ray projection lithography," J. Vac. Sci. Tech. B8, 1519-1523 (1990).

2. V. K. Viswanathan and B. E. Newnam, "Development of reflective optical systems for xuv projection lithography," OSA Proc. on *Soft-X-Ray Projection Lithography,* J. Bokor, ed., (Opt. Soc. Am., Wash. D.C., 1991), Vol. 12, pp. 30-33.

3. C. Wang and D. L. Shealy, "Differential equation method for design of multi-mirror x-ray projection lithography systems," Proc. SPIE Vol. 1547, (1991).

4. See, for example, the tolerance analysis procedures used in Code V, a proprietary code distributed by Optical Research Associates, Pasadena, CA.

5. For an excellent discussion on Zernike polynomials, see M. Born and E. Wolf, *Principles of Optics,* Pergamon Press, 1975.

* Work supported by Los Alamos National Laboratory Directed Research and Development funds and conducted under the auspices of the U.S. Department of Energy.

Tolerances of a Reflective Imaging System

Masaaki Itou and Tsuneo Terasawa
Hitachi, Ltd., Central Research Laboratory
Kokubunji, Tokyo 185, Japan

A number of reflective imaging systems have been designed for use in soft X-ray projection lithography.[1,2] Optical surface figure errors in these imaging systems, however, degrade resolution as well as cause changes in image positions, which in turn degrade overlay accuracy. We therefore evaluate the figure tolerances of a four-mirror imaging system by ray-tracing calculations.

Figure 1 shows a schematic layout of a ring-field imaging system with a 5x reduction ratio. This system consists of concave mirrors M_1, M_3 and a convex mirror M_2. These mirrors are aspherics (conics of revolution), of which the vertices lie on the optical axis. A plane mirror M_4 deflects the X-ray beam to prevent a wafer from obscuring the optical path. Because of symmetry, the image distortion is essentially zero over a ring field of 12 mm radius. To resolve 0.1 μm features, a numerical aperture (NA) of 0.08 is required at a wavelength of λ=14 nm. As shown in Figure 2, the incoherent MTF value is ~50% at a spatial frequency of 5000 lines/mm.

Figure errors with a low spatial frequency are discussed here. We have calculated the optical performance of an imaging system with aspherics of which the conical constants slightly differ from the nominal design. The plane mirror was replaced with a spherical one with a very large radius of curvature. Figure 3 shows rms wavefront aberration as a function of peak-to-valley figure error for each of the four mirrors. To achieve diffraction-limited resolution, the wavefront aberration should be $< 0.07\lambda$. Even if the total error budget is assigned to mirror M_2, which is the most critical, the tolerance is only 1.2 nm. Figure 4 shows change in image position due to figure error. The image displacement should be kept within 10 nm to print 0.1 μm features. In this case mirror M_1 is the most critical, and its tolerance is 1.4 nm assuming that all the other mirrors are perfect.

Taking account of the error budget for assembly, the figure tolerance of each mirror would be < 1 nm. Breakthroughs are needed in the fabrication and testing of high-quality optical surfaces to make soft X-ray projection lithography a production tool.

References
1. T.E.Jewell, J.M.Rodgers, and K.P.Thompson, "Reflective systems design study for soft X-ray projection lithography," J.Vac.Sci.Technol. B8, 1519 (1990).
2. D.L.Shealy, C.Wang, and V.K.Viswanathan, "Design and analysis of multi-mirror soft X-ray projection lithography systems," in Proc. OSA Soft X-ray Projection Lithography (1991).

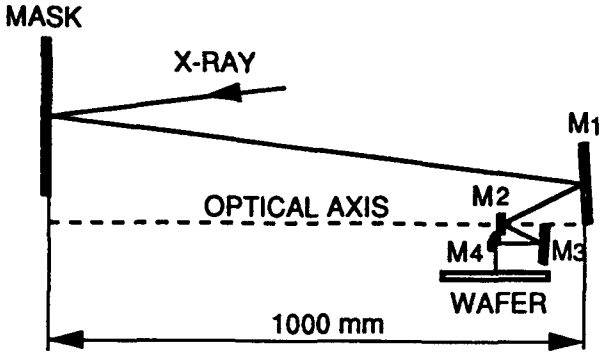

Fig.1. Schematic layout of a four-mirror imaging system.

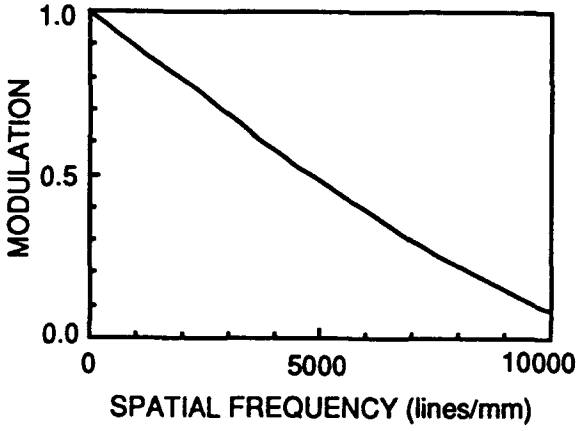

Fig.2. MTF at 14 nm wavelength with NA=0.08.

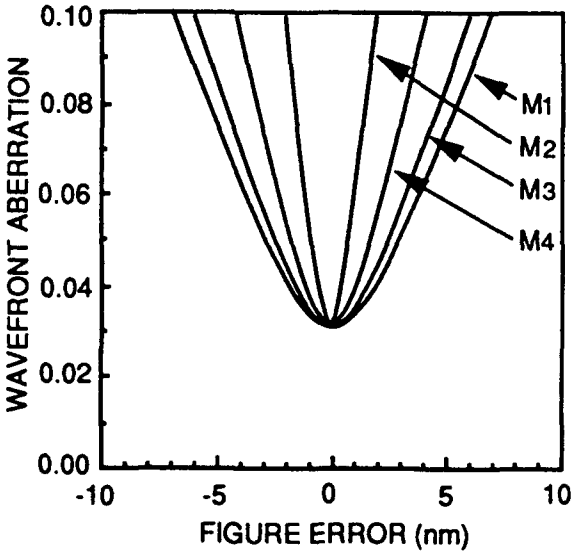

Fig.3. Normalized wavefront aberration at a wavelength of 14 nm.

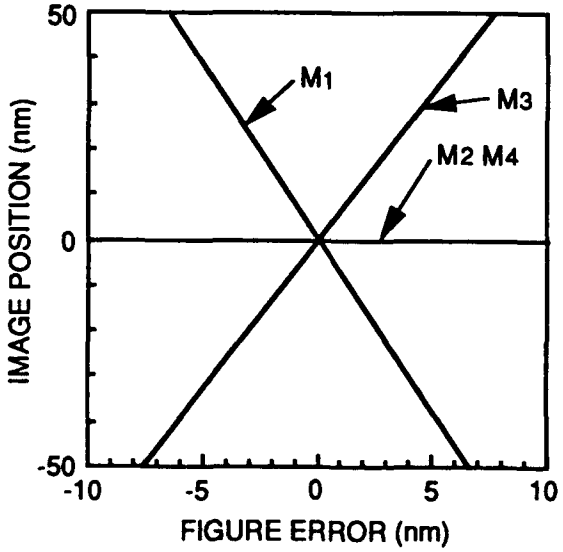

Fig.4. Change in image position.

1× Reflective X-Ray Optics

R.F.W. Pease [1], N.I. Maluf [1], D.A. Markle [2] and G. Owen [3]

[1]Department of Electrical Engineering, Stanford University
Stanford, CA 94305-4055

[2]Ultratech Stepper, [3]Hewlett Packard Company

Using soft X-rays with a wavelength of 13 nm, a diffraction limited projection system with an NA of about 0.09 would have a resolution of about 0.1 μm. The corresponding Rayleigh depth of focus would be about 1.6 μm. Several catoptric reduction designs for use in this regime have been proposed, but they are limited to very small field sizes, because of the difficulty of controlling geometric aberrations. In addition, central obscuration in some designs (e.g. the Schwarzschild), further reduces image modulation. The use of aspheric mirrors can improve the performance, but the figuring and in particular testing of such surfaces at these wavelengths are major challenges. In addition, the alignment of such an aspheric system is a far from trivial undertaking. An alternative approach is to adopt a unit magnification optical system, and make use of the inherent freedom from aberrations such a configuration can posess. Such an approach, using the Offner ring field design, has been proposed by Wood et al [1]. An objection that is often raised to 1× lithography in general is the perceived difficulty of making masks. It is shown that the assumptions customarily made to extrapolate 5× mask specifications down to the 1× level are fallacious. In particular, evidence is presented that error distributions do not, as is commonly assumed, lie on a Gaussian. Even more importantly, the errors are not distributed evenly over the mask: it is shown how this fact, in particular, greatly eases the supposed difficulty of making 1× masks.

[1] O.R. Wood, II, W.T. Silfvast and T.E. Jewell, "Short-wavelength annular-field optical system for imaging tenth-micron features", J. Vac. Sci. Technol. B 7 (6), pp 1613-1615, Nov/Dec 1989.

Precision bending of substrate for high perfomance x-ray optics

D.D. Allred, Y. Shi, M. Berrondo, R.T. Perkins, F. Yuan, L.V. Knight, A. Reyes-Mena
Brigham Young University, Provo, UT 84602

We have investigated producing aspheric mirrors for x rays with order-of-magnitude improvements in surface finish, figure, and lightness for x-ray mirror blanks.

Our study looked at ultrastructure processing *to replace mechanical methods of material removal.* The method starts with a chemical-mechanical polished, flat silicon wafer of the type used in the semiconductor industry. These can be produced with excellent smoothness. Our goal is to preserve the atomic scale smoothness of the surface wafer while the wafer is bent to the desired figure. The wafer is bent to the desired shape by selective, anisotropic etching followed by the build up of stress of predetermined amounts and at predetermined location through either the formation of stressed films or through selective ion plantation. The thin films can be of silicon dioxide, silicon nitride, borophosphatesilicate glass, etc. The bending is modulated to produce complex shapes by controlled thinning of the wafer in selected regions through anisotropic etching of the patterned rear surface of the wafer. The stressed layers together with the etched pattern precisely determine the final topology of the smooth surface. This method is potentially capable of producing an optical element of arbitrarily precise figure which is also atomically smooth.

We have developed codes that accurately predict the figure of substrates that are stressed by thin film deposition. The codes can be written for this specific application and for specific computers. When such codes are coupled to a graphics work station, they are efficient and accurate design tools. Such a system will allow a technician to quickly design a complicated optic.

Our work has shown that the process of fabrication must be iterative. With the first etching and deposition an approximation of the figure will be achieved. The major limitation to the accuracy after the first iteration are the nonuniformity of the deposited film and the substrate. It should be noted that with the proper deposition parameters the thin film will not degrade the nanosmoothness of the substrate since the film is deposited on the back surface of the wafer. The same is true if implantation is used to achieve stress. The codes accurately predict a specific deposition pattern for an arbitrary optical design. However, the accuracy of the actual figure is limited by deposition uniformity and any inhomogeneities of the substrate. It is possible that the thin film thickness will vary from point to point by as much as 10%. This is the present limit on the figure accuracy. It may be possible to produce more uniform films by using atomic layer growth CVD, but some correction will still be required.

The solution to these problems requires the construction of a *correction facility* with real-time metrology and feedback control. [J. R. Kurdock and R. R. Austin] Such a facility will require high precision real-time measurements coupled with fast interaction between the codes and fabrication tools. Taking into account the iterative nature of bending to produce precise figures such a facility would begin with the design code. The codes will tell the fabricator how to etch the substrate and where to deposit the film and other details relative to deposition. The result will be a first, "rough" approximation to the optic. As was mentioned, deviations from the predicted figure will be caused by variation in the

deposited films and substrate thickness, and substrate roughness. These errors can be corrected by depositing or removing small amounts of material in the right places. The key to doing this is that we can measure in situ the effect of these errors to great accuracy with a Twyman–Green interferometer. Then material can be added or subtracted as the interference pattern is monitored electronically. Innovative inversion algorithms—inverse scattering tomography—can control the deposition or removal of material. The implementation of these algorithms directly or to optimize neuro nets is key to making this process practical.

Inverse scattering tomography is used to image properties of materials. This is done by analyzing the scattered energy from different energy sources—dielectric constant and conductivity from electromagnetic energy; bulk modulus, shear modulus, density, bulk viscosity and shear viscosity from elastic waves; etc. The algorithms developed by our collaborators [Borup, D., S. Johnson and M. Berggren] are unique in their accuracy—greatly exceed that of diffraction tomography—and speed—at least 10 times faster than other inverse scattering methods. The algorithm compensates for absorption, refraction and diffraction and gives clear, quantitative images of material properties. It is advantageous to formulate the Inverse Scattering problem as a nonlinear integro-differential equation. However, intrinsic to the nature of these inverse problems is their potential for ill-posedness. Borup, et al. have experience in overcoming ill-posedness of inverse scattering problems. Theoretical and practical results have been achieved in pursuit of *numerically efficient* and *robust* algorithms, i.e. fast algorithms that also mediate the ill-posed nature of some inverse problems. The incident (electromagnetic) energy is diffracting in the cases studied, so that standard Computed Tomographic (CT) algorithms are inadequate for the kind of resolution required for quantitative maps. The need to solve the wave equation exactly, dramatically increases the complexity of the inversion problem. For example, Borup, et al. have solved (in 20 minutes of Cray YMP time) an imaging problem requiring inverting a nonlinear system simultaneously for $\sim$ 50,000 unknown object material values and $\sim$10 million field values (this would require several weeks to terminate successfully on a Cray YMP using naive matrix inversion approaches). By solving the wave equation exactly, within the inversion procedure, they are able to account for the effects of diffraction more accurately, thereby gaining substantial improvement in resolution and accuracy, over standard linearized Diffraction Tomography.

The technology to implement this proscess is within the capabilities of modern deposition and measuring systems. For example the deposition could be done by laser CVD, small aperture sputter guns, laser produced evaporation, or ion implantation. The removal could be done by laser ablation or laser annealing—laser annealing would locally change the stress.

References

[J. R. Kurdock and R. R. Austin] in *Physics of Thin Films*, edited by G. Hass and M. H. Francombe, (Academic Press, New York, 1978)

[Borup, D., S. Johnson and M. Berggren], "Nonperturbative diffraction tomography via Gauss-Newton iteration applied to the scattering integral equation", *Ultrasonic Imaging. (to appear).*

Tuesday, April 7, 1992

Multilayers

TuB 1:00pm–4:10pm
Steinbeck Forum

R. H. Stulen, *Presider*
Sandia National Laboratories

Multilayer Mirror Technology

D. G. Stearns and R. S. Rosen
Lawrence Livermore National Laboratory, P.O. Box 808, Livermore, Calif.

S. P. Vernon
Vernon Applied Physics, P.O. Box 10469, Torrance, Calif.

Recent advances in multilayer (ML) fabrication and characterization have brought this technology to the verge of satisfying the severe requirements posed by soft x-ray projection lithography (SXPL). To enable a viable production SXPL system, the ML coatings must simultaneously demonstrate (1) high normal incidence reflectivity in the range of 65-70% at λ=130Å, (2) ML period errors of less than 0.5% over the optical surface to maintain diffraction-limited imaging and (3) long term stability under realistic operating conditions. In addition, it is possible that certain optical designs will require laterally graded coatings with similar tolerances for the ML period errors. This set of stringent requirements can only be achieved via a thorough understanding and control of the ML deposition process, ML structure and properties.

At Lawrence Livermore National Laboratory we have successfully deposited high performance ML coatings on large area figured optics using dc magnetron sputtering. In our novel approach, we use a combination of large area sources, small source-to-substrate separation and compound planetary motion of the substrates to achieve excellent uniformity. This technique requires no masking to generate a uniform deposition profile, which significantly simplifies the accomodation of different targets, substrates and deposition conditions. Furthermore, since the intrinsic deposition profile is uniform, simple masks can be used to produce axisymmetric variations in the ML period when laterally-graded coatings are required.

We present results of uniform and laterally-graded ML coatings on a variety of substrates. The highest normal incidence reflectivity of 65% at 130Å

has been achieved using ML composed of alternating layers of Mo and Si. The optimum structure, corresponding to smooth pure layers separated by narrow interlayers of mixed composition, is obtained by sputtering at low Ar pressure of ~1.75 mT. Recent studies indicate that an important condition for the formation of smooth layers is a that a critical energy flux be applied on the film surface during growth. In the case of magnetron sputtering at low Ar pressure the energy flux is provided by the reflected Ar neutrals. However, we have observed that high quality ML can be grown at higher Ar pressure (10 mT) by applying a dc bias to the substrate, thereby extracting Ar ions from the plasma which bombard the growth surface.

The optical performance of the ML coatings has been characterized at soft-x-ray wavelengths using synchrotron radiation. Figured substrates as large as 4-inch-diameter with curvatures up to f/3 have been characterized for uniformity, and the uniformity is found to be consistently better than 0.5% across the entire surface. The residual nonuniformities can be accounted for by the variation of the substrate surface area projected onto the target. We have also characterized laterally-graded ML coatings deposited onto 4-inch diameter Si wafers, where the ML period increases radially over the range of Λ=60-100Å. These coatings not only demonstrate the versatility of the deposition system, but additionally provide a controlled study of the variation of the optical performance of Mo-Si ML over an extensive range of x-ray wavelength.

Peak reflectivity is the primary figure of merit for a many-bounce optical system as will be used in SXPL. However, there are x-ray optical applications requiring only one or two reflections where the integrated reflectivity becomes the true figure of merit. The integrated reflectivity of a ML coating can be significantly increased at the expense of the peak reflectivity by varying the ML period continuously through the layer stack. As a demonstration, we have fabricated a series of these "chirped" ML coatings with layer thickness dispersions ranging from 0.01 to 0.1Å per layer. The integrated reflectivity is found to increase systematically up to ~25% for the 0.1Å chirp. This suggests that ML strucutral design can now be matched to a specific optical system to optimize the x-ray throughput.

Controlling short wavelength x-ray multilayer period variation on focussing optics

J.B. Kortright,[1] K. Nguyen,[1] P. Denham,[1] and D.L. Windt[2]

[1]Center for X-ray Optics
Lawrence Berkeley Laboratory
University of California
Berkeley, CA 94720
(510) 486-5960
(510) 486-4550 FAX

[2]AT&T Bell Laboratories
Murray Hill, New Jersey 07974
(908) 582-2367

The variation of multilayer period, or d-spacing, across the reflecting surfaces of soft x-ray normal-incidence focussing optics is of primary importance in the optical performance of these systems. Focussing necessarily implies a specific optimal variation of period across the surfaces, and the multilayer bandpass sets the tolerance scale for acceptable deviations from this ideal variation.[1,2] Mo/Si multilayers for use at wavelengths above 12.4 nm have relatively broad bandpasses, easing these tolerances. Multilayers for use at shorter wavelengths have significantly narrower bandpasses, thus placing significantly greater demands on the control of the period variation. Other design considerations, such as higher magnification systems and larger optics, also place more stringent demands on the control of multilayer period.

With a goal to utilize a multilayer-coated Schwarzschild objective at $\lambda = 7$ nm in imaging experiments, we are developing improved techniques to control the period variation to the required tolerances. These include techniques to tailor the multilayer profile during deposition, and techniques to measure the multilayer optical properties across the curved surfaces. Ru/B_4C multilayers have high normal incidence reflectance (approaching 20%), although the many layers required to achieve such high reflectance results in a narrow bandwidth of roughly 1% FWHM.

The optimal period variation across the surfaces of the primary and secondary mirrors of the Schwarzschild pair are shown in Figure 1 as a function of radial distance from the optic axis. The smaller, primary mirror has the larger optimal variation in d across its clear aperture, making it the more difficult mirror to coat accurately. This variation is large compared to the bandwidth of the multilayer, implying that active control of the multilayer d variation across the surface is required.

Our approach to obtaining the desired control of the d-variation is to make use of the inherent axial symmetry of the Schwarzschild system and an imposed axial symmetry during sputter deposition resulting from planetary rotation of the mirrors about their axis. The introduction of masks oriented radially with respect to the planetary rotation (or optic) axis provides control over the radial d-variation.

Measurement of the d-variation and reflectance of the multilayers as a function of radius is crucial to the development of acceptable period variation, and the measurement techniques themselves

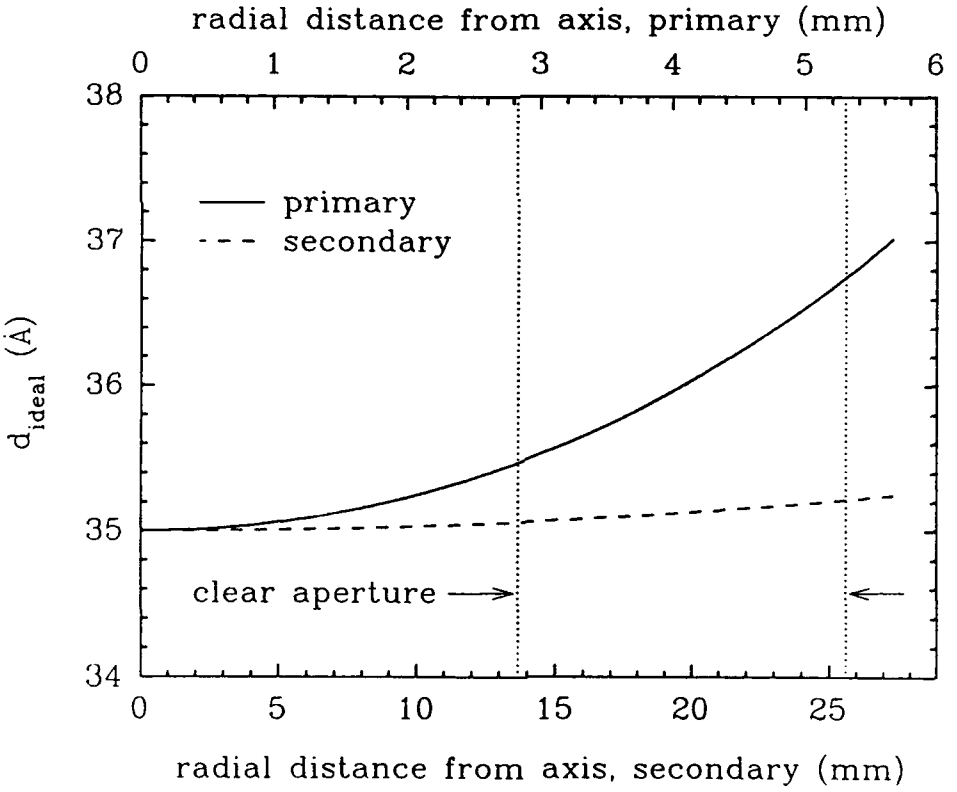

Figure 1. The ideal d-spacing variation across the surfaces of the primary and secondary mirrors of a Schwarzschild objective are plotted as a function of radial distance from the optic axis at that mirror. This period variation would be optimal for operation at 7 nm, neglecting refraction in the multilayer.

are not trivial. We are utilizing two different schemes. One utilizes a small beam of soft x-rays (at the wavelength of interest) to step across the surface of the curved optics to make spatially resolved measurements of the first order multilayer peak. The second utilizes hard x-rays (λ = .154 nm) which can measure many orders of multilayer reflectivity and thus provide a more detailed assessment of the multilayer quality. The drawbacks to utilizing hard x-rays to measure multilayer specular reflectance on curved surfaces is that shallow grazing incidence angles result in a relatively large beam footprint, averaging over a large area, and can preclude the measurement of concave surfaces. We have developed techniques to overcome these difficulties with hard x-ray measurements by tiling the curved surfaces of the optics with sub-millimeter flat substrates which collectively follow the contour of the substrates. After multilayer deposition the small flat substrates are removed from the curved surfaces and their multilayer reflectivity measured individually, providing the variation of multilayer reflectance performance across the curved optics.

Our results to date indicate that we can obtain the required amount of multilayer period variation using these new masking techniques. However, the reflectance in the first peak can be reduced as a result of the introduction of these masks. This paper will focus on our experiences with these important technological issues of improving control over multilayer deposition to unprecedented levels which will be required for successful implementation of soft x-ray projection lithography using multilayer.

This work was supported by the Director, Office of Energy Research, Office of Basic Energy Sciences, Materials Sciences Division, of the U.S. Department of Energy under Contract No. AC03-76SF00098.

References.

1. J.B. Kortright and J.H. Underwood, "Design considerations for multilayer coated Schwarzschild objectives for the XUV," Proc. Int. Soc. Opt. Eng., **1343**, (1990) 95.
2. J.B. Kortright and R.N. Watts, "Multilayer uniformity and performance of soft x-ray imaging optics," OSA Proceedings on Soft X-ray Projection Lithography, Vol. 12, ed. J. Bokor, (1991) 92.

Structural Modification of Mo-Si X-Ray Multilayer Mirrors: Ion-Assisted Sputter Deposition

S. P. Vernon
Vernon Applied Physics
Torrance, CA 90505

D. G. Stearns, R. S. Rosen
Lawrence Livermore National Laboratory
Livermore, CA 94550

The structural properties and soft x-ray normal incidence reflectivity of Mo-Si multilayers fabricated using ion-assisted dc magnetron sputter deposition are reported.

Multilayer Performance for Soft X-ray Schwarzchild Optics

Georgy Gutman, Kevin Parker, James L. Wood
Ovonic Synthetic Materials Co., Inc.
Troy, Michigan 48084

Richard Watts
National Institute of Standards and Technology
Gaithersburg, Maryland 20899

One of the most important requirements for soft x-ray optics is high normal incidence reflectivity. But to ensure a high throughput optical system, Schwarzchild objectives in particular, it is not only necessary to fabricate multilayer coatings with the highest possible reflectivity but to achieve the designed d-spacing uniformity/grading and match the d-spacings of the concave and convex mirrors. The latter is especially important for high throughput multi-mirror lithography optical schemes.[1]

To derive a simple estimate of the throughput requirements, let us assume that the goal is to realize a maximum throughput of a Schwarzchild objective at wavelength λ. Let us suggest that we are coating perfectly figured substrates and analyzing throughput of perfectly adjusted and aligned objective. To be specific we will consider Schwarzchild objective parameters reported in [2,3].

Methods of developing maximum reflectivity in the point (small area) of surfaces are reported elsewhere [4] and will not be considered here. Due to deposition error, first, the actual d-spacing of the multilayer coating, especially for figured optics, will very from point to point over the surface and, second the actual d-spacing for concave and convex pieces can not be matched perfectly. These errors in the d-spacing will degrade the throughput of the objective.

From data given in [2,3] it follows that for the secondary concave mirrors it is necessary to insure uniformity across the region of interest (for λ = 140Å the Bragg angle is 3.3° to 6.3°) with precision better than 0.5%. For the primary convex piece it is necessary to grade the d-spacing across the surface according to the law $d = K(1/\sin\theta)$, where θ is the Bragg angle, with the same precision as the concave piece. A uniform coating on the convex piece would decrease the throughput on the ends of the working region producing a 20% reduction in overall throughput and a significant broadening of the peak of reflectivity.

Error in matching of the d-spacings between concave and convex mirrors can give a more significant degradation of system throughput. An error in d-spacing of +/- 1% can decrease the system throughput by about 20%. We would like to underline however, that a simultaneous change in d-spacing for both optics (when Δd = constant) will not significantly change the throughput

of the system due to a comparatively wide bandpass of synchrotron sources and a broad range of sensitivity for the photoresist.

The obtained variation in multilayer period across a flat or curved surface depends on the specific deposition apparatus used. The planer magnetron sputtering system used is of the rotating drum batch type. It has been modified to include a spinning platform, that revolves with the drum, passing in front of the cathodes on each revolution of the drum. The platform spins on its own axis perpendicular to the axis of the drum (Fig. 1).

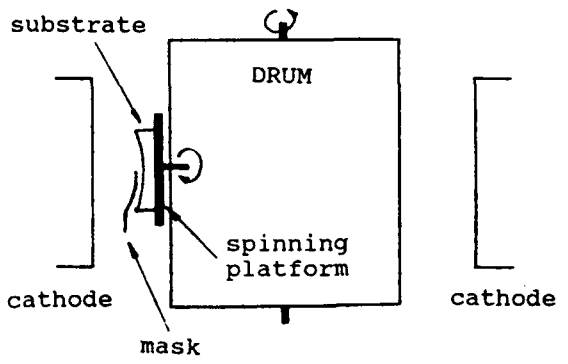

Fig. 1. Magnetron Sputtering machine used to fabricate x-ray multilayer coatings.

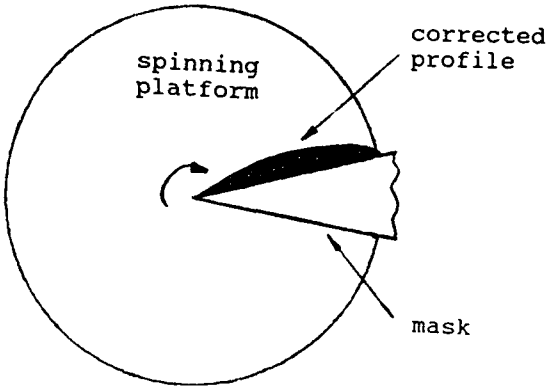

Fig. 2. Mask and corrected profile in front of substrate.

It is known [5] that for curved surfaces the variation in d-spacing across the surface is a function of local height and local angle. To obtain uniform/graded coatings the next approach was used. The curved optic was mounted in the center of the spinning platform. A mask is fixed on the rotating drum just in front of the spinning substrate and the optic is coated. The d-spacings across the surface are then measured and the mask corrected (Fig. 2). The process is repeated again until the desired uniformity/grading is reached (Fig. 3).

Test optics were prepared in accordance with the approach described elsewhere [6,7]. In this method cylindrical multilayers with the same radii of curvature as the Schwarzchild objective were fabricated and characterized as deposited. According to the results of d-spacing measurements done on a Huber goniometer (λ = 1.54Å) the uniformity across the surface was made better than 0.5%. The same piece was then flattened and measured at the SURF facilities at NIST with a 2mm^2 incident beam and fixed detector

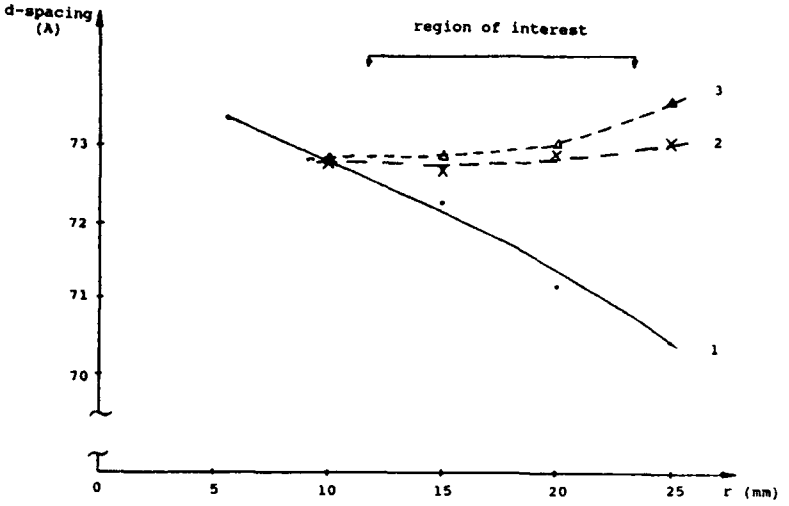

Fig. 3 Uniformity results of masking process for Mo/Si, d = 72.5Å, R = 50mm. 1- With mask. 2- Corrected profile of mask on cylindrical mica (Cu-Kα). 3- Corrected profile mask on spherical secondary mirror (Soft x-ray).

angle. Figure 4 shows that d-spacing measurements at SURF agreed very closely to the previous measurements (uniformity across the surface better than 0.3%) and the reflectivity as expected.

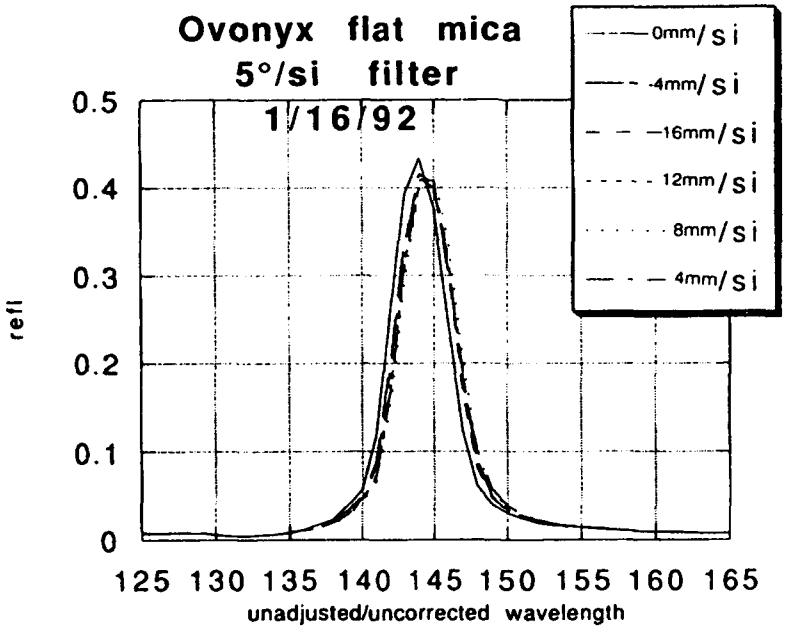

Fig. 4. Uniformity results of mica coated bent then flattened and measured. Corrected wavelenth will shift peaks along wavelength scale but not relative to each other.

To match the d-spacing of the concave and convex spherical pieces both pieces are fixed in spinning platforms 180° from each other and sputtered in the same run. By changing the rotation velocity for each optic while it passes the cathodes we can precisely match the d-spacing. By sputtering the optics at the same time only a short time stability of the deposition is necessary as compared to a need for very precise run to run repeatability.

The method, realizing uniform/graded d-spacing across curved surfaces and matching d-spacings, permits increased throughput of Schwarzchild objectives and multilayer optical systems. It would be advantages to do additional experiments to find the tolerance for radii of curvature of cylindrical test optics which can be flattened without destroying the multilayers. Flat and bent multilayer mirrors sputtered in the same process need to be characterized at Cu-Kα and soft x-rays to find a more precise correlation. This would minimize time of fabrication of curved multilayer mirrors.

REFERENCES

1. J.B. Kortright, R.N. Watts, OSA Proceedings on Soft X-ray Projection Lithography, Monterey, CA 1991.

2. X-ray reduction imaging at the NSLS, Correspondents Report, Synchrotron Radiation News, Vol. 4, No. 2, 1991.

3. J.E. Bjorkholm et al., J. Vac. Tech., 13, vol. 8, No. 8, Nov/Dec, 1990.

4. D.G. Stearns, R.S. Rosen and S.P. Vernon, Proceedings of the SPIE Symposium on Short- Wavelength Coherent Radiation, 152, Vol 11, 1991 OSA.

5. J.B. Kortright, J.M. Underwood, SPIE, vol 1343, X-Ray/EUV Optics for Astronomy, Microscopy, Polarimetry, and Projection Lithography, 1990.

6. G. Gutman et al., SPIE, vol 1546, Multilayers and Grazing Incidence X-ray/EUV Optics, July, San Diago, 1991 (will be published).

7. G. Gutman, J.L. Wood, SPIE, vol 1546, Multilayer and Grazing incidence X-ray/EUV Optics, July, SanDiago, 1991 (Will be published).

Multilayer Damage and Repair Issues in Soft-X-Ray Projection Lithography

D. P. Gaines, R. C. Spitzer
Brigham Young University
Provo, UT 84602

N. M. Ceglio
Lawrence Livermore National Laboratory
PO Box 5508, Livermore, CA 94550

Current soft x-ray projection lithography (SXPL) system designs require multilayer coated optics to operate at levels approaching predicted maximums for near normal incidence reflectivity. Effects that (potentially) degrade multilayer performance in the SXPL environment are discussed. Appropriate repair strategies are suggested, and preliminary results are presented.

Silicide Layer Growth Rates in Mo/Si Multilayers

R. S. Rosen and D. G. Stearns, *Lawrence Livermore National Laboratory Livermore, CA 94550.*
M. A. Viliardos and M. E. Kassner, *Department of Mechanical Engineering, Oregon State University, Corvallis OR 97331*
S. P. Vernon, *Vernon Applied Physics, Torrance, CA 90505*
Y. Cheng, *Arizona State University, Tempe, AZ 85287*

Mo/Si multilayers (ML's) are attractive for x-ray optics due to the relatively high associated reflectivity. However, the reflectivity is known to decrease with the formation of diffuse interlayer regions resulting from interdiffusion at the Mo-Si interfaces [1–2]. Most of the previous studies have reported interdiffusion coefficients [1–4] and effective activation energies [2–4] over a range of temperature assuming that the interdiffusion coefficient is invariant with annealing time. Recent results by the authors [2] have suggested that there may be an initial "surge" contraction (~ 0.1–0.2 nm) of the ML structure. Therefore, it is the objective of this study to perform a series of annealing treatments of Mo/Si ML's at relatively low temperatures to determine the Mo-Si interdiffusion kinetics as a function of time.

The multilayers in this study consisted of 40 bilayers of Mo and Si sputter deposited onto polished single crystal Si wafers. The nominal bilayer spacing was 7.0 nm and the ratio of the Mo layer thickness to the bilayer thickness was ~ 0.4. A detailed description of the vacuum system and deposition procedures is presented elsewhere [5]. The coated Si substrates were then annealed at temperatures of 260–342 °C and times from 1–1000 hours. The structure of the as-deposited (unannealed) and annealed multilayers were examined using small and large angle x-ray diffraction (XRD), normal incidence x-ray reflectance (NIR) measurements using a synchrotron source, and high resolution electron microscopy (HREM).

The unannealed multilayer consists of amorphous Si layers and crystalline Mo layers. These pure layers are separated by thin amorphous interlayer regions of $MoSi_2$ stoichiometry [6]. Annealing causes a contraction of the multilayer structure corresponding with growth of the Mo-Si interlayer regions, consistent with the formation of higher density silicides from the pure layers. As the annealing time increases, the amorphous interlayer regions grow thicker with increasing amounts of crystallized regions. After a sufficient annealing time, the ML structure consists of relatively thick layers of h-$MoSi_2$ separated by thin layers of "unreacted" crystalline Mo. The pure Si layers are completely consumed by the formation of h-$MoSi_2$. Figure 1 shows the Mo-Si interlayer growth rate at 316 °C, shown plotted as the difference of the squares of the interlayer width, $w^2(t) - w^2(0)$ versus time t. The thick interlayer, formed from deposition of Mo-on-Si, is shown to have a higher growth rate than that of the thin interlayer, formed from deposition of

Si-on-Mo. Additionally, both interlayers exhibit a primary "surge" stage of interlayer growth, equal to ~ 0.4 nm. The same behavior was observed in specimens annealed in the range of 260–350 °C. The NIR of the ML's was found to decrease with annealing time and increased annealing temperature. The decrease in measured reflectance of ML's annealed at different temperatures and times were found to correlate with the growth of the interlayer regions over the temperature ranges of this study.

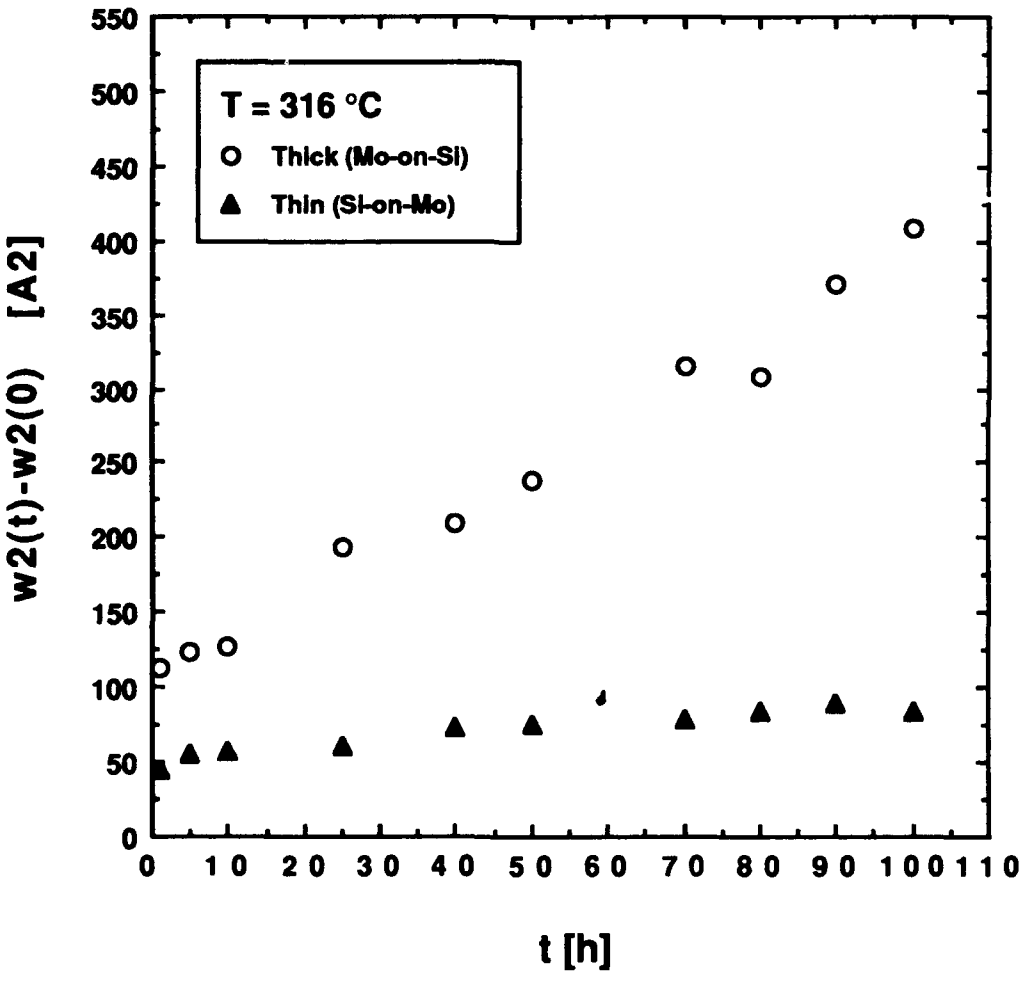

Figure 1. Mo-Si interlayer growth at 316 °C. The thick interlayer is formed from deposition of Mo-on-Si and the thin interlayer is formed from deposition of Si-on-Mo.

The growth kinetics of the Mo-Si interlayers were determined by assuming that the interlayer growth is diffusion limited with constant concentrations at the interfaces between the Mo-Si interlayer and elemental layers, and that the concentration gradient across the interlayer is linear.

The interlayer width $w(t)$ after annealing time t can then be related to the interdiffusion coefficient, $D(t')$:

$$w^2(t) = w^2(0) + 2\Delta C \int_0^t D(t')dt' \quad (1)$$

where $w(0)$ is the initial interlayer width and ΔC is the change in concentration across the interlayer. Assuming that $D(t')$ is constant and integrating, results in the relationship:

$$D = [w^2(t) - w^2(0)]/2t. \quad (2)$$

Figure 2 shows an Arrhenius plot of log D versus $1/T$ for the thick and thin Mo-Si interlayers. Both interdiffusion coefficients for the thick interlayer (Mo-on-Si) are ~ an order of magnitude greater than for the thin (Si-on-Mo) interlayer. The apparent activation energy for both interlayers and growth stages is ~ 2.3 eV, and D_0 is ~ 10 for the primary and ~ 1 cm^2/s for the secondary stages of interlayer growth. These values are comparable to those of bulk diffusion in h-$MoSi_2$.

In conclusion, annealing Mo/Si ML's at temperatures of ~ 250–350 °C for 1–1000 h results in decreased reflectivity. This loss of reflectivity is the result of interdiffusion of Si and/or Mo in the (principally) amorphous Mo-Si interlayer region, causing growth of this interlayer region that eventually crystallizes to h-$MoSi_2$. A plot of the square of the interlayer thickness versus annealing time indicates two distinct stages of thermally activated growth: a primary "surge" of ~ 0.4 nm, followed by a (slower) secondary "steady-state" growth where D is constant with time. The interdiffusion coefficients and apparent activation energy for interlayer growth are comparable to those of bulk diffusion in h-$MoSi_2$.

References

1. D. G. Stearns, M. B. Stearns, Y. Cheng, J. H. Stith and N. M. Ceglio, "Thermally induced structural modification of Mo-Si multilayers," J. Appl. Phys. vol. 67, pp. 2415–2427, March 1990.
2. R. S. Rosen, M. A. Viliardos, M. E. Kassner, D. G. Stearns, and S. P. Vernon, "Thermal Stability of Mo/Si Multilayers," *Proc. Optical Applied Science and Engineering,* SPIE Symposium, San Diego, CA in press.
3. K. Holloway, K. B. Do and R. Sinclair, "Interfacial reactions on annealing molybdenum–silicon multilayers," J. Appl. Phys. vol. 65, pp. 474–480, Jan. 1989.

4. J. Y. Cheng, H. C. Cheng, and L. J. Chen, "Cross-sectional transmission electron microscope study of the growth kinetics of hexagonal $MoSi_2$ on (001)Si," J. Appl. Phys. vol. 61, pp. 2218–2223, Mar. 1987.
5. D. G. Stearns, R. S. Rosen, and S. P. Vernon, "Fabrication of high-reflectance Mo-Si multilayer mirrors by planar-magnetron sputtering," J. Vac. Sci. Tech. A vol. 9, pp. 2662–2669, Sept./Oct. 1991.
6. D. G. Stearns, R. S. Rosen, and S. P. Vernon, "High Performance Multilayer Mirrors for Soft X-ray Projection Lithography," Invited Paper in *Multilayer Optics for Advanced X-Ray Applications*, San Diego, CA, SPIE vol. 1547, 2–13 (1991).

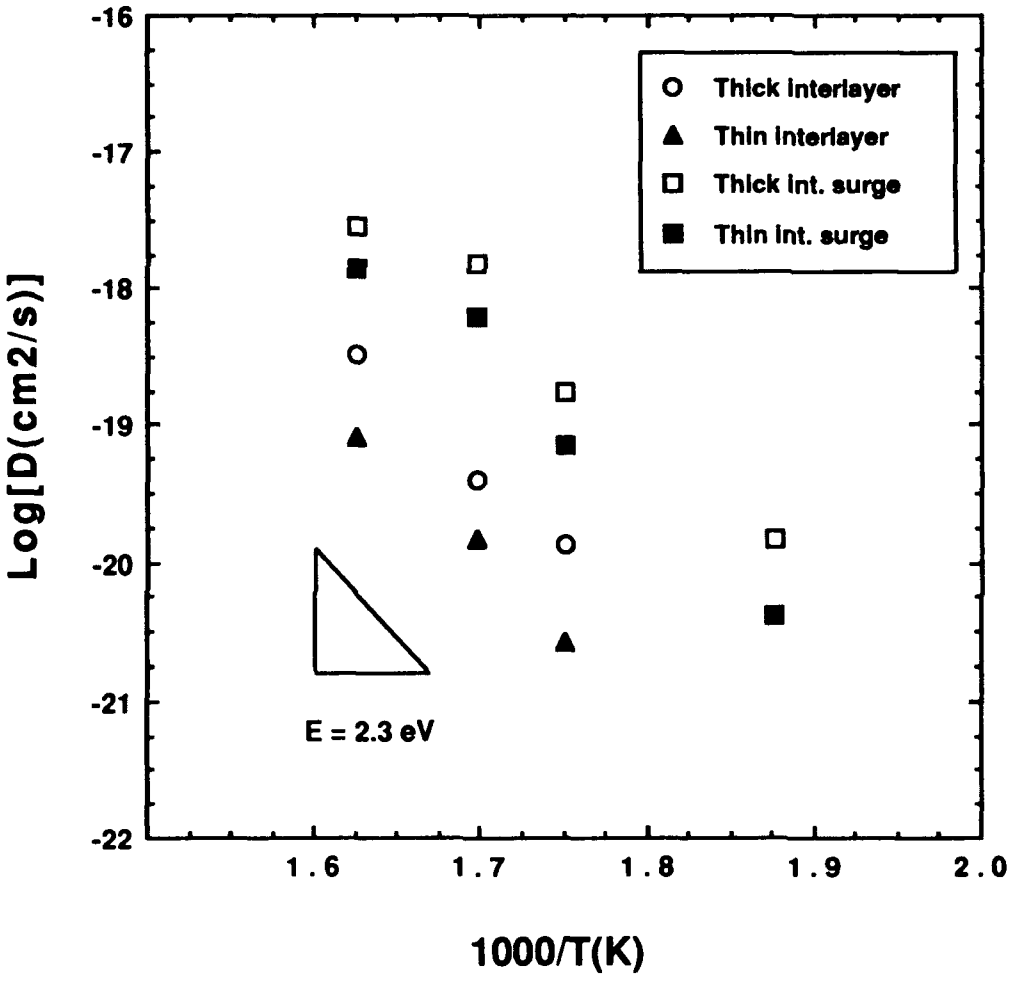

Figure 2. Arrhenius plot of molybdenum-silicon interlayer growth rates in multilayer structures.

Investigation of Distortion and Damage of Mo-Si Multilayer Reflective Coatings with High Intensity UV Radiation

Howard A. Bender and William T. Silfvast

Center for Research in Electro-Optics and Lasers
University of Central Florida
Department of Physics
12424 Research Parkway
Orlando, Florida 32826

Kenneth M. Beck

University of Central Florida
Departments of Chemistry and Physics
Orlando, Florida 32816

Summary

We report on studies of optical distortion and damage thresholds of Mo-Si multilayer soft x-ray reflective coatings using 308 nm pulsed radiation from a XeCl excimer laser to simulate soft x-ray irradiation. Preliminary experimental results yielded values of 260 mJ/cm^2 and 500 mJ/cm^2 for distortion and damage thresholds.

Studies have been performed on the thermal stability of soft x-ray Mo-Si multilayer mirrors under steady state irradiation[1]. Under pulsed irradiation, rapid lattice expansion and increased reflectivity changes have been observed[2]. Also, real time reflectivity decreases and wavelength shifts have been measured under high intensity pulsed x-ray flux[3]. It would be desirable to understand and quantify the specific distortion and damage effects caused by such high flux intensities.

As a preliminary step, optical microscopy was used to analyze gross visual material changes. Low intensity laser flux caused visible discoloration or distortion changes at values above the quoted distortion threshold. When these regions were subsequently illuminated with higher intensities the damage threshold was observed to increase by 50%, suggesting that significant permanent changes in the layers had occurred with the annealing pulse. These changes will be investigated in more detail with electron microscopy.

Time dependent optical reflectivity measurements of the irradiated

regions were also investigated and compared to samples of pure silicon at flux levels which caused melting of the silicon.

The sample multilayer used was a 40 bi-layer Mo-Si coating on a single crystal silicon (100) substrate. Each layer had approximate thicknesses of 40 A.

Calculated values of melting a thin layer of the surface (as a gauge for induced damage) indicated much higher thresholds near 1 J/cm^2. However, these models did not account for the extremely thin layers in relation to heat diffusion depths.

These results will be compared and correlated with values obtained using soft x-ray flux from a laser plasma source.[2,3]

REFERENCES

1. A.V. Vinogradov, unpublished communication, 1991.
2. A. Zigler, J.H. Underwood, J. Zhu and R.W. Falcone, "Rapid Lattice Expansion and Increased X-ray Reflectivity of a Multilayer Structure Due to Pulsed Heating", Appl. Phys. Lett. 51(23), 1873-1875, 1987.
3. B. McGowan, private communication, LLNL, 1992.
4. M. Sparks, "Theory of Laser Heating of Solids: Metals", Journal of Applied Physics, Vol. 47, No. 3, 837-849, 1976.
5. H.S. Carslaw and J.C. Jaeger, Conduction of Heat in Solids, 2nd ed., Oxford University Press, Oxford, 1959.
6. D.H. Auston, et. al., "Time Resolved Reflectivity of Ion-Implanted Silicon During Laser Annealing", Appl. Phys. Lett. 33(5), 437-439, 1978.

Metrology

TuC 4:10pm–5:20pm
Steinbeck Forum

Chris Evans, *Presider*
National Institute of Standards and Technology

An Undulator Facility for Precision Optical Testing

David Attwood
Center for X-ray Optics
Lawrence Berkeley Laboratory
University of California, Berkeley, CA 94720

The development of reflective optics for projection soft x-ray lithography will require new tools, previously available only at longer wavelengths. Among these is a test facility for large numerical aperture interferometry at short wavelengths. As with visible light interferometry this is most effectively done with coherent radiation. In this paper we discuss the spatial and temporal coherence properties of undulator radiation, wavelength tuning range, design tradeoffs involving harmonic content and thermal loading, and challenges associated with at-wavelength interferometry of complex surfaces. Preliminary plans for such a facility at Berkeley's Advanced Light Source will be discussed. This work is supported by DARPA, AFOSR, and DOE/BES.

Propagation error in precision Fizeau interferometry

Chunsheng Huang

GCA Tropel
A Unit of General Signal
60 O'Connor Road
Fairport, NY 14450
(716) 388-3494

1. Introduction

It has long been recognized that aberrations of the optical system comprised of the interferometer cavity and the viewing system can result in distortion of fringes[1-5]. However, what is less understood is that the aberrations of the optical system, especially the viewing system, can influence the optical path difference (OPD) of interference fringes between the reference wavefront and the test wavefront due to the fact that rays from the test surface may not trace the exact same optical path as those from the reference surface. The propagation error that is produced by the optical system and the aberrated surface or optical system under test is basically pupil shear of the viewing system and is referred to here as the shearing error.

The shearing error which may be negligible in conventional interferometric optical testing could be significant errors when testing components intended for use in the soft X-ray region. For most applications, the shearing error is insignificant, first of all because the fringes are usually nulled before taking a measurement meaning that the test wavefront has a small departure from the reference wavefront, i.e, the shearing angle is small. In addition, since most applications do not require a viewing system with high resolution, the aperture stop of the viewing system is very small, which means the aberration of the viewing system is also small which results in a small shearing error.

However, for very high accuracy optical testing or full-aperture asphere testing, the shearing error cannot be neglected. For testing soft X-ray optics, a 100th wave error at a HeNe wavelength (632.8 nm) is equal to about a half wave error at 13 nm. For a non-null asphere test, the return test wavefront has a significant departure from the reference wavefront and results in a significant shearing error.

A simplified vision of the optical system of a Fizeau interferometer is shown in Fig. 1. Unfolding the viewing system, the surface under test is the object of the viewing system. The marginal ray of the Fizeau objective becomes the chief ray of the viewing system. The system can further be reduced to the surface under test, the Fizeau surface, and the entrance pupil of the viewing system as shown in Fig. 2.

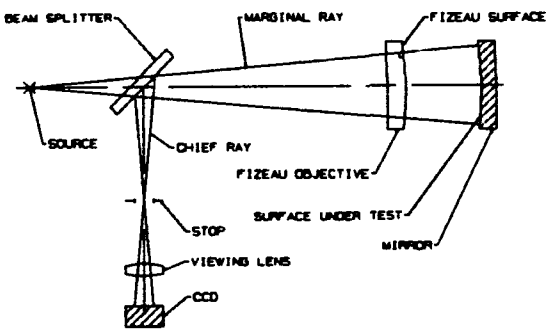

Fig. 1 A simplified Fizeau system where a marginal ray of the Fizeau objective is a chief ray of the viewing system.

The shearing error is governed by the following three equations:

$$W_s(\rho,\theta)=W_v(H,r_1,\theta)-W_v(H,r_2,\theta). \qquad (1)$$

and

$$r_1=-\frac{1}{NAr_e}\frac{\partial W_r(\rho,\phi)}{\partial\rho}, \qquad (2)$$

$$r_2=-\frac{1}{NAr_e}\frac{\partial W_t(\rho,\phi)}{\partial\rho}, \qquad (3)$$

where $W_v(H,r,\mathbb{C})$ is an aberrated wavefront of a Fizeau viewing system including the Fizeau objec-

tive; $W_v(H,r_1,\theta)$ and $W_v(H,r_2,\theta)$ are propagation errors from the reference ray and the test ray as shown in Fig. 2, respectively; H is a normalized field height of the viewing system; ρ is a normalized aperture height of the surface under test and of the Fizeau surface; r is a normalized radius height of the pupil of the viewing system; and θ is the angle between H and r. Note that $H=\rho$ and r and ρ are always at the same plane. Thus $\theta=0$ or π. The r_1 and r_2 are the normalized heights of the reference ray and test ray in the entrance pupil of the viewing system which includes the Fizeau objective. $W_t(\rho,\phi)$ and $W_r(\rho,\phi)$ are return wavefronts from the Fizeau surface and the test surface, respectively. NA is a numerical aperture of the test surface, and r_e is a radius of the pupil of the viewing system. $W_r(\rho,\phi)$ and $W_t(\rho,\phi)$, if the incident wavefront is perfect, represent twice the figure error of the Fizeau figure error and the test surface, respectively.

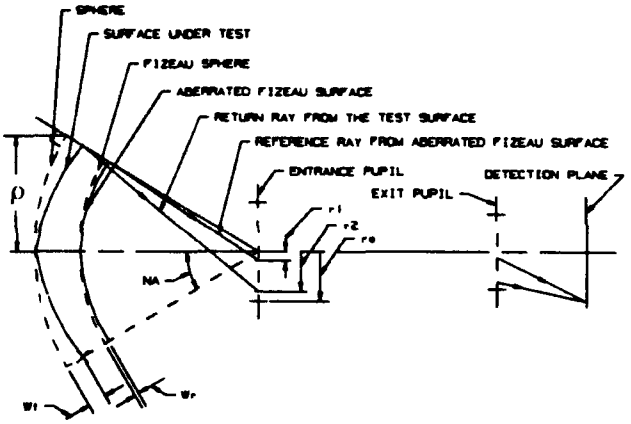

Fig. 2 Optical Diagram of the unfolded Fizeau viewing system where the return rays from the Fizeau surface and the surface under test arrive in the entrance pupil of the viewing system including the Fizeau objective at heights r_1 and r_2, respectively.

2. Numerical Examples

The wave aberration can be expanded as a series of polynomials. A general expression can be written[6-9] as

$$W(H,\rho,\theta)=\sum_{j,k,m}^{\infty} W_{jkm}H^j\rho^k\cos^m(\theta), \qquad (4)$$

where H, ρ, and θ are defined above. For first and third order aberrations only,

$$W(H,\rho,\theta)=W_{111}H\rho\cos(\theta)+W_{020}\rho^2+W_{040}\rho^4+$$
$$+W_{131}H\rho^3\cos(\theta)+W_{222}H^2\rho^2\cos^2(\theta)+$$
$$+W_{220}H^2\rho^2+W_{311}H^3\rho\cos(\theta), \qquad (5)$$

where $W_{111}, W_{020}, W_{040}, W_{131}, W_{222}, W_{220}$, and W_{311} represent tilt, focus, and the third order aberration coefficients of spherical, coma, astigmatism, field curvature, and distortion, respectively. Spherical aberration and distortion are most common aberrations in the viewing system. Tilt, focus, and spherical aberration from the test surface are studied to reveal the shearing error. Let us consider an example in which the Fizeau surface has only spherical aberration for the following cases investigated, i.e.,

$$W_r(\rho)=W_{040}^r\rho^4. \qquad (6)$$

2.1. Spherical Aberration of the Viewing System

Consider that the viewing system has spherical aberration.

$$W_v(\rho,r,\theta)=W_{040}^v r^4. \qquad (7)$$

2.1.1. Shearing Contribution From Spherical and Tilt

Given the tilt of the test surface

$$W_t(\rho,\theta)=W_{111}^t\rho\cos(\phi), \qquad (8)$$

where W_{111}^t is tilt coefficient of the test surface. Substituting Eq. (6), (7), and (8) into (1), (2), and (3), the result is

$$W_s(\rho,\phi)=W_{040}^v\left(\frac{4}{NAr_e}W_{040}^r\rho^3\right)^4-$$
$$-W_{040}^v\left(\frac{1}{NAr_e}W_{111}^t\cos(\phi)\right)^4. \qquad (9)$$

The first term of the above equation results from the Fizeau surface figure error. This term is negligible due to the fact that it is a higher order effect and of much smaller magnitude than the second term. The second term results from tilt in the test surface. The dominant shearing error in this case is the pupil-independent fifth order astigmatism.

2.1.2. Shearing Contribution From Spherical Aberration and Defocus

Given the following focus term of testing surface,

$$W_t(\rho)=W_{020}^t\rho^2, \qquad (10)$$

Repeating the same steps as in the previous section, the resultant shearing error is

$$W_s(\rho)=W_{040}^v\left(\frac{4}{NAr_e}W_{040}^r\rho^3\right)^4-$$

$$-W^v_{040}\left(\frac{2}{NAr_e}W^t_{020}\rho\right)^4. \quad (11)$$

For the same reason above, the first term may be neglected. The shearing error in this case is third order spherical aberration.

It is instructive to assign some reasonable values to the above equations. Assume that the viewing system has one wave of aberration at 632.8 nm, the Fizeau surface has a 50th wave aberration, the surface under test has one wave of defocus, the NA of the surface under test is 0.1, the radius of the viewing system pupil is 10 mm. Then the spherical aberration due to shearing error is $2.6\times10^{-8}\lambda$. Even if there is a 10-wave focus error, the shearing error due to spherical aberration of the viewing system is still negligible.

2.1.3. Shearing Contribution From Spherical Aberrations

Assume that both the Fizeau surface and the testing surface have spherical aberration only. The spherical aberration of the testing surface is given by

$$W_t=W^t_{040}\rho^4. \quad (12)$$

In the same manner, the shearing error is calculated and given by

$$W_s(\rho)=W^v_{040}\left(\frac{4}{NAr_e}W^r_{040}\rho^3\right)^4- \quad (13)$$

$$-W^v_{040}\left(\frac{4}{NAr_e}W^t_{040}\rho^3\right)^4.$$

The resultant shearing aberration is eleventh order spherical. Assume that the surface under test has a 10th wave aberration, the rest assumptions remain the same. The resultant shearing error at the edge of the aperture of the surface under test is about $4.1\times10^{-12}\lambda$. It is clearly negligible. However, when the surface under test is asphere and has 10 waves or greater departure from a sphere, the shearing error is 0.004 waves or larger. This error is significant for soft X-ray surfaces because it represents a 5th wave at a 13 nm wavelength.

2.2. Distortion From the Viewing System

Assume that the viewing system has distortion given by

$$W_v(H,r,\theta)=W^v_{311}H^3r\cos(\theta) \quad (14)$$

where $\theta=0$ or π as previously indicated. Tilt, focus, and spherical aberration of the test surface are investigated in the following sections.

2.2.1. Shearing Contribution From distortion and Tilt

Substituting Eq. (8) and (14) into Eq. (1), (2), and (3), the shearing error becomes

$$W_s(\rho,\phi)=W^v_{311}\rho^3\left(\frac{4}{NAr_e}W^r_{040}\rho^3\right)-$$

$$-W^v_{311}\rho^3\left(\frac{1}{NAr_e}W^t_{111}\right)\cos(\phi). \quad (15)$$

The resultant shearing aberration in this case is third order coma after neglecting the first insignificant term. Assume that we have one wave distortion in the viewing system, (which is equivalent to 6.3 microns at the NA of 0.1), one wave of tilt in the test surface, and that the rest of the parameters are the same as given in Section 2.1.1. The resultant shearing error is 0.0063 waves of coma at a wavelength of 632.8 nm. If there is a 10 wave tilt, the shearing error is a 15th wave of coma at the same wavelength.

2.2.2. Shearing Contribution From Distortion and Defocus

Let the test wavefront be focus error only. Repeating the same calculations as Section 2.1.2 and replacing the viewing system distortion with spherical aberration, the resultant shearing error is

$$W_s(\rho)=W^v_{311}\rho^3\left(\frac{4}{NAr_e}W^r_{040}\rho^3\right)-$$

$$-W^v_{311}\rho^3\left(\frac{2}{NAr_e}W^t_{020}\rho\right). \quad (16)$$

The dominant shearing aberration in this case is the third order spherical aberration. Using the same values as Sections 2.2.1 and 2.1.2 (one-wave focus and one-wave distortion), the resultant shearing error is 0.0127 waves. For 10 waves of defocus, the shearing error is 0.127 waves at 632.8 nm.

2.2.3. Shearing Contribution From Distortion and Spherical Aberration

Let the test wavefront be spherical aberration only. The result is obtained by replacing focus with spherical aberration. The shearing error is then

$$W_s(\rho)=W^v_{311}\rho^3\left(\frac{4}{NAr_e}W^r_{040}\rho^3\right)-$$

$$-W^v_{311}\rho^3\left(\frac{4}{NAr_e}W^i_{040}\rho^3\right). \quad (21)$$

As before, the second term is dominant. The shearing aberration is recognized as the fifth order spherical aberration. Applying the same values (one wave spherical and one wave distortion) given in Sec-

tions 2.1.2, 2.1.3, and 2.2.1 to the above, the resultant shearing error is a 40th wave of the fifth order spherical aberration at the wavelength of 632.8 nm.

In the case of asphere testing with 15 waves of spherical aberration, the shearing error would be 0.38 waves at the same wavelength. This error translates into 128 waves at a wavelength of 13 nm.

3. Discussion and Conclusions

Distortion in the viewing system results in the third order coma if the test wavefront has tilt, third order spherical aberration if the testing wavefront has defocus, and fifth order spherical aberration if the test wavefront has the third order spherical aberration. Third order spherical aberration in the viewing system produces pupil-independent fifth order astigmatism if the test wavefront has tilt, third order spherical aberration if the test wavefront has defocus, and eleventh order spherical aberration if the test wavefront has third order spherical aberration.

Distortion in the viewing system produces the dominant shearing error. Generally speaking, it is tolerable for most applications if the tilt of the test wavefront is kept within one wave. Focus of the test wavefront should be kept within one wave to have a less than a 50th wave shearing error. The test wavefront with one wave of spherical aberration will have a 40th wave shearing error if the viewing system has one wave of distortion.

For soft X-ray surface testing, in order to achieve a 10th wave or better surface measurement accuracy at the wavelength of 13 nm, tilt should be kept to less than 0.2 waves when distortion of the viewing system is one wave at 632.8 nm. Focus of the test wavefront should be less a 10th wave at 683.2 nm for less than a 10th wave of suthe shearing error at a wavelength of 13 nm.

Third order spherical aberration in the viewing system has a small effect on the shearing error. The shearing error resulting from system spherical aberration is a concern only when full-aperture testing of a soft X-ray asphere is attempted because the asphere may have large spherical aberration specification and soft X-ray testing requires a tremendous absolute accuracy.

The Analytical results derived here can be used to evaluate viewing system optical performance. For example, to determine distortion of the system, one can make two measurements with and without tilt. One can then calculate distortion from the shearing coma introduced by the tilt.

References

1. R. Jozwicki, "Influence of spherical aberration of an interferometric system on the measurement error in the case of a finite fringe, " Appl. Opt. Vol 30, No. 22 pp. 3119-3125, Aug. 1991.

2. R. Jozwicki, "Influence of aberrations of Fizeau interferometer elements on measurement errors, " Appl. Opt. Vol. 30, No. 22, pp. 3126-3132, Aug. 1991.

3. J. M. Mehta and W. M. Worek, "Analysis of refraction errors for interferometric measurements in multicomponent systems, " Appl. Opt., Vol. 23, No. 6, pp 928-933, Mar. 1984.

4. K. Kinnstaetter, A. W. Lohmann, J. Schwider, and N. Streibl, "Accuracy of phase shifting interferometer, " Appl. Opt., Vol. 27, No. 24, pp 5082-5089, Dec. 1988

5. C. Evans and W. T. Estler, "Some observations on the performance of commercial phase measuring (Fizeau) interferometers used in surface figure metrology, " ASPE Proc. Vol 4, pp 54-57, Oct, 91.

6. Huang, C., Lawrence, G., Levy, E., McMillan, R., "Performance Analysis of the Multichannel Astrometric Photometer," SPIE, 818-57, San Diego, Aug. 1987.

7. Huang, C. *Design and Analysis of the Astrometrical Telescope Facility,* Ph.D. dissertation, Optical Sciences Center, University of Arizona, 1989.

8. Lawrence, G., Huang, C., "High Accuracy Image Centroiding with a Ronchi Ruling,"Optical Engineering, Vol. 30 No. 5 pp 598-606 May 1991.

9. Huang, C., Jeong, H., Ruff, B., "Optimizing a DUV projection lens with a 442 nm laser interferometer," SPIE, San Diego, July 90.

Status of the Soft X-ray/XUV Optical Metrology Program at the National Institute of Standards and Technology

Richard Watts, David Ederer, Thomas Lucatorto and Charles Tarrio
Division of Electron and Optical Physics
Physics Laboratory
National Institute of Standards and Technology
Gaithersburg, MD 20899
(301) 975-6892; fax (301) 975-3038

The National Institute of Standards and Technology (NIST) has initiated a program devoted to the characterization of soft x-ray optics at the wavelength of use. Although NIST has an operational XUV characterization facility which it is using to make measurements for users across the country, that facility suffers from several deficiencies that will limit its usefulness in the coming years. Therefore, we are constructing an improved monochromator/ reflectometer beamline that will upgrade and extend our XUV measurement capabilities.

In this talk, we will describe the optical properties of the new monochromator, shown schematically in Fig. 1 and detailed in Table 1, and discuss the state of the design of the the new reflectometer. The monochromator is based on a varied line spaced plane grating that uses simple optical elements in a fixed entrance slit/fixed exit slit geometry. Important features of the new instrument include high throughput, simple wavelength scanning, resolutions on the order of 1000 for wavelengths between 40 and 400 Å, and the ability to characterize large (in excess of 30 cm diameter) optical surfaces with small radii of curvature. Time permitting, we will also comment on the status of other XUV optical metrology projects in progress at NIST.

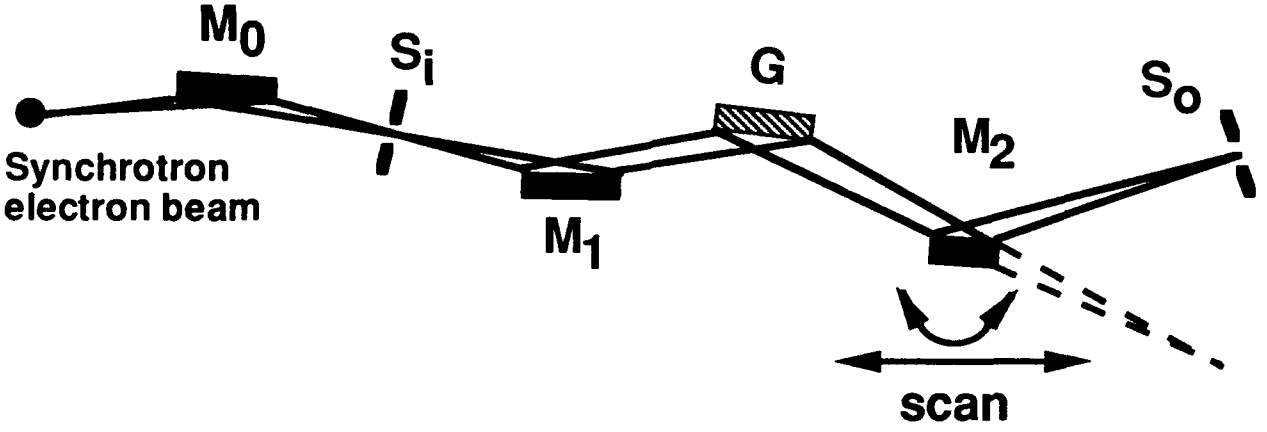

Figure 1. Optical setup for NIST varied line spaced monochromator with entrance slit S_i, toroidal 1:1 focussing mirrors M_0 and M_1, plane varied line spaced grating G, plane scanning mirror M_2, and exit slit S_o.

Table 1
Design Parameters for NIST VLS monochromator (dimensions in cm)

Dimensions:		
Source to M_0	254	
S_i to M_1	325	
M_1 to G	40 (G_1), 50 (G_2)	
G to S_o	285 (G_1), 275 (G_2)	
Transfer mirror (M_0):		
Material:	Nickel coated toroid on Glidcop blank	
Blank size:	6.5 x 15	
Illuminated area:	5 x 15	
Acceptance angle (h x v):	20 mrad x 3 mrad	
Grazing angle of incidence:	3°	
Radii of curvature	R_m= 4,853 R_s= 13.3	
Focus mirror (M_1):		
Material:	Nickel coated toroid on Glidcop blank	
Blank size:	8.5 x 20	
Illuminated area:	7 x 20	
Acceptance angle (h x v):	20 mrad x 3 mrad	
Grazing angle of incidence:	3°	
Radii of curvature:	R_m= 6,210 R_s= 17.0	
Grating (G):	G_1	G_2
Material	Gold coated ULE blank	
Ruling Size:	6 x 14	6 x 10
Nominal line density $1/d_o$:	1500 l/mm	600 l/mm
Grazing angle of incidence:	3.5°	5°
Blaze angle:	2.5°	2.6°
Plane scan mirror:		
Material:	Nickel coated silica	
Blank size:	5 x 12.5	
Grazing diffraction angle scanned:	3 ° - 15°	
Grazing angle of incidence:	3 ° - 15°	
Focal spot properties at 100 Å:		
Size (max)	2 mm x 2 mm	
Divergence (h x v, max)	20 mrad x 7 mrad	
Resolving power	100 - 2000	
Flux (photons/s/0.2 Å)	8×10^{10}	

Imaging Experiments

WA 8:30am–10:10am
Steinbeck Forum

R. F. W. Pease, *Presider*
Stanford University

Soft-X-ray Projection Lithography Experiments using Schwarzschild Imaging Optics

D. A. Tichenor, G. D. Kubiak, M. E. Malinowski,
R. H. Stulen, S. J. Haney, K. W. Berger, L. A. Brown

Sandia National Laboratories
P.O. Box 969
Livermore, California 94551-0969

W. C. Sweatt

Sandia National Laboratories
P.O. Box 5800
Albuquerque, New Mexico 87185-5800

J. E. Bjorkholm, R. R. Freeman, M. D. Himel,
A. A. MacDowell, D. M. Tennant, O. R. Wood, II,

AT&T Bell Laboratories
101 Crawfords Corner Road, P.O. Box 3030
Holmdel, New Jersey 07733-3030

J. Bokor, T. E. Jewell, W. M. Mansfield,
W. K. Waskiewicz, D. L. White, D. L. Windt

AT&T Bell Laboratories
600 Mountain Avenue
Murray Hill, New Jersey 07974-2070

Abstract

Projection imaging experiments are described. A Schwarzschild objective is illuminated with 14-nm radiation using an ellipsoidal condenser and a laser plasma source.

Summary

High-resolution soft-x-ray images have been produced using multilayer-coated Schwarzschild imaging objectives.[1-3] We are continuing to investigate the characteristics of a 20x reduction Schwarzschild using 14-nm illumination provided by a laser plasma source (LPS). Although the field of view achievable using a Schwarzschild design is too small for use in a practical lithography system, 25 μm by 50 μm in this case, this objective is a useful tool for studying the mounting and alignment of soft-x-ray optical elements and the quality and alignment of the condensing optics.

The elements of the imaging objective must be aligned with great precision in order to achieve diffraction-limited performance within an off-axis subaperture of NA 0.1. In this design the nominal separation of the two spherical mirrors must be achieved to an accuracy of ± 5 μm, and the decentration of one element relative to the other must not exceed 2 μm. Imaging results in previous experiments indicate that these tolerances were achieved, but

we were not successful in maintaining the alignment over long periods of time using the original mounting scheme.

A new approach to mounting and aligning the elements is being investigated. The mirrors are kinematically mounted against the optical surfaces to assure that the centers of curvature remain stationary. The objective housing is stabilized by heat treatment and designed for precise adjustment of the optical elements. Final adjustments are made using a Zygo interferometer to examine the full parent aperture in visible light.

The other major area being studied using the 20x Schwarzschild objective is the requirement for surface figure and alignment of the condenser. An ellipsoidal reflector has been designed and fabricated to collect soft x-rays from the LPS and provide Kohler illumination on the mask. In order to be compatible with the existing LPS target chamber, the condenser is located 250 mm from the LPS and reflects the soft x-rays vertically upward at 90 degrees to the incoming rays. A 6x magnification of the LPS is achieved in the decentered entrance pupil of the Schwarzschild, providing an coherency factor of about 0.5. Aberrations are observed in the existing ellipsoidal reflector. Imaging calculations are being performed to determine whether these aberrations are large enough to affect the the image quality.

Alignment errors also introduce aberrations in the illuminating wavefront. In order to achieve an accurate alignment, the object plane focal point f_1 of the ellipsoidal condenser is located off-line using an HeNe laser. A 2.5-mm aperture is attached to the condenser to function as a bore sight. It is centered on f_1 and located at an axial distance of 20 mm in front of f_1. When the condenser with attached bore sight is placed in the experimental chamber, visible emission from the LPS casts a shadow of the bore sight onto an aperture plate covering the condenser. Lateral alignment is achieved to an accuracy of about $\pm$ 0.5 mm by centering the shadow on the aperture plate. Finally, the axial position of the condenser is adjusted for best focus of the soft x-rays at the entrance pupil of the Schwarzschild. The affect of condenser alignment on image quality is being evaluated using numerical simulations.

References:

1. H. Kinoshita, K. Kurinara, Y. Ishii and Y. Torii, J. Vac. Sci. Technol. **B7**, 1648 (1989)

2. J. E. Bjorkholm, J. Bokor, L. Eichner, R. R. Freeman, J. Gregus, T. E. Jewell, W. M. Mansfield, A. A. MacDowell, E. L. Raab, W. T. Silfvast, L. H. Szeto, D. M. Tennant, W. K. Waskiewicz, D. L. White, D. L. Windt, O. R. Wood, II, and J. H. Bruning, J. Vac. Sci. Technol. **B8**, 1209 (1990)

3. D. A. Tichenor, G. D. Kubiak, M. E. Malinowski, R. H. Stulen, S. J. Haney, K. W. Berger, L. A. Brown, R. R. Freeman, W. M. Mansfield, O. R. Wood II, D. M. Tennant, J. E. Bjorkholm, A. A. MacDowell, J. Bokor, T. E. Jewell, D. L. White, D. L. Windt, and W. K. Waskiewicz, Optics Letters **16**, 20 (1991)

Large-Area, High-Resolution Pattern Replication using a Two-Aspherical-Mirror System

Hiroo KINOSHITA, Kenji KURIHARA, Tutomu MIZOTA and Tuneyuki HAGA
NTT LSI Laboratories, 3-1 Morinosato Wakamiya, Atsugi-shi, Kanagawa 243-01
Tel +81 462 40 2607 , Fax +81 462 40 4318

The ability to replicate 0.1 μm patterns using multilayer reduction optics has already been demonstrated[1],. However, if we are to exploit this technology for practical lithography of VLSI devices, the problems of large exposure area and high throughput must be solved.

We have proposed[2] a novel reduction optics design with a ring field width of greater than 20 mm as shown in Fig. 1. This design has a number of significant advantages: (1) high reflective efficiency because the number of reflections is minimized, (2) excellent wavelength matching because multilayers are fabricated on mask substrates and mirrors at the same time, and (3) easier alignment because the mirrors are arranged on an axis.

To clarify whether these various characteristics are actually realized as expected, we have fabricated and assembled a prototype reduction optics consisting of two aspherical mirrors, and put the optics through some tests. Table 1 shows the specification of the optics. The mirrors with a wavelength of 130 Å are made of Mo/Si multilayer. The reflectivity of the reflection mask and optics is about 40%. The substrates for the mirrors are optically polished to an rms surface roughness of 10 Å. The evaluation of the aspherical surface figure has been measured with an interferometer. The maximum error of surface figure is evaluated to be 273 Å ($\lambda/20$) , which is at the measurement limitation of the interferometer.

Using this optics and a reflection mask, demagnified patterns were replicated experimentally. Figure 2 shows a photograph of a reflection mask.

Figure 3 shows an example of the replicated patterns. We can obtain fine patterns in a ring field with a width of 0.06 mm (this is restricted to source size). Up to the present, lines and spaces as small as 0.4 μm were replicated. Exposure time is about 7 seconds using 0.1-μm thick films of PMMA resist which has a measured sensitivity of 35 mJ/cm^2 at a wavelength of 130 Å. This agrees with the calculated exposure time for current of 300 mA at the Photon Factory of the High Energy Physics Laboratory in Tsukuba.

From the above, this system shows the high efficiency and the possibilityc of replicating over a large exposure field, although the evaluation and fabrication of the aspherical mirrors must be improved.

Reference

1. D.W.Berreman, J.E.Bjorkholm, M.Becker, L.Eichner, R.R.Freeman T.E.Jewell, W.M.Mansfield, A.A.Macdowell, M.L.O'Malley, E.L.Raab, W.L.Silfvast, L.H.Szeto, D.M. Tennant, W.K.Waskiewicz, D.L.white, D.L.Windt, and O.R.Wood; Appl.Phys.Lett.56-22 (1990) 28
2. K.Kurihara, H.Kinoshita, N.Takeuchi, T.Mizota, T.Haga and Y.Torii, J.Vac.Sci.Technol.B9-6 (1991)

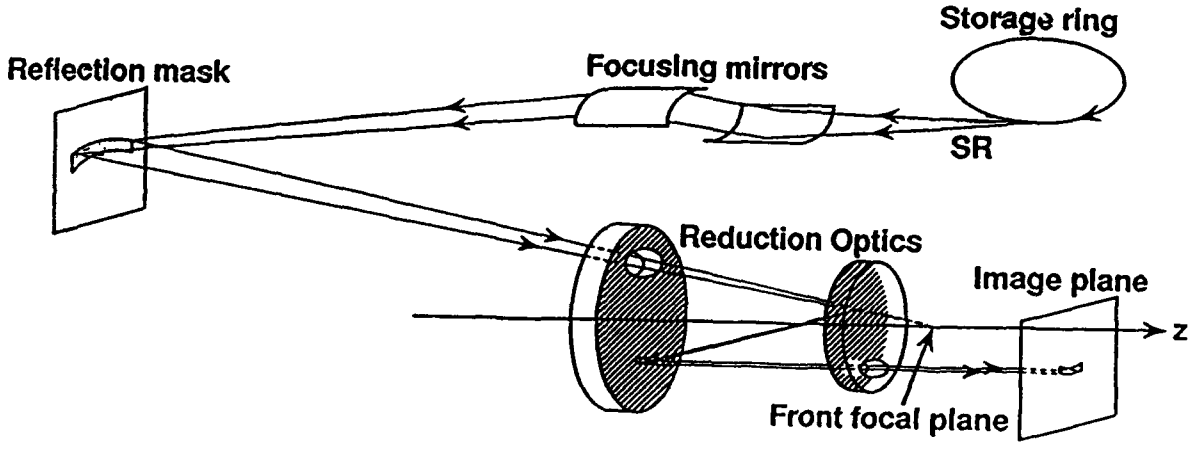

Figure 1. Schematic illustration of a Two-Aspherical-Mirror System

Table 1. Specification of prototype optics

N.A.	0.07
Exposure Area	10 mm X 0.2 mm
Reduction Rate	1/5

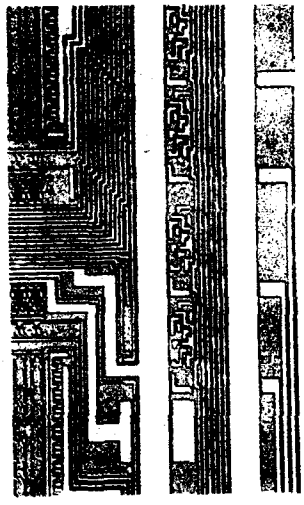

Figure 2. A photograph of a reflection mask pattern

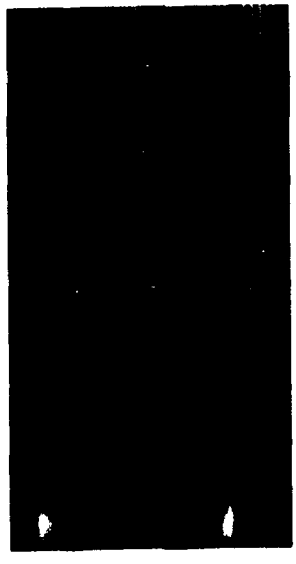

Figure 3. An example of replicated patterns ring field

Soft-X-Ray Projection Imaging Using a 1:1 Ring-Field Optic

A. A. MacDowell
AT&T Bell Laboratories, 510E Brookhaven Lab., Upton, NY 11973

J. E. Bjorkholm, K. Early, R. R. Freeman, M. Himel, P. P. Mulgrew, L. H. Szeto, D. W. Taylor, D. M. Tennant, O. R. Wood II
AT&T Bell Laboratories, Crawfords Corner Road, Holmdel, NJ 07733

J. Bokor, L. Eichner, T. E. Jewell, W. K. Waskiewicz, D. L. White, D. L. Windt
AT&T Bell Laboratories, 600 Mountain Ave., Murray Hill, NJ 07974

F. Zernike
SVG Lithography Systems, Inc., Wilton, Connecticut 06897

The first demonstration of diffraction-limited imaging at 14 nm in the soft-x-ray region, which resulted in the printing of 0.05 μm wide lines and spaces in a 60 nm thick film of PMMA resist, was produced using a multilayer-coated 20:1 reduction Schwarzschild optic.[1] Unfortunately, a Schwarzschild optic possesses a central obscuration and a small image field and, hence, is not a very practical camera. A slightly more complicated optical system, but one that has already been used in a practical camera at visible wavelengths, is the 1:1 Offner ring-field optic.[2] In theory a 0.0835 NA ring-field optic should be able to image 0.1 μm lines and spaces in a 100 micron wide 50 mm radius ring-shaped field at high contrast when illuminated with radiation at wavelengths shorter than 15 nm.[3] In fact, an iridium-coated Offner 1:1 ring field camera was recently used to carry out projection imaging using 42 nm radiation from an undulator in the vacuum ultraviolet storage ring at Brookhaven National Laboratory.[4]

The imaging system used in the work reported in this talk, a ring-field optic from a Perkin-Elmer Model 300 Micralign Projection Printer, was supplied by SVG Lithography. The primary and secondary mirrors of this imaging system were coated with Mo/Si multilayers designed to give maximum reflectance in the soft-x-ray region. For example, the measured peak reflectance of the convex secondary mirror after coating with 40 layer pairs was 55% at 12.7 nm at an incidence angle of 10°. The outside diameter of this mirror which serves as the system stop was reduced with an aperture resulting in a numerical aperture of 0.0835. This NA was previously shown to produce the best compromise between diffraction limited resolution and low aberrations at this wavelength.[3] The distance between the primary and secondary mirrors was adjusted so that the 100 micron wide ring of good aberration correction would lie at 53 mm radius.

The experimental arrangement for soft-x-ray imaging with the multilayer-coated ring-field optic is shown in Fig. 1. The

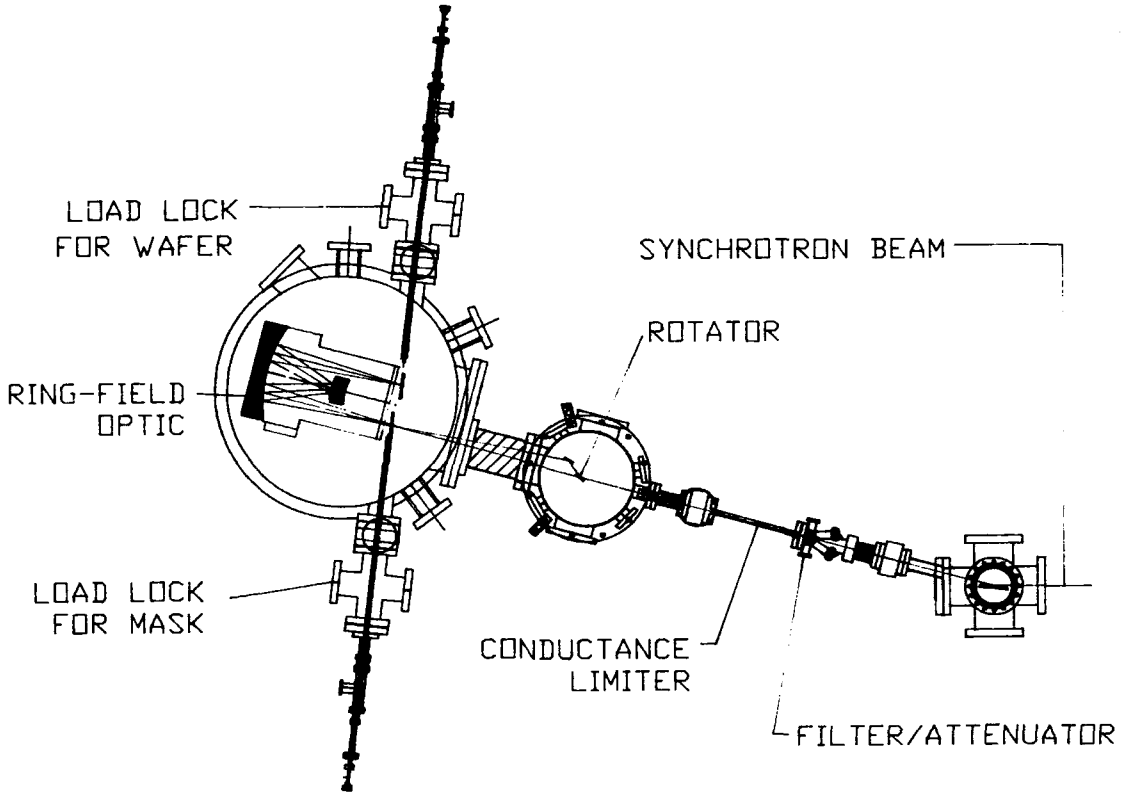

Figure 1. Experimental arrangement for soft-x-ray imaging with a Mo/Si multilayer coated 1:1 ring-field optic illuminated with synchrotron radiation.

soft-x-ray source was the third harmonic of the U13 undulator at the Brookhaven VUV Storage Ring. This undulator is 12 m from the first optical component, a 7.5° grazing incidence, water-cooled silicon mirror. The soft-x-ray beam is filtered with an 7000 A thick silicon membrane. The beam then passes through a conduction limiter (a 2 mm internal diameter tube, 25 cm long) that separates the 10^{-6} Torr vacuum of the experiment from the ultra-high vacuum of the beam line. Following the conduction limiter is a two-mirror device that rotates about the beam axis producing a cone of radiation whose apex (a 2 mm diam. spot defined by the conduction limiter) falls on a transmission mask. The mask is thus illuminated by light from directions defined by the surface of this cone. The rotator results in partially coherent illumination with the degree of partial coherence determined by the cone angle (set to 0.1 in the present experiment).

The transmission mask used in these imaging experiments was fabricated on a 0.7 μm thick silicon membrane. A 0.2 μm Ge absorbing layer was evaporated onto the membrane and was patterned to form a resolution chart comprised of vertical and

horizontal lines and spaces ranging from 1 - 0.15 microns. The combination of Ge on Si results in a transmission mask with a contrast at 12.7 nm greater than 100:1.

The unity magnification image of the mask produced by the ring-field optic was recorded on silicon wafers coated with the negative, chemically-amplified resist, Ray-PN.[5] Figure 2 shows

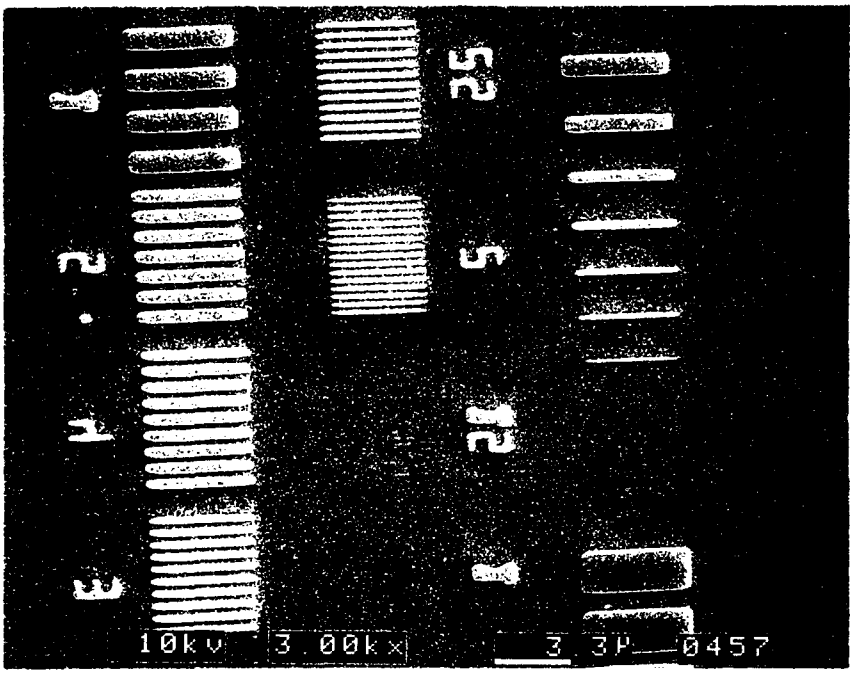

Figure 2. SEM micrograph of the image of a transmission mask in a 70 nm thick film of Ray-PN resist produced using a ring-field optic illuminated with 12.7 nm radiation. The 1.0, 0.5, 0.4, 0.3 0.25, and 0.2 μm lines and spaces are printed. The 0.15 μm lines and spaces (located directly below the 0.2 μm lines on the mask) are not printed. The exposure time was 40 seconds.

an SEM photo of an image of the mask in a 70 nm thick layer of Ray-PN. The exposure time for this image was 40 sec. Immediately after exposure, the resist-coated wafers received a five minute, 105° C bake to drive forward the acid-catalyzed cross-linking reaction. The wafers were then immersion-developed in 0.3 normality AZ Developer for 90 seconds and rinsed in deionized water.

Under our experimental conditions of nearly coherent illumination (sigma=0.1), an ideal Offner optic, operating at 12.7 nm with an NA of 0.0835, should be able to image 0.1 μm lines and spaces with contrasts exceeding 65%.[3] The fact that 0.15 μm lines and spaces are not present in the image shown in Fig. 2 indicates that a) some non-uniformity of the multilayer coatings (or some figuring error of the mirror substrates) is degrading the image or b) the illumination is not resulting in true stationary imaging or c) the imaging system is not sufficiently

mechanically stable. All three of these possibilities are being actively investigated.

1. J. E. Bjorkholm, J. Bokor, L. Eichner, R. R. Freeman, J. Gregus, T. E. Jewell, W. M. Mansfield, A. A. MacDowell, E. L. Raab, W. T. Silfvast, L. H Szeto, D. M. Tennant, W. K. Waskiewicz, D. L. White, D. L. Windt and O. R. Wood, II, J. Vac. Sci. Technol. B8, 1509 (1990).

2. A. Offner, Opt. Eng. **14**, 130 (1975).

3. O. R. Wood, II, W. T. Silfvast and T. E. Jewell, J. Vac. Sci. Technol. B7, 1613 (1989).

4. A. A. MacDowell, J. E. Bjorkholm, J. Bokor, L. Eichner, R. R. Freeman, W. M. Mansfield, J. Pastalan, L. H. Szeto, D. M. Tennant, O. R. Wood, II, T. E. Jewell, W. K. Waskiewicz, D. L. White, D. L. Windt, W. T. Silfvast and F. Zernike, J. Vac. Sci. Technol. B9, 3193 (1991).

5. Hoechst Celanese Corporation, Electronic Products Division, Somerville, NJ 08876.

Schwarzchild microscope for carbon Kα radiation

Katsuhiko Murakami, Hiroshi Nakamura, Tetsuya Oshino, Masayuki Ohtani and Hiroshi Nagata

Research Laboratory, Nikon Corporation,
1-6-3, Nishi-ohi, Shinagawa-ku, Tokyo 140, Japan
(03)3773-1111

1. Introduction

With the development of x-ray multilayers, Schwarzchild optics can be applied to x-ray imaging such as microscopic imaging[1] and projection lithography[2,3].

We have designed and fabricated a Schwarzchild multilayer objective with a magnification of 32 times. In the present experiment, we examine it as a microscope objective by using a conventional carbon Kα radiation source. In the next experiment, we will apply it to use in projection lithography using synchrotron radiation.

2. Design of a Schwarzchild objective

We designed the Schwarzchild objective to realize a resolution of 0.1μm in the demagnification system. The designed characteristics of the objective are listed in Table 1. The resolution determined by the diffraction is 0.03μm in C Kα radiation of 45Å. The aberration in the object plane is 0.06μm on the axis and on the object height of 30μm.

Table 1. Characterizations of the Schwarzchild objective

Magnification	32		
Numerical aperture	0.2		
Concave mirror, diameter	80mm	radius of curvature	135mm
Convex mirror, diameter	16mm	radius of curvature	50mm
Object to image distance	1300mm		

3. Multilayers

We examined suitable material pairs of multilayers for carbon Kα radiation. Figure 1 shows the calculated values of reflectivity (Fig.1(a)) and peak width $\Delta\lambda$ (Fig.1(b)) vs number of layer pairs for normal incidence. Multilayers of Cr/C with 300 layer pairs have 50% of reflectivity, but they have a very narrow peak width. With tolerance of 0.07Å determined by $\Delta\lambda/4$, it is difficult to fabricate such multilayers. We chose the number of layer pairs as 50 in order to obtain wide $\Delta\lambda$. Multilayers of Ni/C and NiCr/C have higher reflectivity than Cr/C multilayers.

These multilayers have an extremely short thickness period. It should be noted that very thin nickel deposition forms island structures, which reduce the performance of the multilayer mirror. We employed 80:20 wt% nickel-chromium alloy which did not form island structures.

Two NiCr/C multilayers with 50 layer pairs and 22Å and 25Å thickness periods were deposited on silicon wafers by ion beam sputtering. Soft x-ray (20-45Å) reflectivities of these multilayers were measured with synchrotron radiation (SR) at the National Laboratory for High Energy Physics, Japan. The smallest incident angle of SR to the sample is limited by the reflectometer[4] and is 8°. We could not measure the reflectivity of the 22Å thickness period multilayers at 45Å. We estimated it from the measured reflectivity (7%) of the 25Å thickness period multilayers at 45Å and from those of two multilayers at wavelengths shorter than 45Å. The estimated value was 3.5%, and the estimated total reflectivity of the Schwarzchild objective was about 0.1%.

Control of the thickness period distribution of the multilayers on the figured substrate is important. We created the desired distribution using appropriately designed deposition masks. The multilayers were coated on spherical substrates made of fused silica.

4. Imaging experiment

The two mirrors of the Schwarzchild objective were aligned by interferometry and rigidly fixed. Figure 2 shows the experimental arrangement of the microscope. A commercial fine-focus x-ray source (RIGAKU Micro-Flex), operated at 10kV and 10μA, with a 2.2μm carbon film target was employed as the light source. A carbon filter was employed to eliminate the visible light emitted with x-rays from the target.

Focusing of the electron beam and adjustment of the objective were performed using a microchannel plate with a fluorescent screen as an x-ray detector for real-time monitoring. The image on the screen was taken with a CCD camera and accumulated. After adjustment, the images were taken on film (Kodak TMAX400). The exposure time was about 1 hour.

Two images of #2000 mesh (12.7μm pitch) are shown in Fig.3. Considerably sharp images were obtained. Figure 3(a) shows the image with the source of 50μm in diameter, where the shadows of the convex mirror and its supports are observed. Figure 3(b) shows the image with the source of 170μm, where the shadow is extinguished and a distinct image of the mesh is observed over the entire area.

The images were analyzed with a microdensitometer. From the slope of the optical density at the pattern edge, the resolution was estimated to be less than 0.5μm. For examination of finer resolution, experiments using a transmission grating as a sample are now under way.

References

1. M.Kado, K.Tanaka, R.Kodama, T.Yamanaka, S.Nakai, K.Yamashita, M.Ohtani and S.Kitamoto, Optics Letters, 16,109 (1991).
2. H.Kinoshita, K.Kurihara, Y.Ishii and Y.Torii, J.Vac.Sci.Technol. B7, 6, 1648 (1989).
3. T.E.Jewell, M.M.Becker, J.E.Bjorkholm, J.Bokor, L.Eichner, R.R.Freeman, W.M.Mansfield, A.A.MacDowell, M.L.O'Malley, E.L.Raab, W.T.Silfvast, L.H.Szeto, D.M.Tennant, W.K.Waskiewicz, D.L.White, D.L.Windt, O.R.Wood, II and J.H.Bruning, Proc.SPIE 1263, 90 (1990).
4. M.Yangihara, M.Niwano, T.Koide, S.Sato, T.Miyahara, Y.Iguchi, S.Yamaguchi and T.Sasaki, Appl.Opt. 25, 4586 (1986).

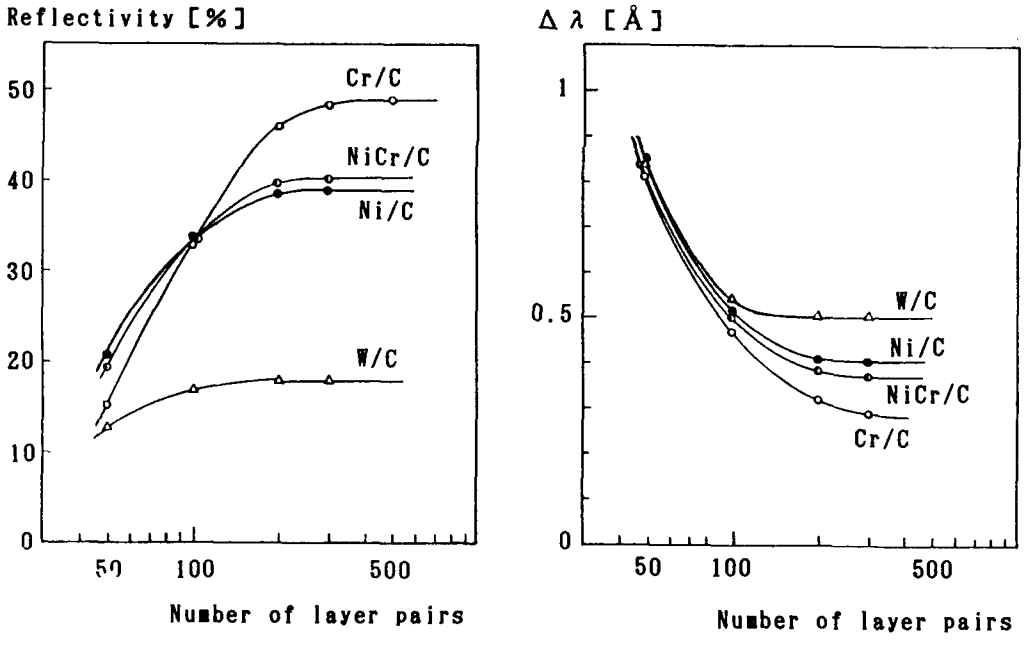

(a) (b)

Fig.1 Calculated (a) reflectivity and (b) peak width $\Delta\lambda$ of multilayers vs number of layer pairs in normal incidence at 45°.

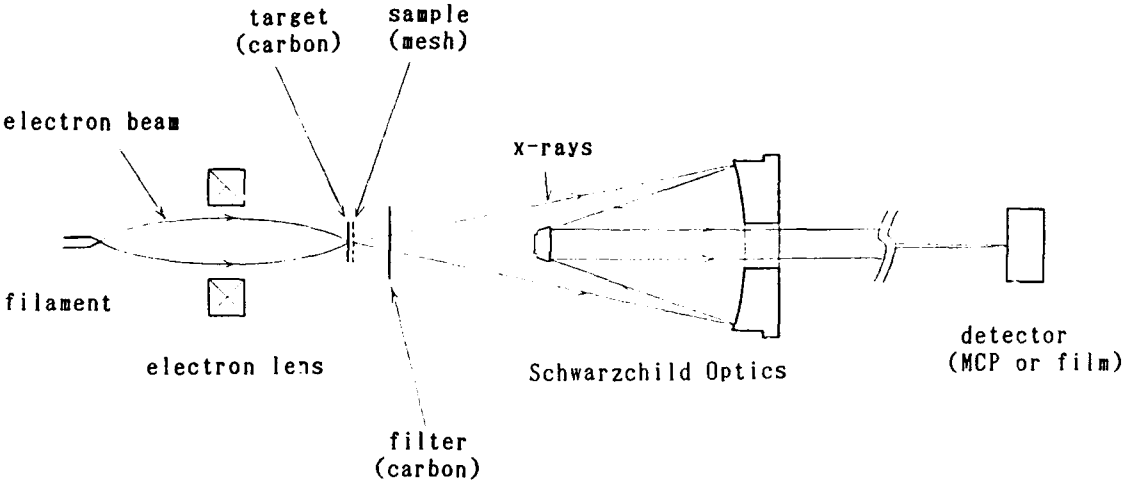

Fig.2 Experimental arrangement of a Schwarzchild microscope.

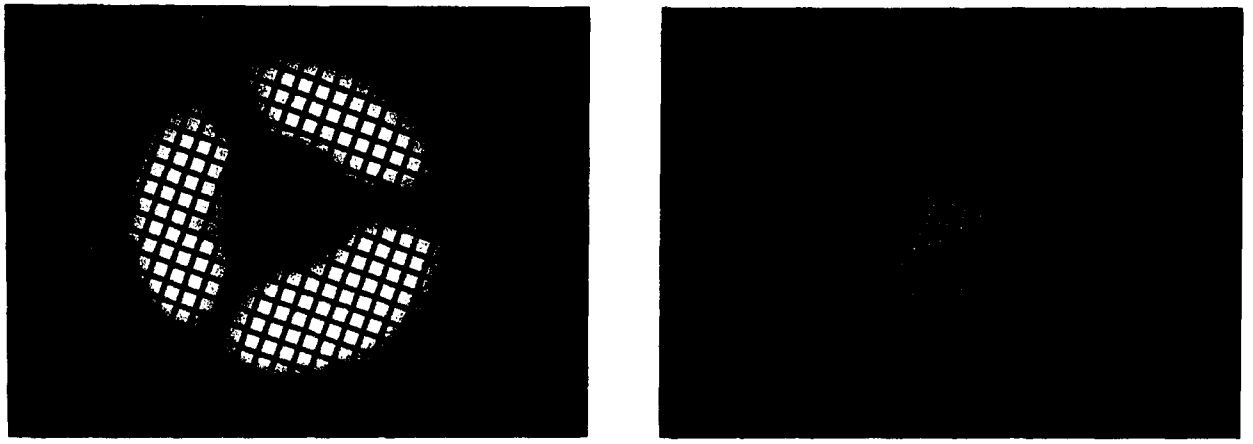

(a) (b)

Fig.3 Images of #2000 mesh (12.7μm pitch) taken with a source size of (a) 50μm and (b) 170μm in diameter.

Sources 2

WB 10:30am–11:50am
Steinbeck Forum

David T. Attwood, *Presider*
Lawrence Berkeley Laboratory

Characterization and Control of Laser Plasma Flux Parameters for Soft-X-Ray Projection Lithography

Martin C. Richardson, William T. Silfvast
University of Central Florida
12424 Research Parkway
Orlando, FL 32826

We discuss particle and plasma emission measurements of, and particle interdiction techniques for, laser plasma sources designed to meet the needs of soft-x-ray projection lithography.

Laser Driver for Projection X-ray Lithography

Lloyd A. Hackel and Raymond J. Beach
P.O. Box 808, L-487
Lawrence Livermore National Laboratory

(510) 422-9009

A projection x-ray lithography system requires a laser system with output of approximately 1 J/pulse, 2 to 3 ns pulselength and a repetition rate of 400 Hz. We have designed a laser diode pumped Nd:YLF rod laser system meeting these requirements It consists of a power oscillator running at 0.5 J/pulse and 20 ns pulselength followed by a 2x power amplifier. The output pulse is shortened to 2.5 ns by an SBS pulse compressor. We discuss the detailed design criteria for the laser and the experiments which support the design.

Small Scale Tokamak for X-Ray Lithography

S. Suckewer
James Forrestal Campus, Princeton University
PO Box 451, Princeton, NJ 08540
L. Bromberg, D. Cohn
M.I.T., Boston, Mass.

A toroidal plasma device (tokamak) with electron temperature in the range of 150-200 eV and density ~10^{13} particles/cm^3 can be built as a very compact and relatively inexpensive machine (~3 M$) . A tokamak with a major radius R ≈ 1m, minor radius r ≈ 0.1m, and confining magnetic field ~ 5k Gauss is not a very attractive for fusion research, however it can be an excellent source of soft X-ray radiation. In particular if operated in a steady state regime or at a high repetition rate it can provide several orders of magnitude more soft X-ray radiation than a small synchrotron with an undulator. This can be seen easily by comparing the total radiated power of a small tokamak and a small sychrotron, taking into account the spectral intensity distribution of line radiation from the tokamak plasma and of continuum radiation from synchrotron. We will present related calculations. Based on the calculations we will discuss the usefulness of a small tokamak for X-ray projection and proximity lithography and simple methods to change the dominant lines in the plasma radiation spectrum.

Resists

WC 1:30pm–2:40pm
Steinbeck Forum

Gary Taylor, *Presider*
AT&T Bell Laboratories

Resist Alternatives for sub-0.35-μm Lithography Using Highly Attenuated Radiation

R. R. Kunz, M. A. Hartney, and M. Rothschild
Lincoln Laboratory, Massachusetts Institute of Technology
Lexington, MA 02173-9108

Resist films that fully attenuate the exposing radiation cannot be processed as conventional resists. Alternative resist chemistries that can accommodate highly absorbed radiation will be the topic of this presentation.

Chemically Amplified Soft X-Ray Resists: Sensitivity, Resolution, and Molecular Photodesorption

Glenn D. Kubiak, Robert Q. Hwang, Michelle T. Schulberg
Division 8342
Sandia National Labs
Livermore, CA 94551-0969
(510) 294-3375

Kathy R. Early
AT&T Bell Laboratories
Crawfords Corner Road
Holmdel, NJ 07733-1988

Resists used for soft x-ray projection lithography must achieve high resolution and exhibit both high sensitivity and reasonable exposure latitude. Additionally, to prevent the deposition of highly-absorbing molecular species on multilayer-coated reflective optics, photon-induced desorption from the resist must be minimized. Chemically amplified resists show promise, exhibiting excellent sensitivity and resolution for e-beam and keV x-ray exposures[1-4], although they have not yet been characterized at wavelengths appropriate to soft x-ray projection lithography (SXPL). One often-noted issue regarding these resists is that the diffusion length of the photogenerated catalysts may limit their ultimate resolution[4]. Characterization of the diffusion length, and its dependence on the post-exposure bake temperature, has not been performed at SXPL wavelengths, however. Lastly, the beam-induced evolution of neutral and ionic molecular species from resists is a well-known phenomenon [5], although such desorption has not been studied for incident extreme ultraviolet (XUV) and soft x-ray radiation.

The sensitivity of three chemically amplified resists, Shipley SAL 601, Hoechst AZ PN114, and Hoechst AZ PF514, has been studied at 140 Å. Sensitivity curves, shown in Fig. 1, were generated using unpatterned monochromatized radiation from a laser plasma XUV source. Exposures required to fully develop 0.2 μm-thick resist films are found to range from 2.5 mJ/cm^2 for the positive-tone AZ PF to 3.5 mJ/cm^2 for the negative-tone SAL 601. Contrast values of 3-4 were typically observed, depending on post-exposure bake temperature and time under vacuum. Lithographic performance of AZ PF and SAL 601 was investigated using a transmissive Si/Ge patterned mask and a multilayer-coated Schwarzschild objective with 20:1 reduction ratio[6]. The variation in minimum resolved feature size as functions of exposure and processing conditions will be discussed.

Using atomic force microscopy, nanometer-scale structural irregularities of exposed and developed films have been examined in both PMMA and AZ PF. For a noncatalyzed positive resist such as PMMA, the minimum size of these structures is related to the range, R_{E_0} , for which the amount of energy deposited in the resist film by scattered secondary electrons is above a threshold dose, E_0. In a catalyzed resist, the size of such structures is related to the temperature-dependent catalyst diffusion length convolved over R_{E_0}. A determination of the minimum sizes of these structures, and their dependence on post-exposure bake temperature, will be presented.

Finally, the time-of-flight mass spectra of ions photodesorbed from PMMA, SAL 601, and AZ PN have been measured for a range of monochromatized wavelengths in the XUV. It is found that the ion mass distributions can be dominated not by the molecular desorption and fragmentation intrinsic to the bulk

resists, but rather by trace contaminants present in atmospheric and vacuum ambients during pre-exposure processing and XUV exposures, respectively. When care is taken to minimize hydrocarbon exposure during pre-exposure baking and vacuum handling, H^+, CH_3^+, CHO^+, $COOCH_3^+$, and $CH_2CH_3CCO^+$ dominate the ion mass spectra photodesorbed from PMMA, while H+, CH_3^+, H_2O^+, and CHO^+ dominate the ion mass spectra for AZPN and SAL601, as shown in Fig. 2. Neutral yields were not measured, but are expected to be 10^3-10^4 greater than ion yields[5]. From these measurements, estimates of the rate of deposition of such fragments on multilayer reflective elements for specific wafer-reflector geometries will be discussed.

1. R. Dammel, et al., Microelectron. Engrg. **9**, 575 (1989)
2. R. U. Ballhorn, et al., Microelectron. Engrg. **13**, 73 (1991)
3. M. DeGrandpre, K. Graziano, S. D. Thompson, H.-Y. Liu, and L. Blum, Proc. SPIE **923**, 158 (1988).
4. H. Oertel, M. Weiss, J. Chlebek, H. L. Huber, R. Dammel, C. R. Lindley, J. Lingnau, and J. Theis, Proc. of SPIE **1089**, 283 (1989).
5. H. Hiraoka, IBM J. Res. Develop. **21**, 121 (1977).
6. D. W. Berreman, J. E. Bjorkholm, L. Eichner, R. R. Freeman, T. E. Jewell, W. M. Mansfield, A. A. MacDowell, M. L. O'Malley, E. L. Raab, W. T. Silfvast, L. H. Szeto, D. M. Tennant, W. K. Waskiewicz, D. L. White, D. L. Windt, and O. R. Wood, II, and J. H. Bruning, Optics Lett., **15**, 529 (1990); D. A. Tichenor, G. D. Kubiak, M. E. Malinowski, R. H. Stulen, S. J. Haney, K. W. Berger, L. A. Brown, J. Bokor, R. R. Freeman, T. E. Jewell, W. M. Mansfield, D. M. Tennant, W. K. Waskiewicz, D. L. White, D. L. Windt, and O. R. Wood, II, Optics Lett. **16**, 1557 (1991).

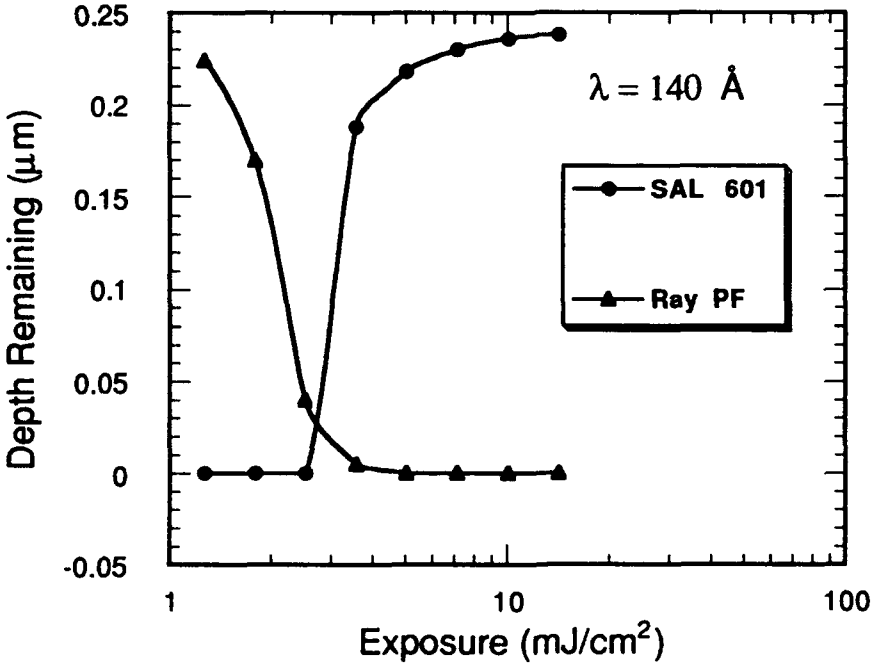

Figure 1. Sensitivity curves for AZPF and SAL 601

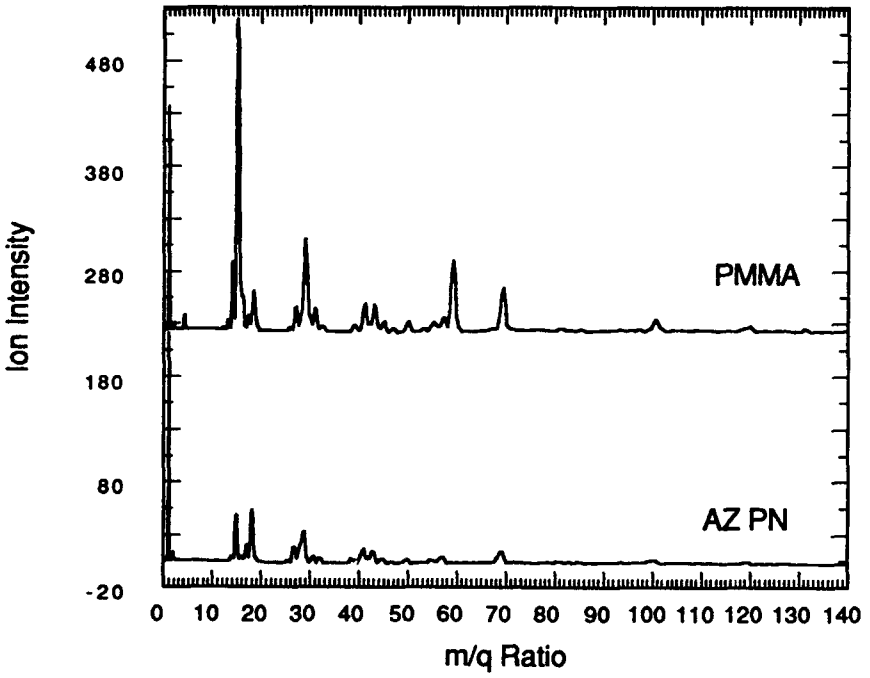

Figure 2. Photodesorption ion mass spectra produced at an incident wavelength of 140 Å

Characterization of Ray-PN Resist for Soft-X-Ray Projection Lithography

K. Early, D. M. Tennant, D. Jeon, P. P. Mulgrew, A. A. MacDowell, and O. R. Wood II
AT&T Bell Laboratories, Crawfords Corner Road
Holmdel, New Jersey 07733-1988, (908) 949-1869

G. D. Kubiak and D. A. Tichenor
Division 8342, Sandia National Laboratories
Livermore, California 94551-0969, (510) 294-3375

To be useful for integrated circuit (IC) manufacturing, a resist process must be capable of high throughput and exhibit good pattern transfer capability, as well as demonstrate high resolution. In 1990, imaging of 50 nm-wide lines and spaces in polymethyl methacrylate (PMMA) resist, using a 20× Schwarzschild optic at $\lambda = 14$ nm, was reported.[1,2] PMMA has long been known for its extremely high resolution and good process latitude, but its low sensitivity and poor plasma etch resistance make it an unlikely candidate for an IC fabrication process.

A difficulty encountered with any resist at $\lambda = 14$ nm is the short absorption length, typically less than 0.2 μm.[3,4] The strong absorption in the resist necessitates a bilevel or trilevel pattern transfer system. In a positive resist like PMMA, even for a relatively thin (0.1 μm-thick) top layer of a trilevel, significant sidewall angles are found in the developed image, in spite of the high MTF of the imaging system. These sloped sidewalls, which are a biproduct of the decrease in dose as a function of depth in the resist film, preclude realizing the $\pm 10\%$ critical dimension (CD) tolerance required in IC manufacturing.

Chemically amplified resists are attractive candidates for use with soft x-ray projection lithography (SXPL) because of their improved sensitivity and their novolak-type resin matrices which provide good dry plasma etch resistance during pattern transfer.[5] A negative crosslinking resist should, in addition, exhibit steep sidewalls as compared with positive resists since the most strongly crosslinked region will be at the resist surface. This strong crosslinking will tend to counteract rather than add to the effect of the developer gradient with depth in the film. We report here on characterization of thin films (50 to 70 nm) of the negative chemically amplified resist Ray-PN[6–8] for use in a trilevel system.

Clean silicon wafers were prepared for resist spinning by dehydration-baking at 200° C for a minimum of 30 minutes. This was followed by vapor-priming with

hexamethyldisilizane (HMDS) to promote adhesion. Thin films were spun-on from resist that had been diluted 1:2 or 1:3 with AZ Thinner.[6] Each wafer then received a 1 minute, 120° C, solvent-drive-off bake. Samples were exposed at the U13UB beamline at the National Synchrotron Light Source (NSLS) at Brookhaven National Laboratory using both the 20× Schwarzschild[1,2] and the 1× Offner ringfield[9] optics. Immediately after exposure, the wafers received a five minute, 105° C bake to drive forward the acid-catalyzed crosslinking reaction. They were immersion-developed in 0.3 normality AZ Developer[6] and then rinsed in deionized water.

Both the prebake and post-exposure-bake (PEB) were carried out using a PMC 730 Series Digital Hotplate to which we added a custom-built vacuum-chuck. The chuck temperature was monitored at a point roughly 0.5 inches beneath the chuck surface. We compared that temperature with the temperature of a probe glued to a wafer surface; the two differed by at most 1° C. From experiments with e-beam writing of fine patterns, we determined that PEB temperatures of 110° and 115° C cause unacceptable pattern distortion for both small and large features. Both the 120° C prebake and the 105° C PEB temperatures were controlled to within ±1° C.

Figure 1 is an SEM micrograph of 0.1 μm line/space pattern that was imaged using the Schwarzschild camera. The exposure dose was a factor of 5 lower than that required to expose PMMA, and hence we estimate it to be $\sim$ 10 mJ/cm^2. (At similar doses, we have also imaged 0.15 μm lines and spaces with the 1× ringfield camera.) Note that the region in the foreground of Figure 1 corresponding to the 0.05 μm line/space pattern is slightly modulated, but not well resolved. At the time of these experiments, the optic numerical aperture (NA) was set to 0.08 which corresponds to a resolution limit of $\sim$ 0.1 μm. However, had the NA been selected for imaging 0.05 μm features, we doubt that they would have been resolved in Ray-PN because 0.05 μm most probably exceeds the resist resolution limit. In Figure 2 we show a close-up of the 0.1 μm line/space pattern. The slight residue remaining between the exposed lines is believed to be due to overdosing of the resist. The granularity seen in the developed images is characteristic of this resist.

This granularity, which is exhibited as both surface and edge roughness appears to be of the order of $\sim 5 - 10$ nm and will be replicated in the pattern transfer to the underlying layer. Unlike PMMA, where the long-chain molecules are fragmented upon exposure and then washed away during development, in Ray-PN the matrix resin is crosslinked in exposed regions and washed away in unexposed regions. The resist resolution will, in some sense, be set by the ability of the developer to select between different molecular weights within the crosslinked resist.[10] Of the crosslinked molecules, the ones that are not developed away are large unfragmented entities, and this is possibly the origin of the resist roughness.

In summary, because of its sensitivity and superior plasma-etch resistance, Ray-

PN is an attractive candidate for a bi- or trilevel resist system in SXPL for CDs down to 0.1 μm. For use in a real IC fabrication line, sufficient process latitude and CD control have yet to be demonstrated. In this regard, edge roughness ($\sim 5 - 10$ nm) may be too severe for a 0.1 μm design rule. Further experimentation is required to determine whether or not thin, pinhole-free, resist layers, which are requisite for high yield, can be produced. A reduction in wavelength to $\lambda = 7$ nm would sufficiently increase the absorption length to possibly allow for a single resist layer, or at least to increase the top layer thickness in a multilayer system enough to allow for spinning of pinhole free films.

[1] J. E. Bjorkholm, J. Bokor, L. Eichner, R. R. Freeman, J. Gregus, T. E. Jewell, W. M. Mansfield, A. A. MacDowell, E. L. Raab, W. T. Silfvast, L. H. Szeto, D. M. Tennant, W. K. Waskiewicz, D. L. White, D. L. Windt, O. R. Wood II, and J. H. Bruning, *J. Vac. Sci. Technol. B* **8**, 1509 (1990).

[2] O. R. Wood II, J. E. Bjorkholm, J. Bokor, L. Eichner, R. R. Freeman, T. E. Jewell, W. M. Mansfield, A. A. MacDowell, L. H. Szeto, D. M. Tennant, W. K. Waskiewicz, D. L. White, and D. L. Windt, *OSA Proceedings on Soft-X-Ray Projection Lithography* **12** (ed. J. Bokor), 2 (1991).

[3] W. M. Mansfield, J. E. Bjorkholm, A. A. MacDowell, R. R. Freeman, L. H. Szeto, G. N. Taylor, D. M. Tennant, W. K. Waskiewicz, D. L. Windt, D. L. White, O. R. Wood II, R. M. D'Sousza, and A. R. Neureuther, *OSA Proceedings on Soft-X-Ray Projection Lithography* **12** (ed. J. Bokor), 129 (1991).

[4] G. D. Kubiak, E. M. Kneedler, K. W. Berger, R. H. Stulen, J. E. Bjorkholm, W. M. Mansfield, and H. Windischmann, *OSA Proceedings on Soft-X-Ray Projection Lithography* **12** (ed. J. Bokor), 124.

[5] J. Lingnau, R. Dammel, and J. Theis, *Solid State Technology*, 105, Sep. (1989) and 107, Oct (1989).

[6] Hoechst Celanese Corporation, Electronic Products Division, Somerville, NJ 08876.

[7] R. Dammel, K.-F. Dössel, J. Theis, H. Huber, H. Oertel, and J. Trube, *Microelectronic Engineering* **9**, 575 (1989).

[8] S. Pongratz, R. Demmeler, C. Ehrlich, K. Kohlmann, K. Reimer, R. Dammel, W. Hessemer, J. Lingnau, U. Scheunemann, and J. Theis, *Proc. SPIE 1089* (A. W. Yanof, ed.), 1989 (1989).

[9] O. R. Wood II, W. T. Sifvast, and T. E. Jewell, *J. Vac. Sci. Technol. B* **7**, 1613 (1989).

[10] Private communication from and G. N. Taylor, AT&T Bell Labs, Murray Hill, NJ.

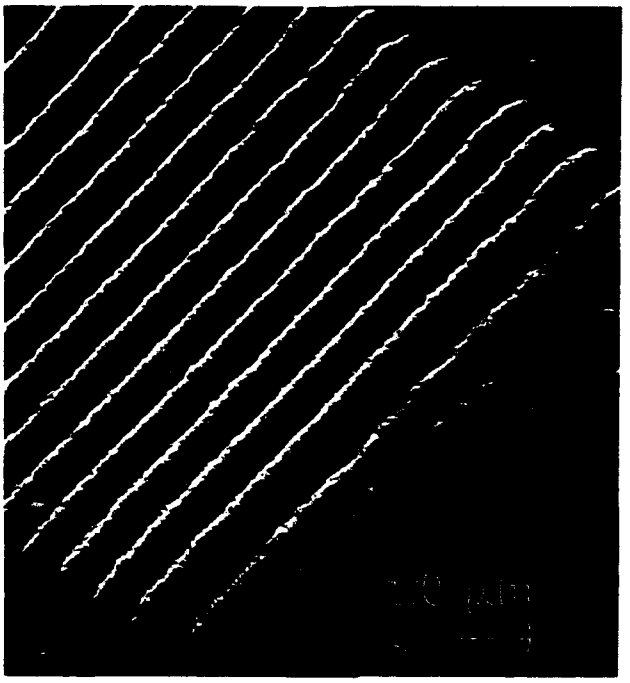

Figure 1: SEM micrograph of 0.1 μm and unresolved 0.05 μm line/space patterns imaged in 50 nm-thick film of Ray-PN resist.

Figure 2: Close-up of 0.1 μm line/space pattern. Note resist granularity.

/ NOTES

Masks

WD 3:00pm–4:20pm
Steinbeck Forum

William G. Oldham, *Presider*
University of California, Berkeley

Mask Technologies for Soft X-ray Projection Lithography at 13nm

D.M. Tennant*, A.A. MacDowell+, P.P. Mulgrew,
J.Z. Pastalan*, W.K. Waskiewicz#, D.L. Windt#, and O.R. Wood II*

AT&T Bell Laboratories
*Holmdel, New Jersey 07733
Murray Hill, New Jersey 07974
+ Brookhaven Laboratory, Upton, New York 11973

Imaging systems using soft X-ray reflective optics can be configured with either a transmission [1] or reflection mask [2] to print onto resist coated wafers. Transmission masks are well suited for high contrast and high resolution imaging. However, thin membranes are needed for such masks which can be fragile and sensitive to heating effects. Ultimately it is therefore desirable to take advantage of the robust nature of a thick reflecting mask. Practical reflective masks intended for use at λ=13 nm require Mo/Si multilayer reflective coatings with minimum features sizes from 2.0 to 0.1 μm in order to demonstrate a 0.1 μm printing capability with systems designed mask to wafer reduction from 20X to 1X, respectively. In this work we compared a variety of technologies for patterning transmissive and reflective masks containing features on this size scale. Transmissive masks which are reported consist of patterned absorbers on silicon membranes with features as small as 0.1 μm. Reflective masks patterned using various methods including: absorbing layers formed on top of multilayer reflectors; reflective coating removal by reactive ion etching (RIE); and ion damage of multilayer regions by ion implantation are also reviewed [2]. With a view to the future,we have begun to assess these reflective masks in a number of areas. Of principal interest are the reflectance contrast; resolution; process complexity; and repairability.

The transmission masks fabricated for use at 13 nm have been of only one type, a Ge absorbing layer patterned on a boron doped silicon membrane. Since the mask reported here is intended for use in a 1X ringfield camera [3] recently adapted for 13 nm, fine features comparable to the camera resolution ($\approx$100 nm) were needed. Good contrast in the mask can be achieved with a relatively thin absorber layer. A 250 nm Ge film gives a transmitted intensity ratio with the membrane of about 1000.

To determine the expected performance of the various reflection mask technologies, the Mo/Si multilayers were modeled assuming a periodic multilayer stack consisting of 60 layer-pairs of Mo/Si, with a period of 68 Å (40% Mo) and measured using a high precision XUV reflectometer. The expected reflectivities in the finely patterned reflection masks were then estimated from large area samples.

Five absorber overlayers were considered : 100 nm thick films of Au, Ge, and 300 nm thick films of three polymers (PMMA, EBR-9, and polyimide). Among these, the Au, Ge, and EBR-9 exhibited the greatest reflectivity changes (>100). Liftoff was employed for both Au and Ge in which a PMMA bilayer [4] was formed on the multilayer. Absorber lines as narrow as 0.1μm were patterned on a multilayer coated wafer. Ge was found to exhibit steeper sidewalls, a much finer grain size than the Au films, and better adhesion to the multilayer. To provide even steeper sidewalls, RIE was used to pattern the Ge absorber material. While Ge is more readily etched than Au, the CF_3 gas used in the process can degrade the Mo surface. To avoid this, we have devised a patterning scheme in which we for Ge pattern on a 300nm layer of polymer atop the Mo/Si multilayer. During the RIE of the Ge absorber the lower polymer acts as as an etch "stop layer" to protect the Mo/Si reflector. The polymer which is uncovered during this step can then be etched down to the Mo surface using RIE in oxygen.

A second mask type is patterning by etching of the multilayers themselves. Mo and Si are etched by RIE in a single gas (CF_3Br) which when patterned on a Si substrate exhibits very high contrast at 13 nm.

The third mask type is patterned ion damage. Since the reflective properties of the multilayers are strongly dependent on the sharpness of the Mo/Si interface, it is possible to intentionally degrade the reflectivity using ion mixing. Since the multilayers represent a depth of 400 nm, energies of 150 keV were necessary to penetrate and damage a significant fraction of the layers. Phosphorus ion doses from 1-5 x 10^{15} were implanted at single and multiple energies. The reflectance contrast was not improved for the multi-energy case over that of the single energy implant, even when a total flux three times higher was used. The reflectance change did increase for increased flux at the highest energy, however. A flux of 5 x 10^{15} /cm^2 was needed to attain a contrast of 20.

PMMA coated wafers were exposed with a 20:1 reduction camera using three different reflection masks: a Ge absorber overlayer applied by liftoff; a Ge on polyimide absorber patterned by RIE; and an etched multilayer pattern made by RIE using a MOP mask. A 100 nm line and space pattern was printed using each mask type. The results were indistinguishable from the transmission mask images and were consistent with the expected throughput.

Repair of defects introduced during mask fabrication is an important criteria when considering any mask technology. Hawryluk et. al. showed that a simulated repair over a large area damaged the multilayer, lowering the reflectivity by about a factor of 3 [5]. During our assessment of whether reflectivity changes were caused by the chemical and plasma cleaning procedures alone, we observed no significant degradation in reflectance, even from plasma cleaning by RIE in a oxygen. This combined with our work using the etched Ge absorber on the polymer layer suggested then that both excess and deficient absorber could be repaired by focused ion beam (FIB) milling and deposition prior to the the etch of the lower layer. To demonstrate this technique we have fabricated a reflection mask for our 20:1 reduction system which contains programmed defects. Once repaired, the "barrier" polymer layer can then be dry etched in oxygen.

References

[1] J.E. Bjorkholm, J. Bokor, L.Eichner, R.R.Freeman, J. Gregus, T.E.Jewell, W.M. Mansfield, A.A. MacDowell, E.L. Raab, W.T. Silfvast, L.H. Szeto, D.M. Tennant, W.K. Waskiewicz, D.L. White, D.L. White, O.R. Wood II, and J.H. Bruning, J. Vac. Sci. Technol. B **8,** 1509 (1990).

[2] D.M. Tennant, J.E. Bjorkholm, R.M. D'Sousa, L. Eichner, R.R. Freeman, T.E. Jewell, A.A. MacDowell, W.M. Mansfield, J.Z. Pastalan, L.H. Szeto, W.K. Waskiewicz, D.L.White, D.L. Windt, and O.R. Wood II, J. Vac. Sci. Technol. **B 9,** 3176 (1991).

[3] A.A. MacDowell, J.E. Bjorkholm, J. Bokor, L.Eichner, R.R.Freeman, J. Gregus, T.E.Jewell, W.M. Mansfield, M.L. O'Malley, E.L. Raab, W.T. Silfvast, L.H. Szeto, D.M. Tennant, W.K. Waskiewicz, D.L. White, D.L. White, and O.R. Wood II, Proc. Microcircuit Engineering 1990

[4] S.P. Beaumont, T. Tamamura, and C.D.W. Wilkinson, in Proc. of the Intl. Conference on Microlithography, ed. by R.P. Kramer (Delft University, Amsterdam, 1981).

[5] A.M. Hawryluk, N.M. Ceglio, D.W. Phillion, D.P. Gaines, R. Browning, R.F. Pease, D. Stewart, and N. Economou, Proc OSA vol.12,45 (1991).

X-Ray Mask Inspection and Qualification

James Wiley
KLA Instruments Corp.
PO Box 49055
San Jose, CA 95161

Summary not available at time of publication.

Reflection Mask Repair for Soft-X-Ray Projection Lithography

A. M. Hawryluk, David P. Gaines
Lawrence Livermore National Laboratory
PO Box 5508, Livermore, CA 94550

Diane Stewart
Micrion Corp.
1 Corporation Way
Peabody, MA 01960

Soft-x-ray projection lithography (SXPL) will use a reflective mask consisting of an x-ray multilayer mirror, patterned with a thin (~50-100 nm) layer of gold. Pattern repair techniques that do not degrade the multilayer mirror reflectivity must be developed if SXPL is to become an acceptable choice for lithography. Mask repair results from both clear and opaque mask repair experiments are discussed and analyzed.

SOFT-X-RAY PROJECTION LITHOGRAPHY

Sponsored by
Air Force Office of Scientific Research
Defense Advanced Research Projects Agency
National Science Foundation

for the
Optical Society of America

ADDENDUM AND POSTDEADLINE PAPERS

APRIL 6–8, 1992
MONTEREY, CALIFORNIA

SOFT X-RAY PROJECTION LITHOGRAPHY
POSTDEADLINE PAPERS

ADDITIONAL PAPERS

Conceptual Design Of a 60-nm Free-Electron Laser for XUV Projection Lithography*

Richard L. Sheffield, Bruce E. Carlsten, K. C. Dominic Chan, John C. Goldstein,
Michael T. Lynch, Brian E. Newnam, Dinh C. Nguyen,
Daniel S. Prono, and Roger W. Warren

Los Alamos National Laboratory
Mail Stop H825
(505) 667-6822
Los Alamos, NM 87545

We present the design and calculated performance for a 20-W XUV-FEL source for 60-nm projection lithography. The compact design features an 85-MeV rf linear accelerator with photoinjector, and a pulsed microwiggler with multifacet resonator optics.

*Work supported by Los Alamos National Laboratory Institutional Supporting Research, under the auspices of the United States Department of Energy.

CONCEPTUAL DESIGN OF A 60-nm FREE-ELECTRON LASER FOR XUV PROJECTION LITHOGRAPHY

Richard L. Sheffield, Bruce E. Carlsten, K. C. Dominic Chan, John C. Goldstein, Michael T. Lynch, Brian E. Newnam, Dinh C. Nguyen, Daniel S. Prono, and Roger W. Warren

Los Alamos National Laboratory
Mail Stop H825 (505) 667-6822
Los Alamos, New Mexico 87545

Introduction

We have designed a free-electron laser (FEL) source for 60-nm XUV-projection lithography. Such a FEL source would enable generation of 0.1-micron feature sizes on semiconductor chips [1]. Our baseline design is for 20 watts output at 60 nm. Imaging optics suitable for 60- and 13-nm lithography have been designed to accommodate the high-average power available from such a XUV-FEL source [2,3]. The overall design goals are: (i) to supply sufficient XUV radiation power to several stepper tools for high-throughput paterning of 60-wafer-levels per hour (30 cm-diameter wafers), and (ii) to maintain a "granular" concept where the size and cost of each individual source are acceptably small.

In general, a FEL has two major subsystems (Fig.1). The first subsystem is an accelerator (rf linear accelerator) which creates a high-energy electron beam. The second subsystem, the wiggler and resonator, converts the energy of the electron beam into useful radiation energy for external use.

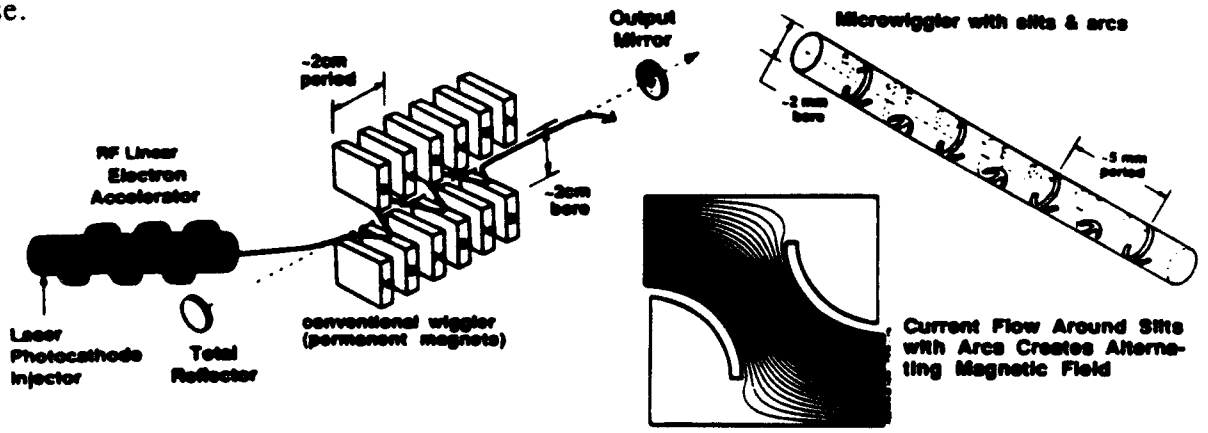

Fig.1. Principles of an FEL; accelerator creates an electron beam that oscillates in a wiggler's alternating magnetic field causing amplification of radiation in the resonator - conventional and microwigglers.

Our design goals require that both FEL subsystems utilize new, emerging technologies. For efficient conversion of electron beam energy into radiation, the electron beam must have high peak current and very low divergence. An accelerator with a photoinjector supplies these parameters. This emerging technology uses a laser to initiate photoemission from a photocathode surface. By making the photocathode an integral part of the accelerator structure, electrons are quickly

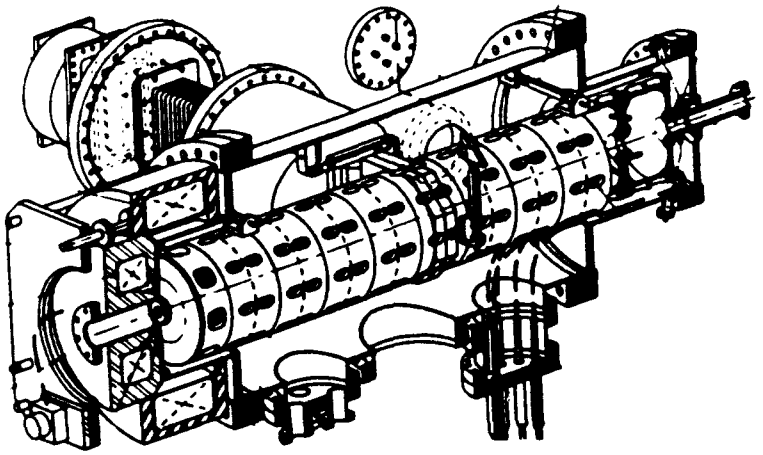

Fig. 3. Schematic of 1.2 m accelerator module undergoing validation tests. Beam parameters are 22 MeV, 3 nC, and <2.5 π mm·mr (rms).

magnets that guide the electron beam through an arc. The function of the chicane is: (i) to allow convenient access for the photoinjector illumination laser, (ii) to enable an extremely compact system since the resonator contains the last accelerator section and the wiggler, and (iii) to compress the electron beam to increase peak current.

The wiggler generates alternating magnetic fields that cause the electron beam to undergo transverse oscillations; during these "wiggles", electron beam energy is converted into coherent 60-nm radiation. Fig. 1 shows a schematic of a conventional wiggler (permanent magnets) and compares its dimensions to a pulsed microwiggler. The one-half-turn current loops of the microwiggler generate the requisite intense and alternating magnetic field. Because the slots (precisely formed by a spark-cutting device to tolerances <1/10,000 inch) can be closely spaced, and since pulsed high currents energize the wiggler, the wiggler period can be very small even while maintaining large field amplitudes [5]. These features enable XUV radiation to be generated by a very small-sized wiggler which can efficiently extract energy from relatively low energy electron beams. By tuning accelerator and wiggler parameters to optimize lasing on the third harmonic, we further reduce the necessary electron beam voltage. A microwiggler structure is currently undergoing validation tests at Los Alamos.

A Proof-of-Principle photolithography experiment (sponsored by DOE) is being carried out at Los Alamos. This experiment will use the existing los Alamos APEX FEL (40-MeV linac) with a 5-mm period, pulsed microwiggler to convert a 40-MeV electron beam into third-harmonic radiation at 250-nm. Scientists from Los Alamos, Motorola, and Texas Instruments are preparing to conduct lithographic exposures at this wavelength to evaluate the characteristics of this UV-FEL source. The proposed XUV-FEL design uses an identical wiggler with third-harmonic generation; operation at 60 nm is attained only by upgrading the electron beam parameters.

accelerated to relativistic velocities without degrading the electron beam quality [4]. The decision not to employ superconducting cavities was based partly on economics and partly on stability issues that limit high beam current in superconducting cavities. To further minimize the accelerator and rf power system cost, the FEL operates on the third harmonic of the FEL fundamental frequency. The wiggler is a new pulsed-electromagnetic microwiggler. A microwiggler generates high axial magnetic field with very short wiggler periods; this gives high optical gain and increases efficiency. The photoinjector and microwiggler lead to dramatic reductions in overall system size and cost. Finally, the ring resonator, which maintains radiation propagating through the wiggler, utilizes multifaceted metallic mirrors, developed at Los Alamos [1], with net reflectance of ~80% at 60 nm. Based on total external reflectances, such low-loss reflectors increase system efficiency and allow lasing with relatively modest single-pass gain. With these technologies, our design for a 20 W/60-nm XUV-FEL facility has an approximate floor space requirement of 20m x 6m.

Technical Discussion of Sub-Systems

The FEL-XUV source is schematically shown in Fig. 2. Two stations of modulators and rf klystrons (35 MW peak, 33-μs macropulse duration [e.g. Litton klystrons #3702]) supply 1300-MHz power to energize the photoinjector and accelerator modules. Each linac module is 2.2 m in

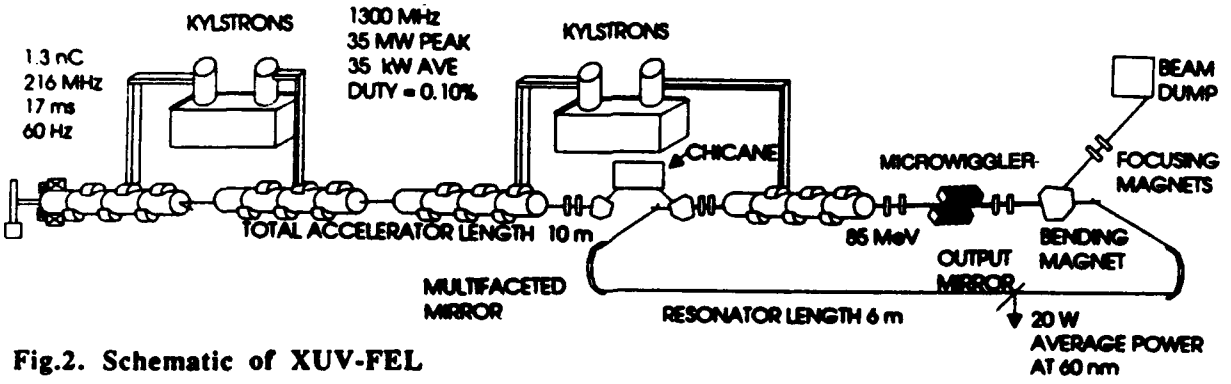

Fig.2. Schematic of XUV-FEL

length. A cryogenic photoinjector-accelerator module (Fig. 3) is currently undergoing validation testing at Los Alamos. This structure is optimized to produce the high-brightness electron beams required in our design. The 60-nm design uses four similar accelerator modules to attain a final energy of 85 MeV. The accelerator is interrupted by the chicane which is comprised of a series of bending

Discussion of Predicted Performance

We have used the numerical simulation codes PARMELA and FELEX [6] to model total system performance. These codes have been validated by numerous FEL experiments. In Table 1 we summarize the expected performance and specify additional parameters that characterize the XUV-FEL source. We note that the output radiation power is not limited by the physics parameters (accelerator and wiggler operational values), but rather by the rf power duty factor (duty factor = macropulse duration x repetition rate).

Table 1. Operational Parameters for a 60-nm XUV-FEL

Accelerator	Wiggler / Resonator
Energy - 85 MeV	Wiggler period - 5 mm
Energy stability - 0.05%	Wiggler length - 37.5 cm
Peak current - 500 A	Wiggler axial field - 3 T
Micropulse charge - 1.25 nC	Wiggler bore - 0.18 cm
Normalized (rms) emittance - 2π·mm·mrad	Resonator mirror reflectance(9 facets)- 82.4%
Micropulse rep-rate - 216 MHz	Outcoupling fraction - ~30%
Rf macropulse duty factor - 0.1%	Peak/average output power - ~2.5 MW/~20 W

References

1. B. E.Newnam, "Development of Free-Electron Lasers for XUV Projection Lithography," Proc. SPIE 1227, pp. 116-133, 1990.
2. B.E. Newnam, and V.K. Viswanathan, "XUV Projection Lithography System Design based on Single-Surface Reflecting Optics," presented at this conference, 1992.
3. V. K. Viswanathan, "Practical Tolerancing and Performance Implications for XUV Projection Lithography Reduction Systems," Proc. SPIE 1671, to be publ. 1992.
4. R. L. Sheffield, "Photo-Cathode rf Guns," AIP Conference Proc. 184, Vol II, 1500 - 1531, (1989).
5. R.W. Warren, "Design Considerations for Pulsed Microwigglers," Nucl. Instr. and Meth. in Phys. Res. A304, 765-769, (1991).
6. B.D. McVey, "Three-Dimensional Simulations of Free-Electron Laser Physics," Nucl. Instr. and Meth. in Phys. Res. A250, 449-455 (1986).

High-Speed Tape Target Transport for Laser Plasma SXPL Source*

Steve Haney, Kurt W. Berger, and Glenn D. Kubiak
Sandia National Labs
Livermore, CA 94551-0969
(510) 294-3375

Paul D. Rockett and John Hunter
Sandia National Labs
Albuquerque, NM 87185

Abstract

We describe a vacuum-compatible, high-speed tape target drive for use in a high-repetition-rate laser plasma SXPL source. Preliminary results are presented for its operation in vacuum using commercially-available tape and a ~1 J/pulse KrF excimer laser operating at 92 Hz.

High-Speed Tape Target Transport for Laser Plasma SXPL Source*

Steve Haney, Kurt W. Berger, and Glenn D. Kubiak
Sandia National Labs
Livermore, CA 94551-0969
(510) 294-3375

Paul D. Rockett and John Hunter
Sandia National Labs
Albuquerque, NM 87185

Abstract

High-power laser plasma sources are needed for the development of a compact soft x-ray projection lithography (SXPL) tool. Such sources have already been shown to achieve ~ 1% conversion efficiency (CE) into a 4.5% spectral bandwidth near 140 Å when driven by a commercially-available, 150 W excimer laser[1]. Laser plasma source targets must be developed which maximize CE while simultaneously minimizing the production of solid and gaseous debris. Mass-limited targets, which incorporate a layer of metal having a thickness approximately equal to the laser pulse-integrated ablation depth on a thin plastic backing, exhibit extremely low debris emission rates. Such tape targets have been proposed for several years for use in a low-repetition-rate commercial laser plasma source for proximity x-ray lithography[2]. Proposed laser drivers for SXPL, however, will operate at repetition rates of up to 1 kHz, imposing severe requirements on tape target advance speeds. Additionally, the source and target drive system must operate in vacuum and permit rapid replacement of spent target material.

We have constructed a high-speed tape drive system for use in a laser plasma source operating at repetition rates of ≥ 200 Hz. The system, shown schematically in Fig. 1, comprises two 8-inch diameter tape reels, retractable tape transport rollers, two independent servo motors and controllers, a vacuum enclosure, and an isolation gate valve to allow rapid tape replacement. The tape reels hold approximately 1100 meters of tape having thickness and width of 25 microns and 1.27 cm, respectively. Alternatively, 2200 meters of 12.5 micron-thick tape may be used. The tape reels are driven by two independent servo motors and controllers. The take-up reel motor controls the tape acceleration, deceleration, and velocity, while the supply reel motor, operating in a constant-torque mode, provides a constant tension or braking of the tape. The tape reels and transport rollers are internal to a vacuum enclosure attached the laser plasma source (LPS) chamber. The tape is supported by a slotted roller assembly to maintain precise positional control of the tape at the laser focus. This roller assembly is retractable and is vacuum-isolated by a gate valve. This feature allows spent tape to be replaced without venting the LPS vacuum chamber and its associated condensing and imaging systems. Following tape replacement, the tape enclosure is rapidly evacuated to ~10^{-5} Torr; the tape enclosure is then opened to the LPS chamber and the tape roller lowered for additional runs.

Using the tape target transport and a ~ 1 J/pulse KrF excimer laser operating near 100 Hz, we find that the required tape speed is 30 cm/sec, providing one hour of uninterrupted plasma radiation. This tape speed corresponds to a modest reel rotation rate of no more than 92 RPM. The reels have been operated at up to 800 RPM, suggesting that this tape drive will support laser repetition rates of up to 1

kHz. Target debris and soft x-ray conversion efficiency studies using a selection of tape formulations and target materials are in progress.

1. P. D. Rockett, J. A. Hunter, R. Kensek, R. E. Olson, G. D. Kubiak, and K. W. Berger, Proc. OSA Topical Meeting on Soft X-Ray Projection Lith., J. Bokor, ed. (1991).

2. U. S. Patent Numbers 4,700,371, 4,837,793, and 4,896,341.

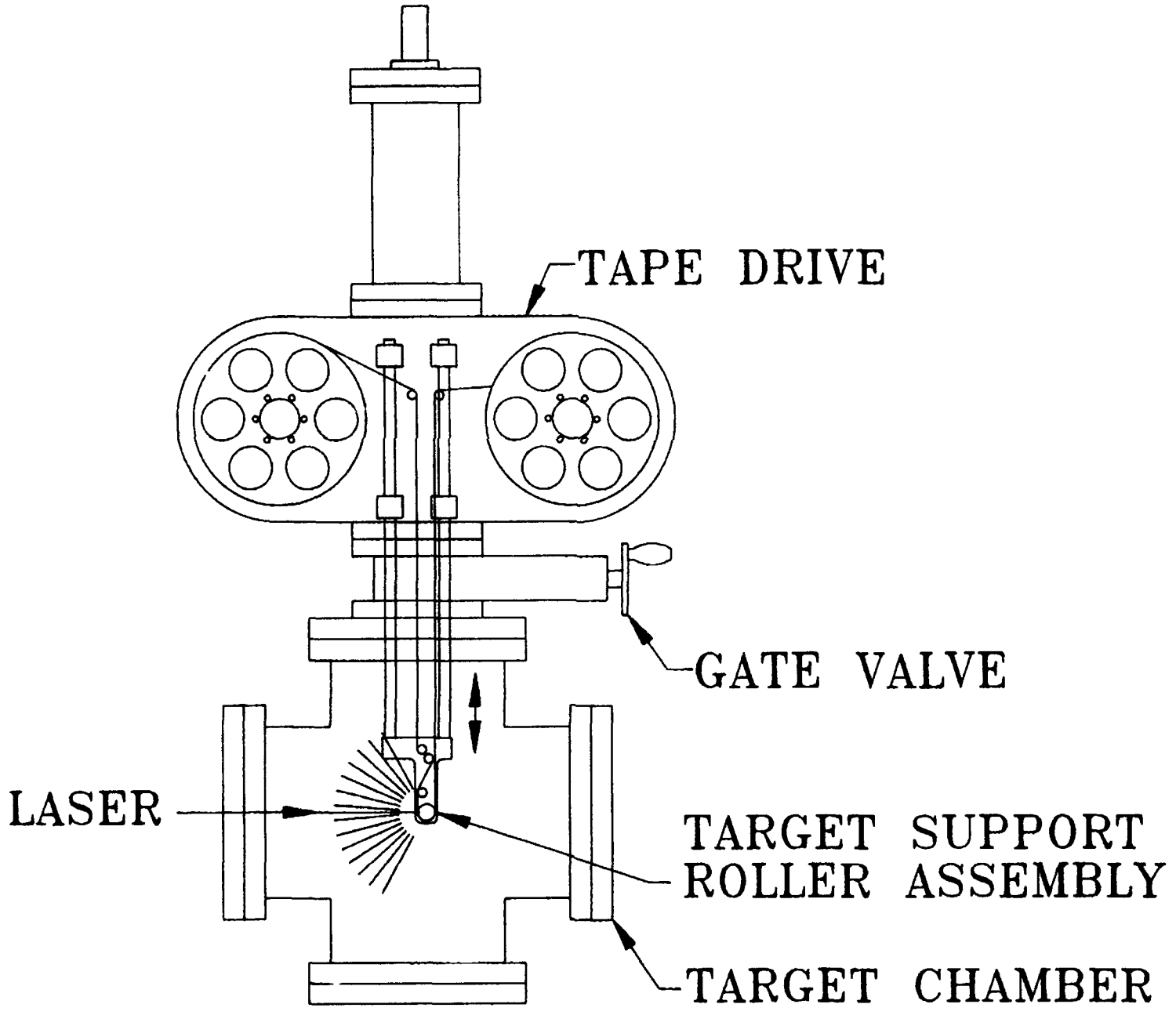

Figure 1. Schematic diagram of the high-speed tape target transport system.

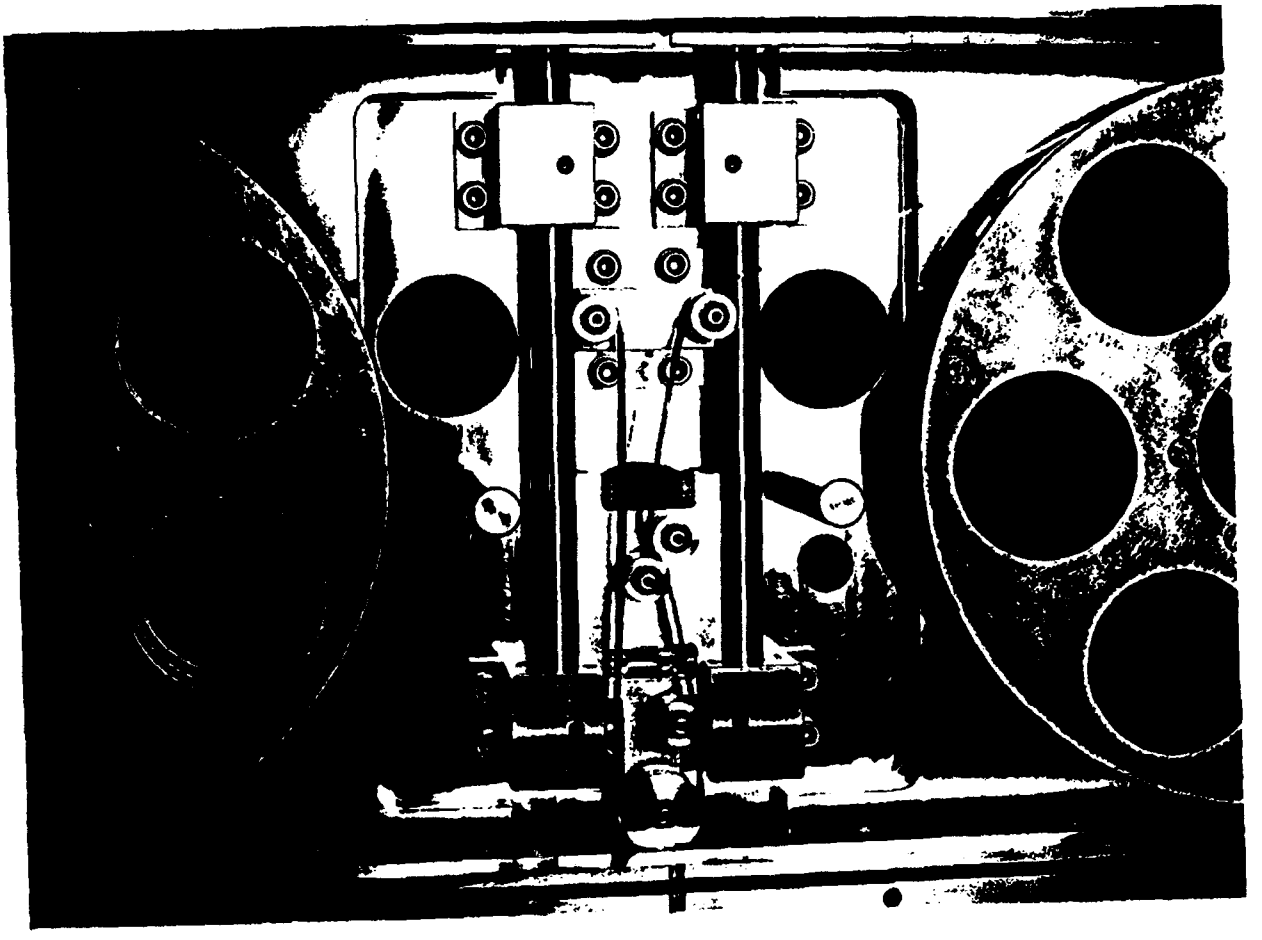

Figure 2. Photograph of the tape reels and transport roller assembly.

*Work supported by the United States Department of Energy under contract number DE-AC04-76DP00789 and by DARPA.

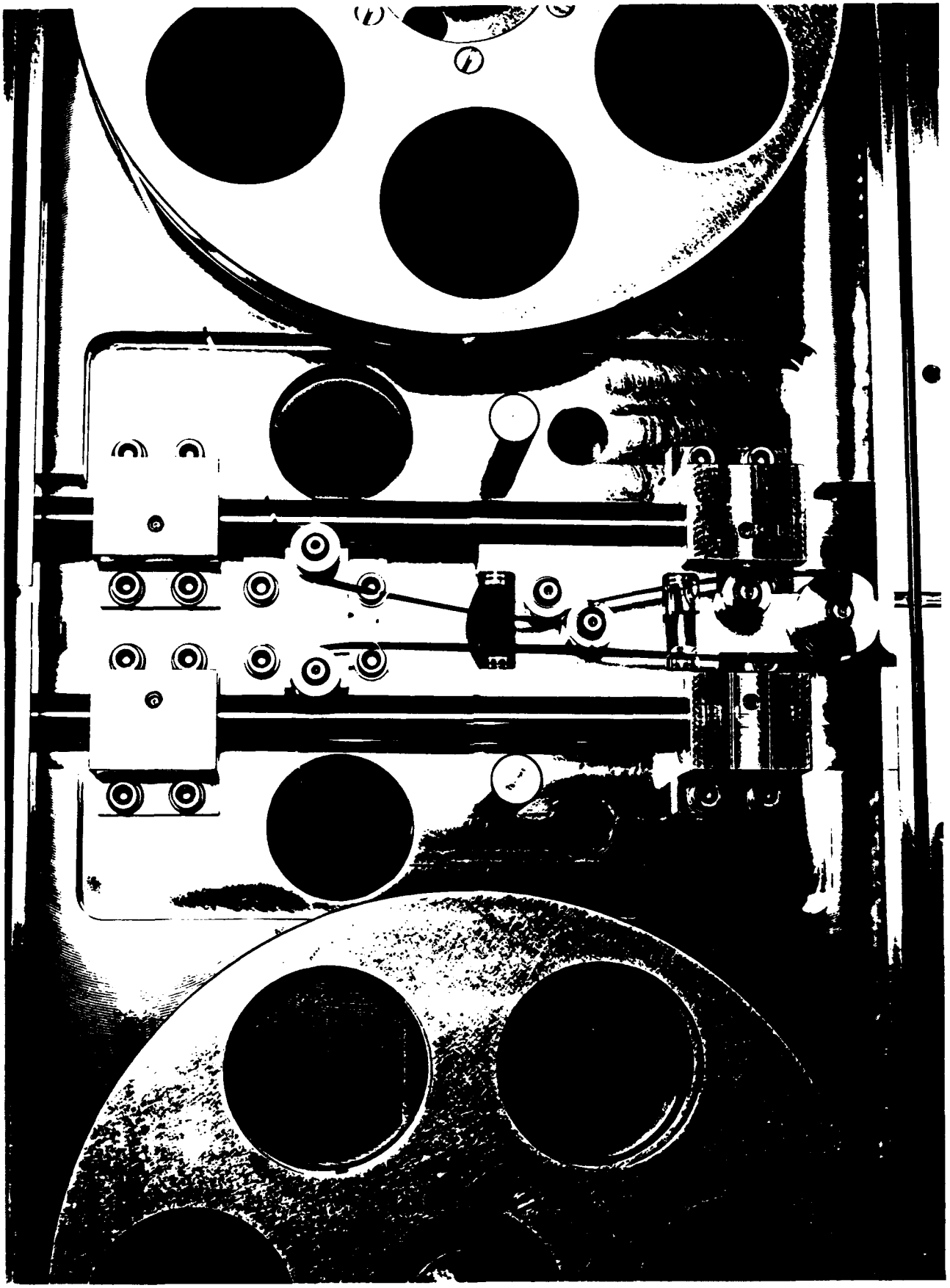

Pd2-5

Contamination Studies of XUV Reflecting Surfaces for Projection Lithography

Brian E. Newnam
Chemical and Laser Sciences Division, MS J564
and
Marion L. Scott
Materials Science and Technology Division, MS E549
Los Alamos National Laboratory
Los Alamos, New Mexico 87545
505/667-7979

Abstract

The results of carbon and oxide contamination experiments with Al, Si, Rh, and Ag films and surfaces quantify certain film growth rates and parameter dependences.

*Contamination Studies of XUV Reflecting Surfaces for Projection Lithography**

Brian E. Newnam
Chemical and Laser Sciences Division, MS J564
and
Marion L. Scott
Materials Science and Technology Division, MS E549
Los Alamos National Laboratory
Los Alamos, New Mexico 87545
505/667-7979

Summary

Optical projection lithography, if extended to extreme-ultraviolet (XUV) exposure wavelengths from 10 to 100 nm, has the potential to produce large chips (10 cm^2) with ≤0.1-μm minimum features and with sufficient process latitude for commercial production. However, surface contamination of these all-reflective illumination and imaging systems is a serious issue. Numerous experimenters[1-3] have reported that operation of optics in a vacuum while exposed to intense XUV and X-radiation results in contamination by carbon deposits and, for some materials, oxide epifilms. The carbon films derive from partial pressures of carbon-containing gases, such as CO, CO_2, and CH_4, that are cracked by photon-induced, secondary electrons emitted from the adjacent optical surfaces. Oxide films form on surfaces reacting with residual O_2 and H_2O in the vacuum.

We report results of an extensive set of oxide and carbon film contamination experiments with Al, Si, Rh, and Ag films and surfaces to quantify the film growth rates and parameter dependences. These four materials were selected initially because they exhibit total external reflectance at moderate angles of incidence, e.g. >45°, as needed for high-reflectance multifacet mirrors. In addition, these materials are candidate films for single-surface and multilayer mirrors at normal incidence as well as transmission filters in XUV projection lithography optical systems.

Our initial studies consisted of monitoring the growth of carbon and oxide contamination layers using Auger electron spectroscopy. In a second series we used *in situ* ellipsometry to directly measure the thickness of oxide films growing on Al and Si films, freshly deposited on Si substrates in a UHV environment (2 x

*Work supported by the Division of Advanced Energy Projects of the Office of Basic Energy Sciences of the U.S. Department of Energy.

10^{-10} Torr), versus partial pressures of O_2 and H_2O. In a third series we measured the time-dependent XUV reflectance *(in situ)* of Al and Si films at the He discharge wavelength of 58.4 nm.

Our primary observations were:

1. Carbon film and oxide growth rates depend on the substrate material. As seen in Fig. 1, carbon films grow rapidly on Rh, but not on Ag surfaces. Oxide films grow most rapidly on Al, and not at all on Ag surfaces.
2. Ionizing sources, including ion gauges and ion pumps (and high-energy photons), greatly increase the rate of carbon film accumulation on Rh, Al, Si, but again not on Ag.
3. Oxide growth rates on Al and Si are inversely dependent on partial pressure of O_2 and water vapor. Water vapor doesn't cause oxide formation on silicon.
4. After the first oxide monolayer has formed, further growth proceeds at a much slower rate; the monolayer acts as a diffusion barrier to penetration by oxygen to virgin metal. See Fig. 2.
5. Oxide films form on silicon at a rate 1/5 that on aluminum.
6. A fresh Al film maintained in a good UHV environment (10^{-9} Torr), where the residual gas was primarily helium, maintained its reflectance for at least one month as seen in Fig. 3. We estimate that no more than 0.25 monolayer of surface contamination (of any kind) had built up over this period.

Since some materials such as Ag *(Si)* attract carbon *(oxide)* contamination layers much less than others, it is possible that thin overcoats of these films will protect other films that have superior optical properties. The calculations of Fig. 4 indicate that a film of Al on a polished CVD-SiC substrate can greatly enhance the reflectance. Addition of a thin coating of silicon (0.7-nm thickness - three monolayers) should significantly reduce the oxide formation rate while producing a minor reduction in initial reflectance. In a practical lithography system, such optical design tradeoffs may advantageous. Even so, our studies indicate that maintaining the optics in UHV of $\leq 10^{-9}$ Torr with periodic *in situ* surface cleaning will probably be necessary.

1. J. R. Roberts, J. Kerner, and E. B. Saloman, Physica Scripta **41**, 9 (1990).
2. M. Yamamoto, et al., Physica Scripta **41**, 21 (1990).
3. V. Rehn, in *Vacuum Design of Synchrotron Light Sources*, AIP Conf. Proc. **236**, pp. 235-265 (1990).
4. D. Windt, et al., Appl. Opt. **27**, 279 (1988).
5. D. Y. Smith, E. Shiles, and M. Inokuti, in *Handbook of Optical Constants of Solids*, E. D. Palik, Ed. (Academic Press, NY, 1985), pp. 369-406.
6. D. F. Edwards, ibid., pp. 547-569.

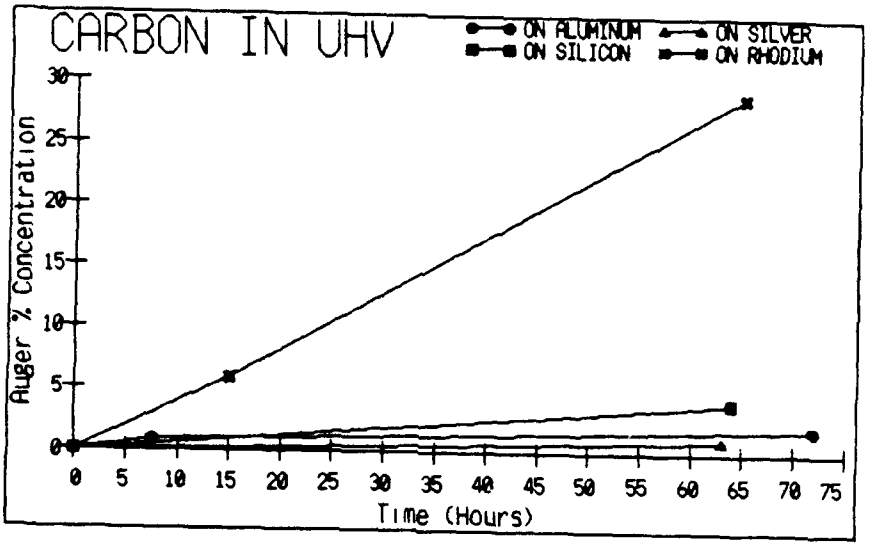

Figure 1. Auger electron spectroscopy study of surface carbon formation on four surfaces in a UHV system (10^{-9} Torr) with no ion gauges or Auger filaments operational.

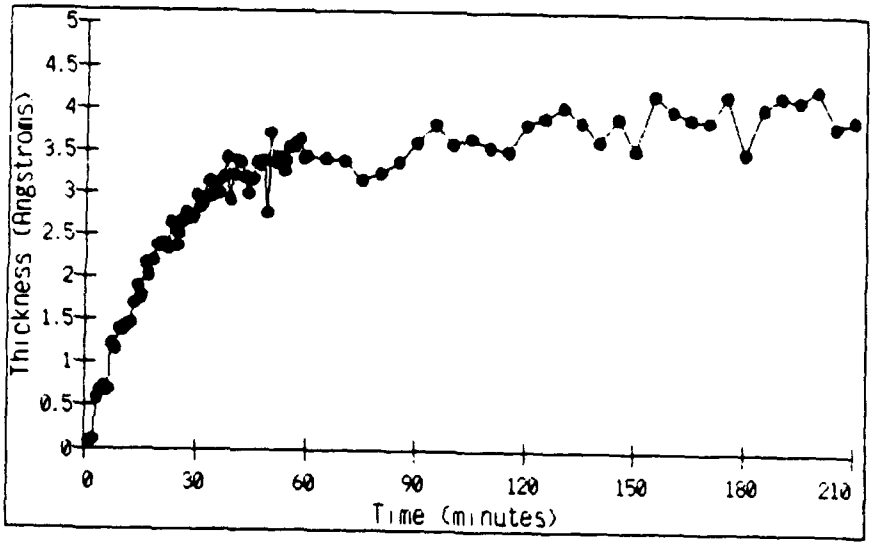

Figure 2. Formation of an aluminum oxide layer on aluminum while the oxygen partial pressure was maintained at 2×10^{-8} Torr. One hour was required to form one oxide monolayer.

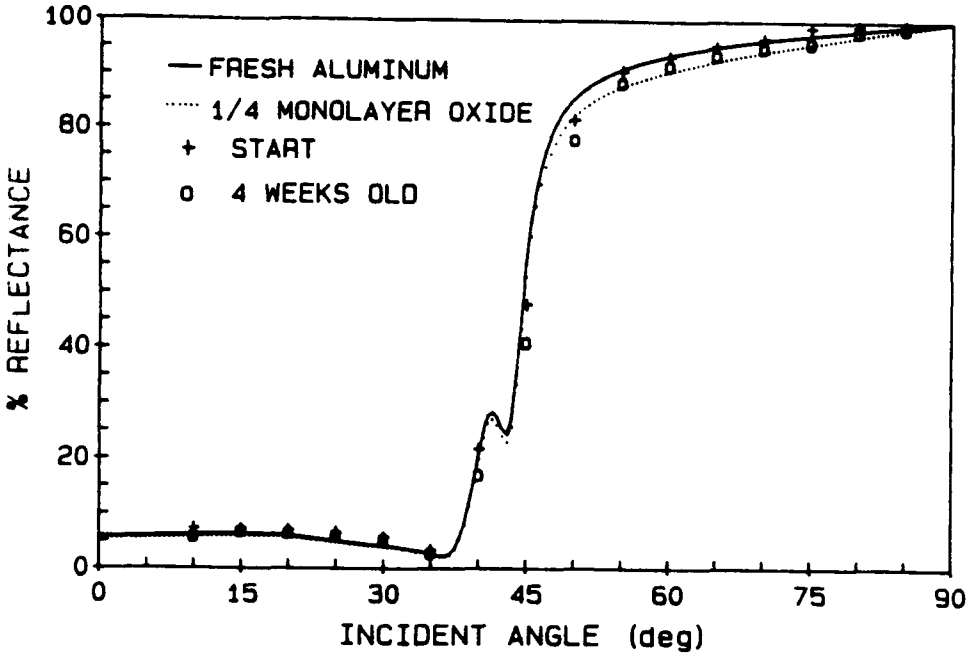

Figure 3. Reflectance vs angle of incidence at 58.4 nm for a fresh Al film deposited on an oxidized Al film on a Si substrate. After four weeks in a UHV system, maintained at a He pressure of $\geq 2 \times 10^{-9}$ Torr, reflectance measurements for this same film indicated formation of only a one-quarter of an oxide monolayer.

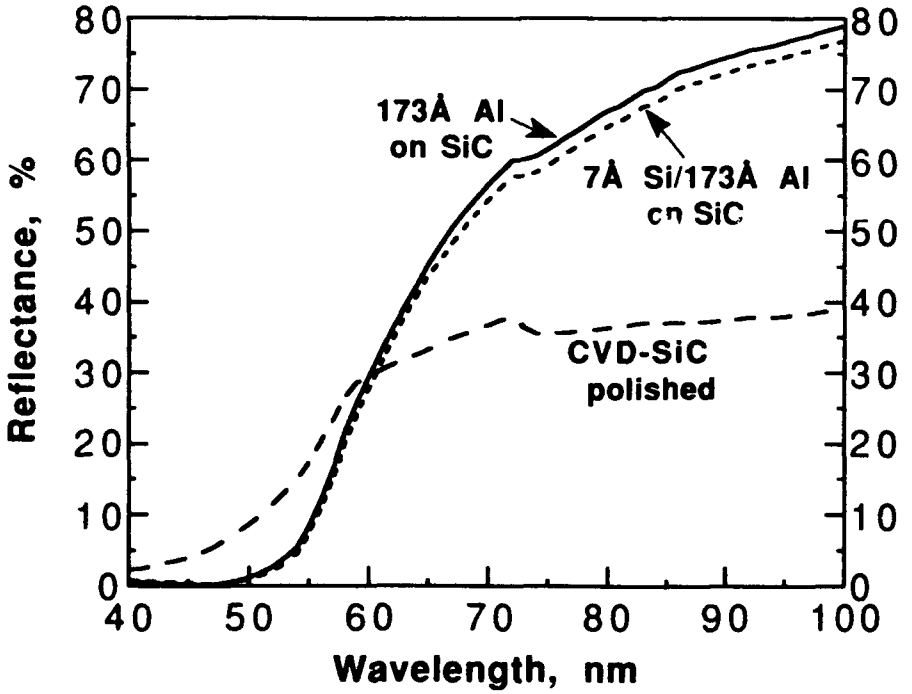

Figure 4. For XUV wavelengths ≥60 nm, a single-layer Al overcoat can provide substantial reflectance enhancement over that measured for polished CVD-SiC.[4] Susceptibility to oxidation should be reduced by a factor of five by using a protective, 7Å-thick (3 monolayers) Si epilayer. Reflectance calculations at normal incidence used empirical optical constant tabulations for CVD-SiC,[4] Al,[5] and Si.[6]

ATOMIC LAYER GROWTH OF TUNGSTEN AND BORON FOR MULTILAYER X-RAY OPTICS.

J.K. Shurtleff, D.D. Allred, R.T. Perkins, L.V. Knight and J.M. Thorne
Center for X-ray Imaging, Brigham Young University, Provo, UT 84602.

J.D. Phillips
MOXTEK, Box 7070, University Station, Provo, UT 84602.

Abstract

We are investigating atomic layer growth which can produce crystalline superlattices or amorphous multilayers with smaller periods and better uniformity than currently available.

Summary

X-ray lithography, x-ray microscopy, x-ray spectroscopy and x-ray astronomy have fueled the growth of x-ray optics. Multilayer x-ray optics are man-made periodic structures consisting of a stack of alternating high and low atomic weight materials. The periodic structure of a multilayer diffracts x-rays in the same way as the periodic structure of a natural crystal. The Bragg equation, $n\lambda = 2d \sin\theta$, is used to predict x-ray diffraction from periodic structures. This equation shows that a smaller period (d) will diffract shorter wavelength x-rays. The total x-ray reflectivity is degraded by nonuniformities in the period (horizontal and vertical), interdiffusion between layers and roughness of the multilayers. Currently, most multilayer x-ray optics (MXOs) are produced by sputtering and evaporation. These techniques can produce a minimum period of approximately 40 Å. Atomic layer growth (ALG) is a new technique for producing MXOs which can produce crystalline superlattices or amorphous multilayers with smaller periods and better uniformity.

ALG is a chemical vapor deposition (CVD) technique which deposits a monolayer of atoms during each cycle of the deposition process. ALG enables the thickness of the material to be controlled to within a monolayer, the interfaces between materials to be atomically abrupt and the material to be uniform over large areas and complex geometries. The deposition of tungsten using tungsten hexafluoride and hydrogen illustrates the ALG deposition process. In the first step, tungsten hexafluoride is introduced into the deposition chamber. It reacts until a monolayer of tungsten hexafluoride is adsorbed onto the substrate surface. In the second step, the deposition chamber is purged and evacuated to remove any excess tungsten hexafluoride. In the third step, hydrogen is introduced into the deposition chamber. It reacts with the monolayer of absorbed tungsten hexafluoride to produce a monolayer of tungsten and hydrogen fluoride gas. In the fourth step, the chamber is again purged and evacuated to remove the hydrogen fluoride and any excess hydrogen. The thickness of the material is determined by the number of four step cycles performed. To produce a

multilayer, this process is repeated for a different material.

We have investigated the deposition of zinc sulfide, zinc selenide, tungsten, boron, carbon and silicon dioxide by ALG. ALG has been used to deposit amorphous materials. Crystalline materials can be grown by atomic layer epitaxy (ALE) by carefully matching the crystal structures of the material and substrate. Most of the III-V and II-VI semiconductors have been deposited by ALE. We have successfully deposited zinc sulfide and zinc selenide by ALE; however, these materials are not ideal for producing MXOs. We calculated the theoretical x-ray reflectivity for several different multilayers to replace the TLAP organic crystals currently used in x-ray spectrometers. A carbon/tungsten multilayer is approximately 100 times more reflective than a zinc selenide/zinc sulfide multilayer with the same period. We have pioneered the deposition of single elements, such as tungsten and boron by ALG. We use two criteria to determine if a material has been deposited by ALG. First, the film thickness must be independent of reactant concentrations, equilibration time and deposition temperature as long as they are greater than some minimum value. Second, the film thickness divided by the number of cycles must be constant for fixed deposition parameters.

We performed a statistically designed experiment to investigate the deposition of tungsten by ALG using tungsten hexafluoride and hydrogen. The overall reaction is $WF_{6\,(g)} + 3H_{2\,(g)} \rightarrow W_{(s)} + 6HF_{(g)}$. We performed a series of twenty-two depositions varying the deposition parameters. We measured the thickness and optical constants of the deposited films using ellipsometry. The results are shown in Table I.

Table I. Statistically Designed Experiment

Run #	Temp. (°C)	WF_6 Flow	H_2 Flow	Eq. Time (s)	Thickness (Å)
1	275	3125	2000	0	20
2	275	1375	4000	0	22
3	425	3125	2000	0	808
4	425	1375	2000	0	-
5	275	3125	4000	10	36
6	275	1375	4000	10	28
7	425	3125	4000	0	260
8	350	2250	3000	5	40
9	275	3125	2000	10	41
10	425	1375	2000	10	836
11	425	1375	4000	10	759
12	425	1375	4000	0	460
13	425	3125	2000	10	541
14	350	2250	3000	5	-
15	500	2250	3000	5	834
16	275	1375	2000	10	35
17	275	1375	2000	0	24

18	350	4000	3000	5	418
19	425	3125	4000	10	715
20	200	2250	3000	5	23
21	275	3125	4000	0	26
22	350	500	3000	5	1202

Table I shows that the film thickness depends on the deposition temperature, but is relatively insensitive to the reactant concentrations or equilibration time. This is the expected result for deposition by ALG. If the material was deposited by CVD, the film would be thicker for higher reactant concentrations and longer equilibration times. However, the film thickness divided by the number of deposition cycles is not constant and it does not equal a monolayer of tungsten per cycle. The refractive indices measured by ellipsometry also differed significantly from the value expected for tungsten. We concluded that the films we deposited during these experiments were actually tungsten oxide due to oxygen contamination in our deposition system. We also decided that that a more reliable technique for measuring the thickness of the films was needed.

After the initial tungsten ALG experiments, we redesigned and rebuilt our ALG deposition system. We were able to eliminate the oxygen contamination, increase the substrate diameter from two inches to four inches and increase the deposition temperature from a maximum of 500 °C to 900 °C. We also developed techniques for etching a step in the deposited film so that we could measure the thickness of the film using optical profilometry. We have performed several tungsten depositions in the new ALE system. We obtained shiny metallic tungsten films and we could not detect oxygen in the films using EDXA on a SEM. We etched a step in the tungsten film. We had to coat it with evaporated aluminum to prevent phase shifting between the tungsten film and the silicon substrate. We measured the step on a Wyko optical profilometer. The total thickness was 815 Å. The thickness divided by the number of cycles is 815 Å / 500 cycles = 1.63 Å/cycle, which corresponds to a monolayer per cycle. We concluded that we can deposit tungsten by ALG; however we require further depositions and measurements to confirm these results.

We have performed preliminary research on the deposition of boron by ALG using diborane and chlorine. The overall reaction is $B_2H_6(g) + 3Cl_{2\,(g)} \rightarrow 2B_{(s)} + 6HCl_{(g)}$. The deposition temperature had to be less than 350 °C to prevent thermal decomposition of the diborane. We selected a deposition temperature of 200 °C. The deposited film was a metallic gray color similar to the amorphous boron films we have deposited by conventional CVD. We determined the thickness of the boron film using optical profilometery. The thickness divided by the number of cycles is 401 Å / 500 cycles = 0.80 Å/cycle, which is slightly less than one monolayer per cycle. The use of chlorine damaged our deposition system; therefore, we recently changed the reactants to boron trichloride and hydrogen. The overall reaction is $BCl_{3(g)} + 3/2H_{2(g)} \rightarrow B_{(s)} + 3HCl_{(g)}$. We have been unable to determine the crystal structures of the ALG deposited materials; however, the edition of a

Scintag thin film x-ray diffractometer to our analytical capabilities should help us resolve this problem. We are confident that we can deposit boron by ALG, but more deposition and analysis is required.

We have investigated the deposition of amorphous and crystalline materials by ALG and ALE. We have successfully deposited tungsten by ALG and we are confident that we can deposit boron by ALG. We have made considerable process toward our goal of producing MXOs with this technique. We have attempted to deposit a W/B multilayer with a period of 30 Å by ALG, but we were unsuccessful. We will continue to investigate the deposition of tungsten and boron by ALG and we will expand our capabilities to include the deposition of rhenium, molybdenum, carbon, silicon, silicon dioxide and other materials in the future.

SOFT X-RAY MULTILAYER MIRRORS

Fan Zhengxiu
Shanghai Institute of Optics and Fine Mechanics,
Academia Sincia, P.O.Box 800-211, Shanghai, 201800, P.R.China

ABSTRACT

The present status of studies on soft x-ray multilayer mirrors in our institute are described. These include the optimum design, deposition technique and the preliminary characterizations.

INTRODUCTION

After the initiation of modern x-ray multilayer fabrication by Spiller[1] and Barbee[2] and coworkers, the interest in use and production of these superstructures is still growing. Combined with the needs of x-ray laser research program we have designed and studied soft x-ray multilayer mirrors.

During the last sereral years we have tried to prepare the multilayer by employing a high vaccum elcetron beam deposition system and plane magnetron sputtering system. Employing both quartz oscillator monitor and time-monitor techniques we have successgully fabricated some multilayers which were designed for mirrors of various wavelength. Measurements of low angle x- ray diffraction, Auger Electron spectroscopy and Transmission Electron Microscopy are done for these multilayers.

Reflectometer has been established in our laboratory. Samples of single layer and multilayer were measured in this reflectometer. The results of reflectivity of x-ray multilayer and optical constants of materials, such as W, C, Si, Mo, in the x ray region have been first obtained in China.

DESIGN

The normal incidence x-ray multilayer mirrors is built up with two mnaterials: H for the heavy material, L for the light material. The structure consists of N identical pairs with a period thickness $d=d_H+d_L$. In all our designs and analyses[3,4], we used the theory based on the classical optical thin-film matrix method. Refering to the optical constants of materials reported by other authors[5-8], we

can choose a proper pair of materials for a specific wavelength and then determine the proper thickness for each layer (d_H, d_L) and the optimum layer numbers (N).

There are a number of ways in which the multilayer structures differ from the ideal structure. The principal imperfections include the surface roughness of the outmost layers and the interfaces roughness, the layer thickness monitor random errors and the diffusion in the interface between two materials. For investigating the effects of these imperfections, the thickness monitor random errors of each layer were introduced by the Gauss-distribution random numbers which its standard deviation (SD) and average value (AV) presents the magnitude of errors. The roughness of the layers surface were divided into two cases: (1) The rms roughness of the outmost layer was simulated by a Debye-Waller[2, 9] factor, (2) The gradient layers which is assumed to be same thickness were instead of the roughness of the interfaces, and we assumed the optical constants to be the cosine function distribution. Figure 1 show the effects of these imperfections.

To meet the needs of x-ray laser research, the wavelengths we choosen to make normal-incidence x-ray multilayer mirrors were 105A, 114A, 135.5A, 171.4A, 234A. The multilayers of Mo/Si, Ag/Si[10], W/C, Mo/Al[3] and Ta/Si[11] are selected for these wavelengthes. Table 1 listed the design results of these multilayers.

FABRICATION

Our deposition system was equipped with a 6KW electron gun and two plane magnetron sputtering guns. So both high vaccum electron-beam (EB) and plane magnetron sputtering deposition system can be employed simultaneously or separately in the fabrication of the multilayers. The base pressure of the system was 5×10^{-6}Torr with a diffusion pump. During deposition the pressure in the chamber is about 5×10^{-5}Torr when using EB or about 2×10^{-3} Torr when using sputtering gun. At present stage no special device is used for cooling or heating the substrate.

Our sputtering deposition system was equipped with two plane magnetron sputtering guns fixed symmetrically, the sizes of targets are Φ80mm. Two guns were drived using 1KW radio frequency power supply for light materials (such as C, Si) and a 1KW direct current power supply for heavy (metal) material (such as Ta, W, Mo) respectively. Fig 2. is the schematic of this system, the target-to-substrate vertical distance is adjustable from 0 to 16cm, there are a movable shutter and a fixed shutter between the substrate table and the guns, where the movable shutter keep the particles of predeposition out of the substrates, the hollow of the fixed shutter make the substrates scan in the well distributed sputtering area.

The counter is used to close the movable shutter as soon as the number of period reaches the design number.

The thickness of each layer was monitored mainly with time-monitor technique together with two quartz crystal oscillator monitors. A 160L-CZ004 motor make the substrates table rotate with the stableness ±0.2%. The argon pressure was controlled by an automatic pressure control instrument with the stability about ±0.05mTorr. The deposition rates for various materials were previously calibrated by depositing films with sufficiently thickness (about 1500-3000A) to be accurately measured using a precision optical interferometer. Table 2 shows that these deposition rates have fine identity for difference deposition periods which indicates the stability of our deposition system is satisfactory.

In the fabrication, after several minutes predeposition, then we open the movable shutter, the substrates contimuously moved over the guns so as to be alternately deposited two defferent materials and bring us the high regular periodic multilayer. We have prepared the multilayers mentioned above with this sputtering system.

TEST AND EVALUATION

1. Structural characterization

The structural characterization can obtain detailed information on the periodicity, interdiffusion at the interfaces, crystal structure, entrapped gases, surface roughness etc. In our works, low angle x-ray diffraction(LXD), auger electron spectroscopy(AES), electron diffraction(ED) and transimission electron microscopy(TEM) are employed. We have improved the numberically simulation method to determine the period thickness, the surface roughness, interdiffusion at the interfaces and the thickness random monitor errors from x-ray diffraction curve. For data reduction the merit function used in this simulation was defined as follows with the nonlinear laeast-quare curve-fitting technique:

$$F=\sum_{i=1}^{M}[\log R_m(\theta_i)-\log R_c(\theta_i)]^2$$

where R_m are the measured reflectivity, R_c are the theoretical results which based of the optical constants from the atomic scatter factors f' and f''[12] for 1.54A. We have infered the imperfections of these multilayers as listed in Table 3.

2. Reflectance measurements

Our home-made reflectometer has resently been established[13]. The absolute reflectance at a particular incidence angle was measured by determining the ratio of the reflected intensity to the incident beam internity, both measurements were done with the same

detector, which is free to rotate about the sample from near-normal incidence to grazing incidence. The light sources used the characteristic x-radiations. There are eight wavelengths in our reflectometer, such as CuKα, CoKα, TiKα, TiLα, AlKα, MgKα, CKα, SiKα. Figure 3 show the measured results of some of these multilayers for 44.7A and 27.44A x-rays.

3. Determination of optical constants.

In design and analyses the structure of multilayers, it is extremely important to have accurate optical constants of materials for soft x-rays, especially in the form of thin film which the thickness less than 300A. However, the optical constants are related to the thickness of coatings and the production method, so we must investigate these so that we can accurately design and evaluate our multilayers.

In the present study, we improve the reflectivity method by analyzing the R-θ curve, using the orthogonal experimentation statistical method to deduce the first results, and the Gauss-Newton method to give the final results.[13] Table 4 listed our preliminary results by taking advantage of this method.

CONCLUSION AND DISCUSSION

As the first steps, we have researched the design and fabrication technology and founded the equipments and method for fabricating and testing x-ray multilayer.

We have fabricated and charactizited several x- ray multilayers However, for improving the properties of x-ray multilayer so as to meet the needs of x-ray laser and another application and enhace the resist the laser and plasma damage ability,, we have to improve the deposition system to enhance the uniform and the stabi- lity of the layer and the monitor techniques of layer thickness to achieve optimum layer thickness. We have also to employ the supersmooth substrates to obtain a low scattering x-ray multilayer.

REFERENCE

[1]. E. Spiller, et al., AIP conference Proceeding, No. 75, 124 (1981)
[2]. T. W. Barbee, Jr., AIP Conference Proceeding, No. 75, 131 (1981)
[3]. Jin Lei, et al., Optical Coatings-Proceedings of international Symposium (23-25 May 1989, Shanghai, China), pp. 176-179.
[4]. Fan Zhengxiu, et al., Chinese Journal of Lasers (In Chinese), Vol. 19, No. 1, 74 (1992)
[5]. B. L. Henke et al., Atomic Data and Nuclear Data Tables, Vol. 27, No. 1, 1 (1982)
[6]. B. L. Henke et al., AIP, No. 75, 340 (1981)

[7]. David L. Windt, et al., Applied Optics, Vol. 27, No. 2, 246 (1988)
[8]. David L. Windt, et al., Applied Optics, Vol. 27, No. 2, 279 (1988)
[9]. R. P. Haelbich, et al., Appl. Phys. Lett. Vol. 34, 184 (1979)
[10]. Shao Jianda, et al., SPIE, Vol. 1519, 298 (1991)
[11]. Shao Jianda, et al., 'Sputtering Deposition Ta/Si Soft X- ray Multilayer Mirror', Submitted to this topical meeting
[12]. D. T. Cromer et al., J. Chem. Phys. 53, 1891 (1970)
[13]. Guo Yonghong et al., SPIE, Vol. 1519, 327 (1991)

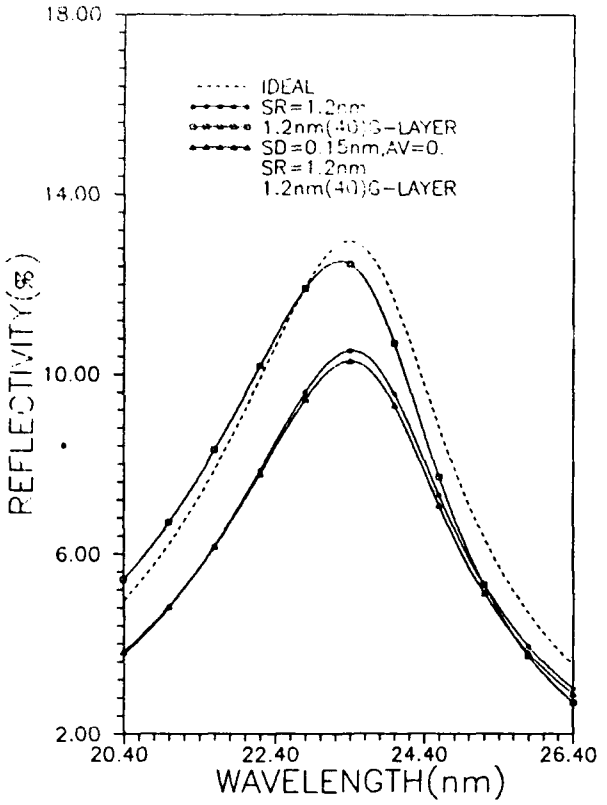

Figure 1. The effects of imperfections. where SR is the rms surface roughness, SD is the standard deviation and AV is the average value of Gauss-distribution random numbers. G-layer is gradient layer.

Table 1. Design parameters and results

λ (A)	Incidence angle	Materials	Layers number	Optimum thickness (A)	Reflectivity (%)
105	0	Mo/Si	20	25/30.5	5.3
114	0	Ag/Si	40	33.6/26.4	35.2
135.5	0	W/C	30	32/39	3.
171.4	0	Mo/Al	20	41/47	44.1

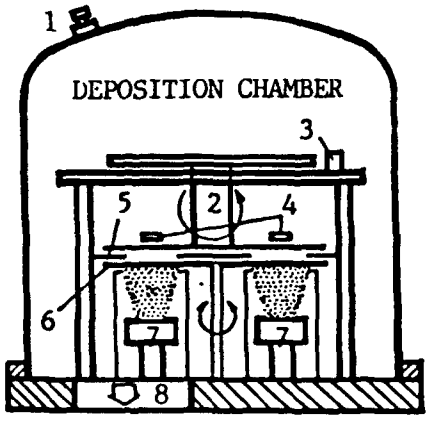

Figure 2. Schematic view of sputtering deposition chamber.
[1]. Pressure control vavle
[2]. Substrates table
[3]. Counter
[4]. Quartz oscillator sensors
[5]. Fixed shield
[6]. Movable shield
[7]. Magnetron sputtering guns
[8]. To pump

Table 2. The deposition rates for different periods

Periods (min)	2	6	8	10	12	16
Rates (A/min)	15.27	16.02	16.11	15.38	15.71	15.86

Table 3. The imperfections deduced numberically with simulation method.

Multilayers	Thickness errors		rms surface	G-layers
	SD (A)	AV (A)	roughness (A)	thickness (A)
Mo/Si	1.3	0.5	10	12.3
Ta/Si	1.5	0	12	12
Ag/Si	0.9	0.2	15	23
W/C	0.7	0	9	11

Table 4. The optical constants of Al, W and C for different wavelengths

Materials	Thickness (A)	Wavelength (A)	n	k
Al	~1000	44.7	0.9936	0.0020
Al	~1000	27.44	0.9963	0.0004
Al	~1000	7.12	0.9989	0.0002
W	~1100	44.7	0.9952	0.0045
W	~1100	27.44	0.9975	0.0020
W	~1100	7.12	0.9992	0.0002
W (W/C)	32	44.7	0.9956	0.0043
C (W/C)	39	44.7	0.9998	0.0002

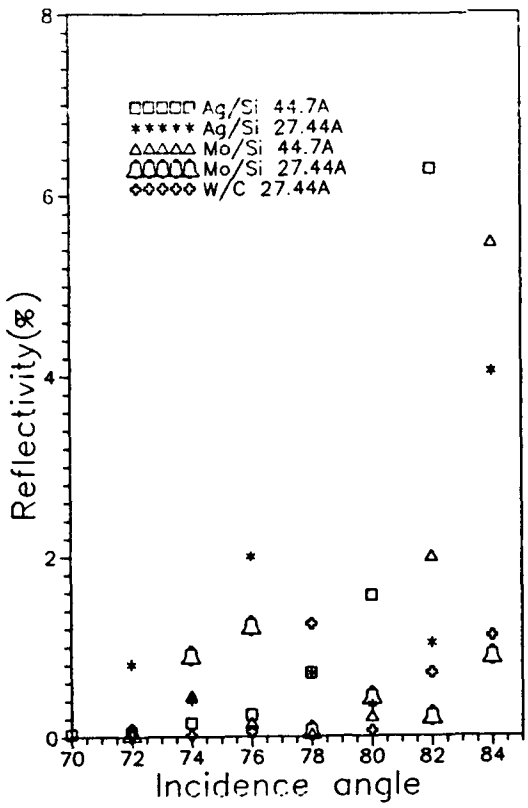

Figure 3. The measured reflectivity of Ag/Si, Mo/Si and W/C for 44.7A and 27.44A x-rays in our home-made reflectometer.

SPUTTERING DEPOSITED Ta/Si SOFT X-RAY MULTILAYER MIRROR

Shao Jianda and Fan Zhengxiu

Shanghai Institute of Optics and Fine Mechanics
Academia Sincia, P.O.Box 800-211, Shanghai
201800, P.R.China

ABSTRACT

30 layers of Ta/Si alternative structure prepared by plane magneton sputtering has been choosen for 234A x-ray mirror. Its characterizations indicated that it is expected to get the real reflectivity of about 10%.

INTRODUCTION

A number of excellent results has proved that sputtering[1], evaporating[2], and laser deposition[3] techniques have allowed effcient multilayer mirrors to be fabricated when we began to study soft x-ray multilayer mirrors. Now in our laboratory, two plane magnetron sputtering guns together with a 6KW electron gun had been laid in a deposition system. The multilayers can be prepared by employing sputtering and evaporating techniques. In this paper, 30 layers Ta/Si multilayer mirror was fabricated only using sputtering technique.

Characterizations of this multilayer have been done with low angle x-ray(CuKα radiation) diffraction (LXD), auger electron spectroscopy (AES) and absolute R-θ reflectivity measurement at 4.47nm. Simulated the LXD curve, the layer thickness monitor errors, rms surface roughness and interdiffusion in the interfaces are investigated. On the basis of these, the 10% real reflectivity of this mirror for design wavelength can be deduced.

In order to analyze annealing-induced variations in interface, the sample were annealed for 2 hours at temperature up to 300℃. Characterizations of this annealed multilayer show that no obvious variations occurs, its interface is also fairly sharp.

DESIGN AND FABRICATION

In resent study, for keeping up to date with the x-ray laser research program in our institute, the wavelength we chosen to make multilayer is 234A. Suitable materials for multilayer mirrors can be selected by the criteria summarized in reference[4] . Carbon has been the spacer of choice for much of the X-UV and soft x-ray spectrum due to its low absorption and the smooth interfaces that form when interlayered with many metals[1, 5]. However, silicon has lower absorption than carbon at wavelength just below the carbon K-edge at 44.7A and also at wavelengths immediately above the silicon L-edge at 124A[6, 7]. The study of Si/metal multilayers is also of interest is itself because of the possible fabrication of fully crystalline multilayers. These could withstand the effects of high intensity radiation much better than polycrystalline or amorphous ones.

Unfortunately, when we started to design multilayer structure, a difficulty emerged, i.e. there wasn't adequate data of the optical constants for the 200A wavelength region in the reference on hand. As a rough method, refering to the optical constants reported by D.L.Windt[8, 9], we have to utilize the linear interpolation method to determine the optical constants of Ta and Si, its results were listed in the table 1.

According to these optical constants, we have determined the optimum thickness of each layer using the theory based on the classical optical thin film matrix method as listed in table 2.

Our sputtering deposition system was detailed discribed in reference [10]. During deposition the argon gas controled by an automatic pressure control instrument was 2×10^{-2} Torr with the stability about ±0.05mTorr. The deposition rates for Si and Ta were approximately 15A/second and 8A/second respectively, with a target-to-substrate vertical distance of 90mm. These rates had previously been calibrated by depositing films with sufficiently thickness (about 1500A) to be accurately measured using a precision optical interferometer. In fabrication, 99.99% pure si and 99.9% pure Ta disks were used as targets, the purity of Ar is $>99.999\%$.

Φ30mm K9 glass with rms surface roughness about 8A was chosen for the substrate of this multilayer. A initial thick Si film about 500A thickness was first deposited so as to reduce the rms surface roughness of the substrate to about 5A on the basis of our experiments in advance. The substrates were initially at room temperature, and no effort was made to cool their temperature during deposition. Ta film is the outmost layer.

CHARACTERIZATION

The structure characterizations of this multilayer was done with LXD, AES and x-ray reflectivity measurement.

1. Low Angle X-ray diffraction

Determination of the imperfections from the measured performance of a multilayer has been discussed by many authors[10, 11]. In our laboratory we have improved a method which simulate the performance of multilayer with the thickness errors, interdiffusion layers and surface roughness from the LXD curve. The optical constants used in simulation for 1.54A were listed in table 3.

Figure 1. shows our simulation curve and measured curve. In this simulation curve, 1.5A standard deviation of a Gauss- distribution ramdon thickness error, 12A thickness of interdiffusion layers at the interfaces and 11A rms sureface roughness were drawn into. We can find these two curves are fairly coincidence.

2. Auger profile analysis

The AES spectrum of this multilayer is reported in figure 2. The tantalum and silicon contributions appear clearly and are in opposition. This profile indicates structure is fine regular in agreement with the LXD analysis.

3. 44.7A x-ray reflectivity measurement

The absolute reflectivity measurement had done using 44.7A CKα radiation with the reflectometer in our laboratory. Figure 3 reported our measurement results and the simulation curve with the imperfections mentionded above. Table 4 presented the optical constants for 44.7A.

4. Characterization of annealled sample

Experiment of thermal stability had done through annealling for 2 hours at temperature up to 300℃ at atmosphare. Characterizations of this annealled sample indicated that no obvious variations occurs. The results of LXD, AES and the absolute reflectivity measurement of annealed sample essentially coincides with previous results.

CONCLUSION

We have designed and fabricated 30 layers Ta/Si multilayer mirror for 234A x- ray. The imperfections have been numerical determined with a simulating method. On the basis of these results we estimated the reflectivity of this mirror for 44. 7A and the measured results of reflectivity indicated that our estimation agree with these perfectly. So we think that the reflectivity of this multilayer can also be estamited using this technique, Figure 4

reported this estimation, the reflectivity of 10% is expected for 234A x-ray.

REFERENCE

[1]. T.W.Barbee, Jr., AIP Conference Proceedings, No.75, 131(1981)
[2]. E.Spiller, et al., AIP conference Proceedings, No.75, 124(1981)
[3]. S.V.Gaponov, et al., Opt. Commun., 38, 7(1981)
[4]. A.G.Michette, Optical Systems for Soft X Rays, Plenum Press, New York(1986)
[5]. E.Spiller, et al., Appl. Phys. Lett. Vol.37, 1048(1980)
[6]. T.W.Barbee, Jr., et al., Appl. Opt. Vol.24, 883(1985)
[7]. J.L.Wood, et al., Proc. SPIE Vol.563, 238(1985)
[8]. D.L.Windt, et al., Applied Optics, Vol.27, 246(1988)
[9]. D.L.Windt, et al., Applied Optics, Vol.27, 279(1988)
[10]. Fan Zhengxiu, 'Soft X-ray Multilayer Mirrors', Submitted to this topical meeting
[11]. E.Spiller, et al., Optical Engineering, Vol.25, No.8, 954(1986)
[12]. P.G.Harper, SPIE Vol.984, 150(1988)

Table 1. The optical constants for 234A

Materials	n	k
Ta	0.8465	0.1790
Si	0.9455	0.0321

Table 2. Design Parameters and Results

λ (A)	Incidence angle	Materials	Layers number	Optimum thickness (A)	Reflectivity
234	0	Ta/Si	30	4.5/8.35	0.13

Table 3. The optical constants for 1.54A

Materials	$\delta \times 10^6$	$\beta \times 10^6$
Ta	39.4524	3.1201
Si	7.6216	0.1766

Table 4. The optical constants for 44.7A

Materials	n	k
Ta	0.99054	0.00951
Si	0.99524	0.00211

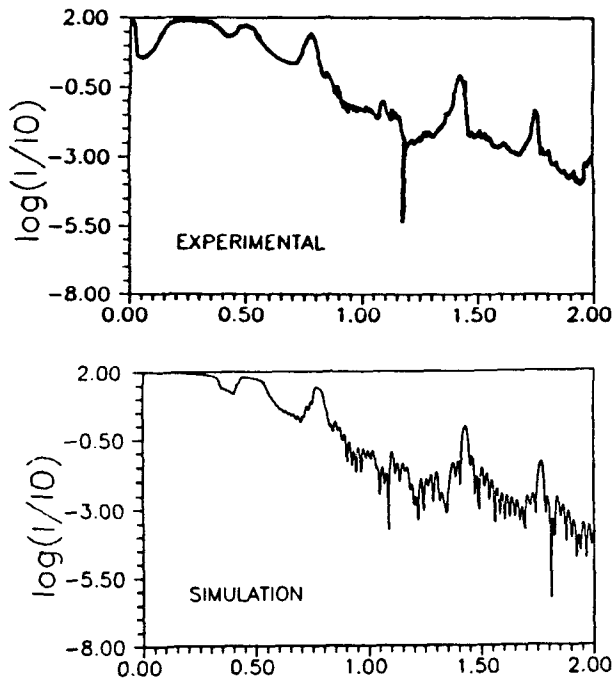

Figure 1. Experimental and simulated low angle x-ray diffraction curves.

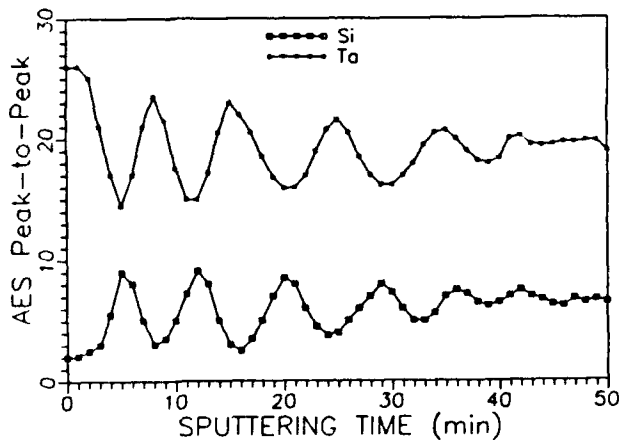

Figure 2. Auger profile analysis.

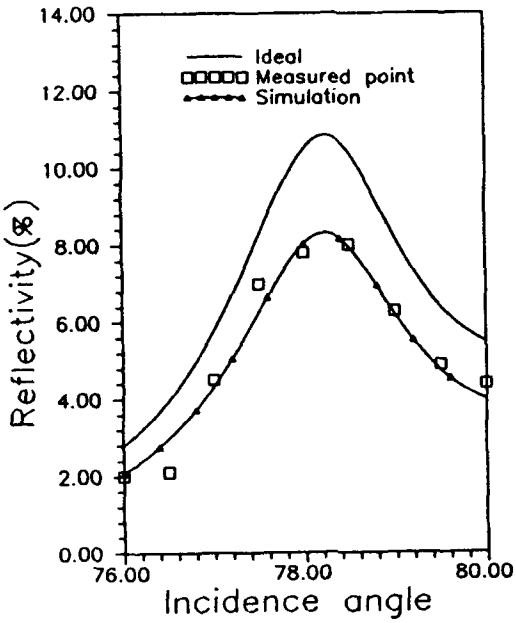

Figure 3. Ideal, simulation and measured reflectivity curves for 44.7A

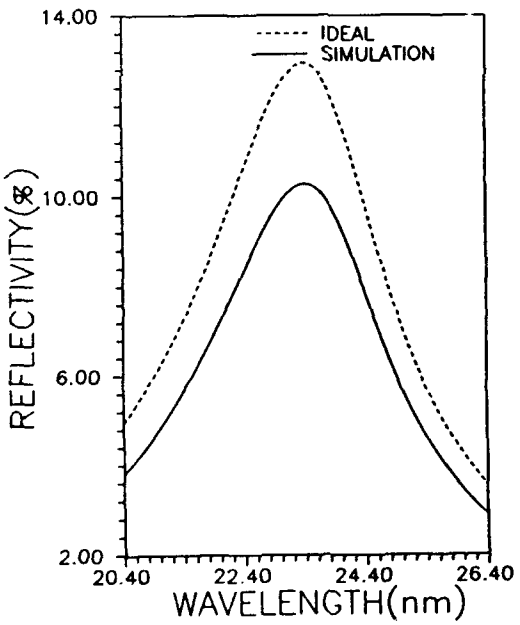

Figure 4. Ideal and simulation reflectivity curves for 234A

Observation of Influence of Electrical Isolation of Dielectric Substrates on Structure and Reflectivity of Mo/Si Multilayer Coatings

Georgy Gutman
Ovonic Synthetic Materials Co., Inc.
Troy, Michigan 48084

Richard Watts
National Institute of Standards and Technology
Gaithersburg, Maryland 20899

SUMMARY

One of the most important general requirements for soft X-ray optics, and X-ray lithography in particular, is high reflectivity at normal incidence for long wavelength X-rays. Dependence of the multilayer structure on the deposition parameters and identification of appropriate conditions for the growth of multilayers having optimally smooth and sharp interfaces has been reported elsewhere[1,2,3,4].

A schematic depiction of the RF magnetron sputtering system used to deposit the Mo/Si multilayer mirrors is shown in Figure 1. Two nominally identical superpolished (RMS roughness < 1Å) 10mm thick quartz substrates were coated in the same run with 40 layer pairs of Mo/Si with the target Γ of 0.5. The substrates were mounted side by side on a spinning platform which was in turn mounted on a rotating drum. In the usual way, the rotation of the drum brought the spinning substrates first under the Mo target and then under the Si target producing one layer pair for each revolution of the drum.

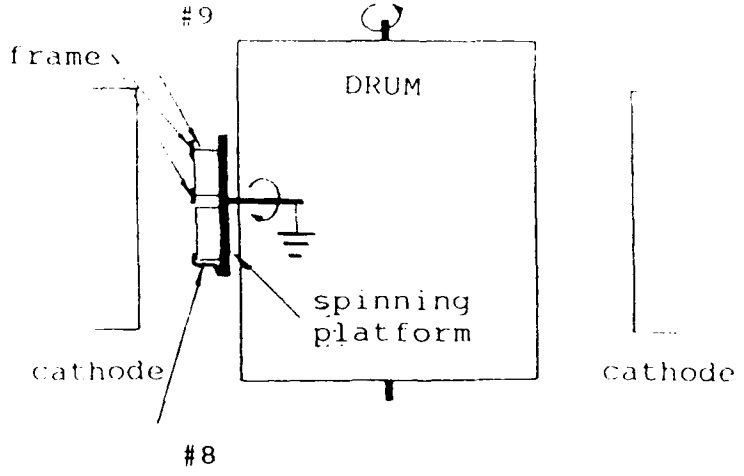

Fig. 1. Schematic diagram of the RF sputtering system.

In every way the substrates were identically mounted except that an electrical path to ground was provided for the surface of substrate #8. The surface of substrate #9 was electrically isolated from the grounded spinning platform. To insure that substrate #9 did not become grounded during the deposition process by coating of the sides of the substrate electrically connecting the surface to the spinning platform, a frame mask of Kapton tape was affixed to the surface of substrate #9. A similar frame mask was placed on substrate #8 to insure identical conditions for the deposition.

The electrical connection on substrate #8 was made in such a way that the first layer of deposition completed the conduction path across the front surface of the substrate. A test of the continuity to ground of both the substrates after deposition showed the surface of substrate #8 connected to ground through a 16 ohm resistance and surface of substrate #9 still electrically isolated from ground with a measured resistance greater than 1 megohm.

Figure 2 shows diffraction curves determined under identical conditions using λ=0.154nm x-rays. Three observations can be made concerning these data sets: (1) The bilayer spacing of the isolated substrate is 7% greater than that of the grounded substrate, (2) the number of orders of reflection is significantly reduced in the isolated substrate than the grounded substrate and (3) the Γ's of the two coatings are significantly different judging from the ratios of the second and third orders in each case.

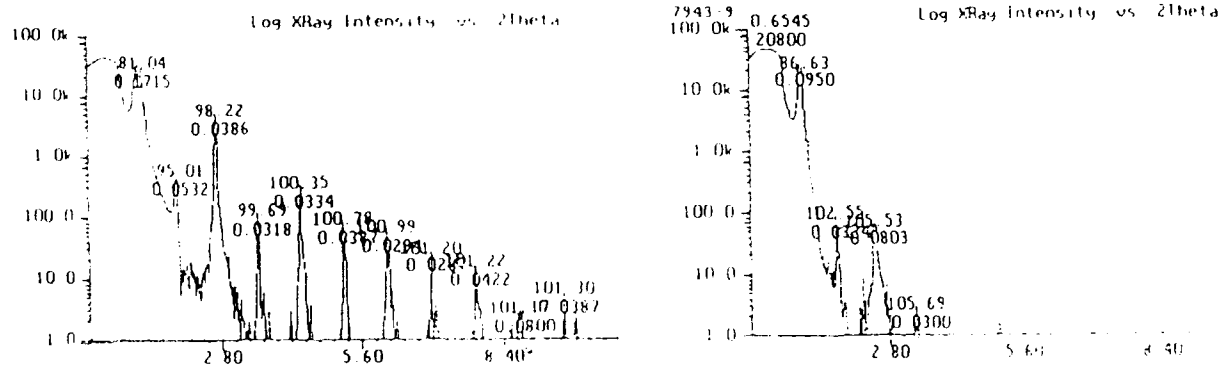

Fig2. θ-2θ x-ray diffraction curves at λ =0.154nm. Left #8, grounded; Right #9, isolated.

Figure 3 shows reflectance versus wavelength measurements performed under identical conditions at 45° angle of incidence. These results have two important features (1) the reflectivity of the coating on the isolated substrate is half the value of the reflectivity measured on the grounded substrate and (2) the effective bilayer spacing at these longer wavelengths varies by approximately 5%, with the isolated substrate having the larger bilayer spacing.

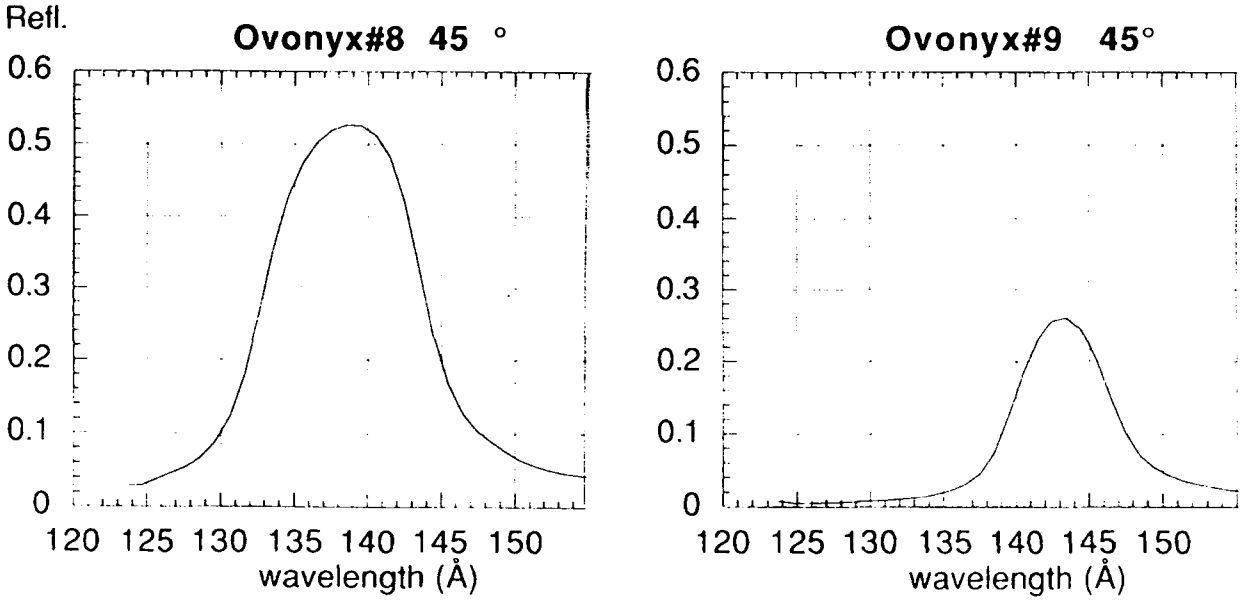

Fig. 3. 45 degree incidence reflectivity of a Mo/Si multilayer coating.

Similar results have been obtained on replications of this experiment and on Si wafer substrates.

We conjecture that the difference in charged ion bombardment of the growing multilayer is the primary factor influencing the growth of the films. It is possible that increased ion bombardment of the grounded substrate increases deposited atom surface mobility and results in the differences observed in the film growth. We stress that these are preliminary conjectures and that further work is being pursued at our laboratories to fully elucidate the origins of these observations.

ACKNOWLEDGEMENT

We would like to thank John Keem for useful discussions.

REFERENCES

1. D.L.Windt, et.al. "Interface Imperfactions in Metal/Si Multilayers", J.Appl.Phys. **71**(6), 2675 (1992).

2. S.P.Vernon, et.al. "Multilayer Coatings on Figured Optics", Proceeding SPIE Multilayer Optics for Advanced X-Ray Applications, Vol. 1547, San Diego, CA, July 1991.

3. J.E.Bjorkholm, et.al., "Reduction Imaging at 14nm Using Multilayer-Coated Optics: Printing of Feartures Smaller than 0.1μm", J. Vac. Sci. Technol., Vol. D., No.6, Nov/Dec 1990.

4. D.G. Stearns, et.al. "High Performance Multilayer X-Ray Optics," Proceedings OSA Topical Conference on Soft X-Ray Projection Lithography, Monterey, CA, April 1991.

Resist Alternatives for Sub-0.35-μm Lithography Using Highly Attenuated Radiation

R. R. Kunz, M. A. Hartney, and M. Rothschild
Lincoln Laboratory, Massachusetts Institute of Technology
Lexington, MA 02173-9108

Introduction

Traditional optical lithography uses semitransparent single-layer resists where the exposing radiation produces a latent image throughout the thickness of the resist, and an isotropic liquid-based development step is used to create the desired resist profile. However, resolution of 0.25-μm or better, which is required for 256 Mbit DRAM chips and beyond, cannot be obtained with conventional photolithographic technology (250-400 nm wavelength). Shorter wavelengths are required, such as 193-nm (DUV-193), soft-X-ray (10-50 nm) or hard-X-ray (1-2 nm) radiation. Unfortunately, between the wavelengths of 10 and 220 nm few materials are semitransparent. For example, at 193 nm novolac resins commonly used at longer wavelengths have an absorption depth of only 40 nm, and at the 13-nm wavelength it is 400 nm. New resist processes capable of accommodating a latent image confined to the near-surface region must therefore be developed. The lithographic process must now include an additional processing step, namely pattern transfer into the bulk of the resist. This step must be highly anisotropic so that the pattern in the surface layer is faithfully reproduced at the resist-substrate interface. These general considerations were outlined already in 1984 by Taylor et al.[1]. They apply also to other forms of strongly absorbed radiation such as ion beams. (For instance, a 30 keV Ga^+ beam has a projected range of only 34 nm in photoresist.) Today, surface imaging processes have been demonstrated not only for soft X-ray projection (SXP) [2] and deep ultraviolet (DUV) lithographies [3], but are being considered for manufacturing processes at optical wavelengths as well [4]. In this paper we review some of the recent developments in the areas of surface imaging and multilayer resists, with emphasis on application to 193-nm lithography. It should be noted, however, that some of the reviewed resist concepts may be applicable to SXP lithography as well.

Silylation Processes

The surface-imaging chemistry most widely adopted is based on area-selective silylation of novolac- or phenol-based resins. Figure 1 shows a typical process flow for a positive-tone silylation process. This scheme requires the resist exposure to crosslink the resin, either directly [3] or through a subsequent acid-catalyzed reaction activated during a post-exposure bake step [5]. The crosslinking acts to impose diffusion-rate contrast of the silylating reagent between the crosslinked and uncrosslinked areas. Once the silylating reagent has diffused into the resin, it reacts with phenol groups to form a silyl ether. The silicon incorporated in the resist acts as an etch mask during the oxygen-plasma development step. This approach has been demonstrated using electrons [5] and ions [6], as well as SXP (13.5 nm) [2], 248 nm [7], and 193 nm [8]. An example of patterning using this process is shown in Figure 2, where the imaging was performed using 193 nm. The commercial product Shipley FSC is a typical resin that can be used for the uncatalyzed process, whereas Shipley SAL 601 and SNR 248 are acid catalyzed systems.

Since the diffusion depth of silylating agent is often greater than the crosslinked depth, diffusion of silylating agent under the crosslinked area could limit the resolution to only coarse features. However, Hartney et al. [8] have examined diffusion profiles of the silylating reagent for features as small as 0.3 μm and found no evidence of underdiffusion. It has been proposed [8] that stress created by the differential swelling of crosslinked and uncrosslinked areas results in anisotropic diffusion profiles. This same restricted diffusion, however, can lead to proximity effects where silylation depths for tightly spaced gratings are smaller than for large, uncrosslinked fields. Modeling is under way [9] to examine the process latitude and limitations of this surface imaging scheme at sub-0.25-μm feature sizes.

Other silylation chemistries have been developed which are based on photogeneration of silylation sites [10]. The principle here is not to inhibit the diffusion of the silylating agent, but rather to prevent its reaction with the resin in selected areas. In this scheme, the original resin contains pendant tertiarybutoxycarbonyloxy (tBOC) groups and a photoacid generator (PAG). Upon exposure, sufficient acid concentration is generated to remove the majority of tBOC groups during a post-exposure bake, the result being a phenol-like polymer which can be readily silylated. In contrast to the system based on crosslinking, this process is negative tone. Use of this approach in surface imaging has thus far been limited to 248 nm [11].

With either of the silylation chemistries described above, anisotropic pattern transfer must be performed using an oxygen plasma etch through the unsilylated resist. Since silylation depths are often only 100 to 200 nm thick [3], etch selectivities of the order of 20:1 must be achievable to transfer the pattern through 2 μm of underlying film. In addition, for this process to meet large throughput requirements, high etch rates will be necessary. Horn et al. [12] have evaluated several commercially available etch tools for the purpose of comparing etch selectivity, profiles, and rates for a 193-nm based silylation process. With proper choice of the etching tool, selectivities as high as 25:1 and novolac-resin etch rates of greater than 1 μm/min can be obtained. Issues such as the etch profile and critical dimension control are also under investigation for a variety of commercially available etching tools, but further study is required to determine the process limits.

Novel approaches

For specialized applications, such as deep-trench etching into silicon, resist approaches that depart radically from traditional silylation-based surface-imaging chemistry may find utility. One such approach uses WO_3. This material has long been evaluated as a particle-beam resist [13], but recently Rothschild and Forte [14] have examined its application as a 193-nm resist. Surface-imaging of high-optical-density (O.D. = 1.5), ultrathin (~50 nm) WO_3 films, followed by a fluorine-plasma development step and oxygen reactive ion etching for pattern transfer, has enabled patterning of 0.35-μm structures into novolac polymer. In addition, initial results at 4.47 nm (C Kα) indicate the process may be transferable to the X-ray regime [15].

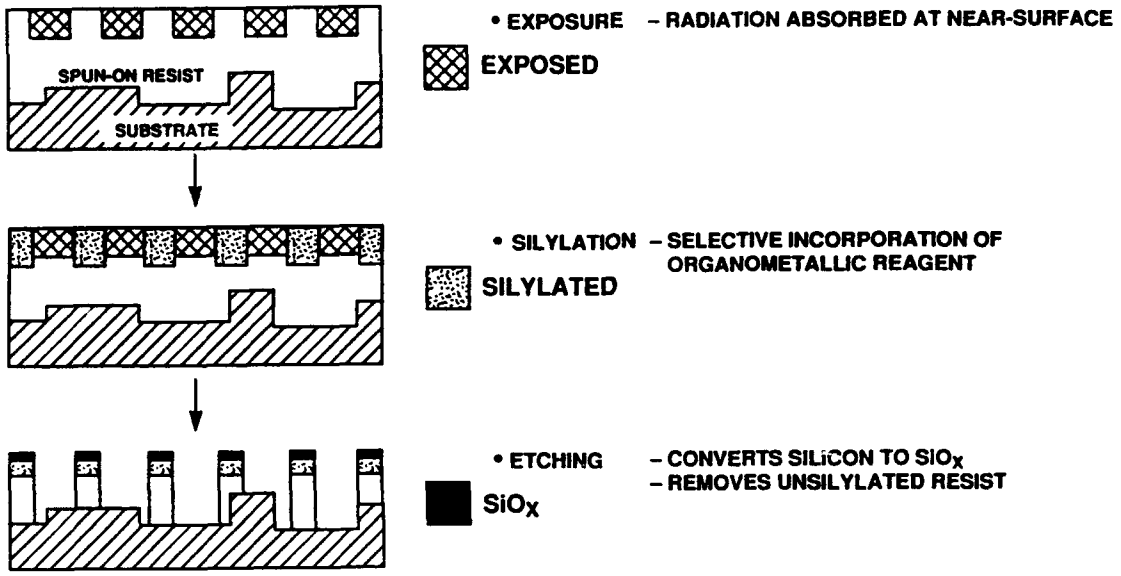

Figure 1. Process flow for a positive-tone silylation process in which the diffusion selectivity is based on radiation-induced crosslinking of the resin.

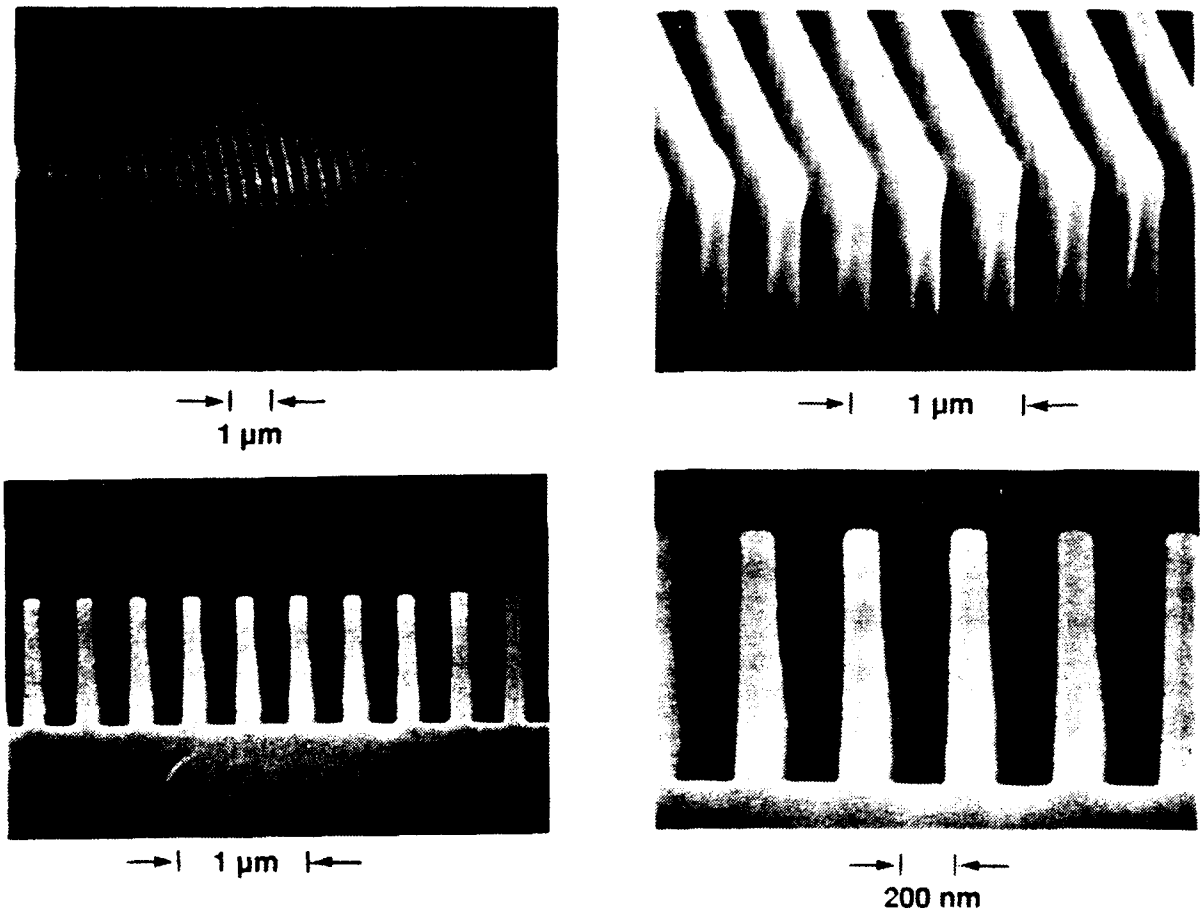

Figure 2. Scanning electron micrographs taken at four different magnifications, of 0.2-µm lines and spaces printed in polyvinylphenol using 193-nm projection lithography. The exposure was 100 mJ/cm^2 and the silylating agent was TMSDMA. The pattern transfer was performed using oxygen reactive ion etching.

Another novel approach involves photochemical manipulation of adsorbed molecular layers [16]. With appropriate chemical pretreatment, a Pd-containing electroless plating catalyst can be selectively deposited from solution after patterned exposure. The result is the area-selective electroless deposition of copper or nickel. Using this technique and 248-nm illumination, 0.65-μm patterns have been transferred into silicon, where electroless copper was the etch mask in a fluorine-plasma reactive ion etch pattern transfer step [17]. Another method [18] involves deposition of the Pd catalyst onto a resist that has already been exposed. The Pd in the exposed areas is then lifted off during a wet development step. Electroless Cu or Ni plating and pattern transfer then yield the desired resist image. This second scheme is being evaluated at i-line (365 nm) by National Semiconductor Corporation under the auspices of the MANTECH program [19]. The catalyst, and copper- and nickel-plating chemicals are commercially available as Shipley Cataposit 44, Cuposit 328, and Niposit 468, respectively.

It should be noted that all the schemes mentioned above do not require a special ambient during exposure. Further resists have been developed at 193 nm, which rely on photooxidation of silicon-containing polymers in air. Unexposed portions of ultrathin (~30-150 nm) films of highly absorbing silicon polymers spun on organic films are thus selectively etched [20] or dissolved [21], and the pattern is then transferred with oxygen reactive ion etching.

Conclusion

Surface-imaged resist systems unhindered by strong absorption of the incident radiation have been demonstrated now for over five years. Systems based on area-selective silylation are slowly becoming accepted as a viable generation of resist technology, and extension of these processes into the VUV and soft X-ray arenas has begun. As new sources and optics become available, additional resist technologies such as those mentioned here, that are suitable for strongly absorbed radiation will undoubtedly be developed and together with silylation find a place for lithography in the 0.10 to 0.35 μm range. In addition to higher resolution, the new resist processes must satisfy increasingly stringent requirements in etch latitude and control of critical dimension. Novel resist processes that can provide significant improvements in these areas may ultimately provide the best overall process performance.

Acknowledgment

This work was sponsored by the Defense Advanced Research Projects Agency.

References

1. G. N. Taylor, L. E. Stillwagon, and T. Venkatesan, *J. Electrochem. Soc.* **131**, 1658 (1984).
2. G. N. Taylor, R. S. Hutton, D. L. Windt, and W. M. Mansfield, *Proc. SPIE* **1343**, 258 (1990).
3. M. A. Hartney, R. R. Kunz, D. J. Ehrlich, and D. C. Shaver, *Proc. SPIE* **1262**, 119 (1990).
4. C. M. Garza, G. R. Misium, R. R. Doering, B. Roland, and R. Lombaerts, *Proc. SPIE* **1086**, 229 (1989).
5. T. G. Vachette, P. J. Paniez, and M. Madore, *Proc. SPIE* **1262**, 205 (1990).
6. M. A. Hartney, D. C. Shaver, M. I. Shepard, J. S. Huh, and J. Melngailis, *Appl. Phys. Lett.* **59**, 485 (1991).
7. J. W. Thackeray, J. F. Bohland, E. K. Pavelchek, G. W. Orsula, A. W. McCullough, S. K. Jones, and S. M. Bobbio, *Proc. SPIE* **1185**, 2 (1990).
8. M. A. Hartney, M. Rothschild, R. R. Kunz, D. J. Ehrlich, and D. C. Shaver, *J. Vac. Sci. Technol. B* **8**, 1476 (1990).
9. M. A. Hartney, *Proc. SPIE* **1672** (1992) (to be published).
10. H. Ito, and C. G. Wilson, *Polymer Eng. Sci.* **23**, 1012 (1983).
11. C. A. Spence, S. A. MacDonald, and H. Schlosser, *Proc. SPIE* **1262**, 344 (1990).
12. M. W. Horn, M. A. Hartney, and R. R. Kunz, *Proc. SPIE* **1672** (1992) (to be published).
13. M. Baba and T. Ikeda, *Jpn. J. Appl. Phys.* **20**, L149 (1981); N. Koshida and O. Tomita, *Jpn. J. Appl. Phys.* **24**, 92 (1985).
14. M. Rothschild and A. R. Forte, *Appl. Phys. Lett.* **59**, 1790 (1991)
15. M. Rothschild, unpublished results.
16. C. S. Dulcey, J. H. Georger, V. Krauthamer, D. A. Stenger, T. L. Fare, and J. M. Calvert, *Science* **252**, 551 (1991).
17. J. M. Calvert, M. S. Chen, C. S. Dulcey, J. H. Georger, M. C. Peckerar, J. M. Schnur, and P. E. Schoen, *J. Vac. Sci. Technol. B* **9**, 3447 (1991).
18. G. S. Calabrese, L. N. Abali, J. F. Bohland, E. K. Pavelchek, P. Sricharoenohaikit, G. Vizvary, S. M. Bobbio, and P. Smith, *Proc. SPIE* **1466**, 528 (1991).
19. K. Radigan and S. Liddicoat, *Proc. SPIE* **1672** (1992) (to be published).
20. R.R. Kunz, M. W. Horn, P. A. Bianconi, G. M. Wallraff, R. D. Miller, R. B. Goodman, E. J. Ginsburg, D. A. Smith, and J. R. Eshelman, *Proc. SPIE* **1672**, (1992) (to be published).
21. R. R. Kunz, P. A. Bianconi, M. W. Horn, R. R. Paladugu, D. C. Shaver, D. A. Smith, and C. A. Freed, *Proc. SPIE* **1466**, 218 (1991).

TECHNICAL PROGRAM COMMITTEE

Natale M. Ceglio, *Chair*
Lawrence Livermore National Laboratory

William T. Silfvast, *Chair*
University of Central Florida (CREOL)

Jeffrey Bokor
AT&T Bell Laboratories

John H. Bruning
GCA/Tropel

E. Michael Campbell
Lawrence Livermore National Laboratory

Hiroo Kinoshita
NTT LSI Laboratories, Japan

David Markle
Ultratech Stepper

William Oldham
University of California, Berkeley

Richard H. Stulen
Sandia National Laboratories

Gary N. Taylor
AT&T Bell Laboratories

John Warlaumont
IBM

Frits Zernike
SVG